**Title**

Delineating mechanisms of cutaneous wound healing and regeneration in adults



**Author**

Guerrero-Juarez, Christian Fernando

**Publication Date**

2018

Peer reviewed|Thesis/dissertation

UNIVERSITY OF CALIFORNIA,
IRVINE

# Delineating mechanisms of cutaneous wound healing and regeneration in adults

DISSERTATION

submitted in partial satisfaction of the requirements
for the degree of

DOCTOR OF PHILOSOPHY

in Biological Sciences

by

**Christian Fernando Guerrero-Juarez**

Dissertation Committee:
Assistant Professor Maksim V. Plikus, Chair
Assistant Professor Sha Sun
Associate Professor Ali Mortazavi
Professor Xing Dai
Professor David Gardiner

2018

# DEDICATION

To

My parents – *Gricelda Juarez Morales* and *Fernando Guerrero Cano*

# TABLE OF CONTENTS

# LIST OF FIGURES

# LIST OF TABLES

# ACKNOWLEDGMENTS

I would like to express my foremost appreciation and gratitude to my Doctorate advisor, Dr. Maksim V. Plikus, for his continued support, encouragement and guidance throughout my tenure at the University of California, Irvine. With his support, I have been able to participate in several research projects – on and off campus, which have been invaluable in my formation as a scientist. Such opportunities have furthered my horizons, expanded my knowledge and enhanced my skills set. They have served as drivers for both, my academic and personal growth. I am indebted to Dr. Plikus and couldn't have been happier to have been part of his research team.

I would like to thank my committee members – Drs. Ali Mortazavi, Sha Sun, Xing Dai and David Gardener, who have provided insightful comments, constructive criticism, and continued commitment to my dissertation work.

I would like to thank my mentors at UC Irvine and CSU San Bernardino, especially Drs. Marlene de la Cruz, Luis Mota-Bravo, Belisario Ventura, Sanders McDougall, Cynthia Crawford and Laura L. Newcomb for their continued advice and mentoring throughout the years. Their guidance and support made my graduate and undergraduate career a valuable one.

I would like to thank the undergraduate students whom I have had the opportunity to work with and mentor throughout the years – especially Sarah Konopelski, Amanda Ramirez, Christina Dang and Yuchen Liu. Your continued efforts, commitment and diligence helped our research program tremendously.

I would like to thank my friends and extended family for their support. Especially, I would like to thank Drs. Alvaro P. Villarreal-Ponce and Rolando Ruiz-Vega for their friendship and advice over the past few years.

I would like to express my foremost, sincere appreciation and gratitude to my parents – Fernando Guerrero Cano and Gricelda Juarez Morales, for their endless support throughout the years, for always believing in me, and for their always wishing the best for me. Your hard work and sacrifices have always been appreciated and you have become a driving force in my academic studies and future career goals. I Love you both.

I would like to thank my brother, Alexis Hiram Guerrero-Juarez, for his continuous support. You are a tenacious young man and I am ecstatic to see what the future holds for you. I am sure all your hard work and dedication will pay off. Go on and change the world!

I would like to thank the collaborators of the Plikus laboratory with whom I had the opportunity to work with both on and off-campus.

I thank the University of California, Irvine Developmental and Cell Biology Department, Center for Complex Biological Systems, Sue and Bill Gross Stem Cell Research Center, FACS and Stem Cell COREs, and the UCI Genomic High Throughput Facility, especially Dr. Melanie Oakes and Valentina Ciobanu, for their support and patience these past years.

I would like to thank the National Science Foundation Graduate Research Fellowship Program (DGE-1321846), training grant from Initiative for Maximizing Student Development (GM055246), MBRS-IMSD Travel Award, Developmental and Cell Biology Department Travel Student Awards, Susan V. Bryant Fellowship Award, Howard A. Schneiderman Fellowship Award, UC Irvine Public Impact Fellowship Award, CCBS Opportunity Award and Associated Graduate Student Travel Award for their financial support.

I would like to thank past and current members of the Plikus laboratory for their criticism, advice and fun days in the laboratory. I wish all of you continued success in your current and future endeavors.

# CURRICULUM VITAE


## Christian Fernando Guerrero-Juarez

Depts. of Developmental and Cell Biology & Center for Complex Biological Systems
Ayala School of Biological Sciences
Sue and Bill Gross Stem Cell Research Center
University of California, Irvine
845 Health Sciences Road, Irvine, CA 92697-4716, USA
Laboratory: +1 (949) 824-1260 | Mobile: +1 (909) 583-1571 | E-mail: cfguerre@uci.edu


**PERSONAL HISTORY**

Full Name: Guerrero-Juarez, Christian Fernando
Place of Birth: Morelia, Michoacán de Ocampo, México | Date of Birth: December 1st, 1989
Citizenship(s): United Mexican States (Native), United States of America (Naturalized)
Language(s): Castilian Spanish (Native), English (Academic – Fluent)

**EDUCATION AND TRAINING**

University of California, Irvine — 09/12-06/18
Doctor of Philosophy (Ph.D.) – Biological Sciences
Master of Science (M.S.) – Biological Sciences

California State University, San Bernardino — 09/07-06/12
Bachelor of Arts (B.A.) – Biochemistry
Bachelor of Science (B.S.) – Biology

**RESEARCH AND TRAINEE FELLOWSHIPS**

| | |
|---|---|
| National Science Foundation Graduate Research Fellowship Program | 06/14-06/17 |
| National Institutes of Health MBRS-IMSD Fellowship Program | 06/13-05/14 |
| National Institutes of Health MARC Training Program | 06/09-06/11 |

**PATENTS**

1. Plikus MV, **Guerrero-Juarez CF**, Cotsarelis G. Methods for scar reduction by converting scar fibroblasts into adipocytes with hair follicle-derived signals. (2017). P-80804-USP. (Submitted to USPTO).

**BIBLIOGRAPHY – PEER-REVIEWED PUBLICATIONS**


1. **Guerrero-Juarez CF**, Plikus MV. (2018). Emerging non-metabolic functions of skin fat. ***Nat Rev Endocrinol***. Review. Jan 12. doi: 10.1038/nrendo.2017.162.

2. Zwick R*, **Guerrero-Juarez CF***, Horsley V, Plikus MV. (2018). Anatomical, physiological and functional diversity of adipose tissue. ***Cell Metabolism***. Jan 9;27(1):68-83. doi: 10.1016/j.cmet.2017.12.002. Review. (*Equal contribution).

3. **Guerrero-Juarez CF**, Astrowski AA, Murad R, *et al*. (2018). Wound regeneration deficit in rats correlates with low morphogenetic potential and distinct transcriptomic profile of epidermis. ***J Invest Dermatol***. pii: S0022-202X. (18)30005-8. doi: 10.1016/j.jid.2017.12.030.
COMMENT IN: 1) Hair regeneration under stress (*J Invest Dernatol*).

4. Hughes MW, Ting-Xin J, Plikus MV, **Guerrero-Juarez CF**, Chein-Hong L, Maxson C, Widelitz R, Chuong CM. (2018). *Msx2* supports epidermal competency during wound-induced hair follicle neogenesis. ***J Invest Dermatol***. pii: S0022-202X(18)31736-6. doi: 10.1016/j.jid.2018.02.043

5. Wang Q*, Oh JW*, Lee H, Dhar A, Peng T, Ramos R, **Guerrero-Juarez CF**, *et al*. (2017). A multi-scale model for hair follicles reveals heterogeneous skin domains driving rapid spatiotemporal hair growth patterning. ***eLife***. 11;6. pii:e22772. (*Equal contribution).
COMMENT IN: 1) Regional differences (*eLife*).

6. **Guerrero-Juarez CF**, Plikus MV. (2017). *Gli*-fully halting the progression of fibrosis. ***Cell Stem Cell***. Review. Jun 1;20(6):735-736.

7. Plikus MV*, **Guerrero-Juarez CF**, Ito M, *et al*. (2017). Regeneration. Regeneration of fat cells from myofibroblasts during wound healing. ***Science***. 17;355(6326):748-752. (*Corresponding author). (*≥52 citations*).
COMMENT IN: 1) Fibroblasts become fat to reduce scarring (*Science*). 2) Repeal and replace: Adipocyte regeneration in wound repair (*Cell Stem Cell*).

8. Wang X*, Hsi TC*, **Guerrero-Juarez CF**, Pham K, Cho K, McCusker CD, Monuki ES, Cho KW, Gay DL, Plikus MV. (2015). Principles and mechanisms of regeneration in the mouse model for wound-induced hair follicle neogenesis. ***Regeneration***. 2(4):169-181. (*Equal contribution).

9. Chen CC, Wang L, Plikus MV, Jiang TX, Murray PJ, Ramos R, **Guerrero-Juarez CF**, *et al*. (2015). Organ-level quorum sensing directs regeneration in hair stem cell populations. ***Cell***. 161(2): 277-90. (*≥60 citations*).
COMMENT IN: 1) A collective path toward regeneration (*Cell*).

10. Zhang LJ, **Guerrero-Juarez CF**, Hata T, Bapat SP, Ramos R, Plikus MV, Gallo RL. (2015). Innate Immunity. Dermal adipocytes protect against invasive *Staphylococcus aureus* skin infection. ***Science***. 347(6217):67-71. (*≥126 citations*).
COMMENT IN: 1) Infection. Double skin protection (*Nat Rev Immunol*). 2) Physiology. Killer fat (*Science*). 3) Staphylococcus aureus infections: adipocytes join the fight (*Pert Dial Int*).

11. Plikus MV, **Guerrero-Juarez CF**, Treffeisen E, Gay DL. (2014). Epigenetic control of skin and hair follicle regeneration after wounding. *Exp Dermatol*. 23(7). Review.

12. **Guerrero-Juarez CF**, Ramos R, Oh JW, Hsi TC, Plikus MV. (2014). Light-emitting hair follicles: studying skin regeneration with *in vivo* imaging. *J Invest Dermatol*. 134(6):1496-98. Commentary.

13. Sanchez A, **Guerrero-Juarez CF**, Ramirez J, Newcomb LL. (2014). Nuclear localized Influenza nucleoprotein N-terminal deletion mutant is deficient in functional vRNP formation. ***Virol J***. 11(155).

14. Oh JW, Hsi TC, **Guerrero-Juarez CF**, Ramos R, Plikus MV. (2013). Organotypic skin culture. ***J Invest Dermatol***. 133(11). Review.

15. Ramos R, **Guerrero-Juarez CF**, Plikus MV. (2013). Hair follicle signaling networks: a dermal papilla-centric approach. *J Invest Dermatol*. 133(10):2306-8. Commentary.

16. Whitaker EL, Filippov V, Fillippova M, **Guerrero-Juarez CF**, Duerksen-Hughes PJ. (2011). Splice variants of *mda-7/IL-24* differentially affect survival and induce apoptosis in U2OS cells. *Cytokine*. 56(2):272-81.

**BIBLIOGRAPHY – NCBI SEQUENCES**

1. **Guerrero-Juarez CF**, Patel P, Pham B, Tavoc K, Shamansky LM. Partial sequence of the glyceraldehyde-3-phosphate dehydrogenase-2 (GAPC-2) gene from *Oxalis triangularis* subspecies *papilionacea*. (2012). (Accession No. JX280919.1).

**ACCOLADES AND HONORABLE MENTIONS**

| | |
|---|---|
| Department of Developmental and Cell Biology Travel Student Award ($300.00) | 05/18 |
| University of California Chancellor's *ADVANCE* Postdoctoral Fellowship Program | 04/18 |
| LEAD Francisco J. Ayala School of Biological Sciences Award | 04/18 |
| UC Irvine Latino Excellence and Achievement Award (LEAD) Nominee | 04/18 |
| Deutsches Krebsforschungszentrum Postdoctoral Fellowship Program | Offered/Declined |
| Associated Graduate Student Travel Award ($600.00) | 07/17 |
| Department of Developmental and Cell Biology Travel Student Award ($300.00) | 07/17 |
| Center for Complex Biological Systems Opportunity Award ($10,000.00) | 06/17 |
| Howard A. Schneiderman Graduate Fellowship Award ($5,000.00) | 06/17 |
| Ford Foundation Diversity Dissertation Fellowship Honorable Mention | 03/17 |
| Department of Developmental and Cell Biology Travel Student Award ($300.00) | 04/17 |
| Department of Developmental and Cell Biology Travel Student Award ($300.00) | 07/16 |
| UC Irvine Public Impact Fellowship Honorable Mention ($1,000.00) | 11/15 |
| Susan V. Bryant Graduate Fellowship Award ($1,000.00) | 06/15 |
| Fine Science Tools Graduate Travel Award in Developmental Biology ($500.00) | 06/15 |
| Department of Developmental and Cell Biology Travel Student Award ($300.00) | 06/15 |
| NIH MBRS-IMSD Travel Award ($500.00) | 04/13 |

*University of California, Irvine*

| | |
|---|---|
| Department of Biology Outstanding Undergraduate Student | 06/12 |
| University Honors | 06/12 |
| Department of Biology Honors | 06/12 |
| $22^{nd}$ Annual CSU Student Research Conference – $1^{st}$ Place Award | 03/12 |
| LSAMP Scholarship ($2,000.00) | 11-12 |
| Associated Students Incorporated Scholarship ($1,000.00) | 11-12 |
| Associated Students Incorporated Scholarship ($1,000.00) | 10-11 |

Ronald E. McNair Scholars Program 06/11-08/11
MARC U-STAR Scholars Program 09/09-06/11
China-Taiwan Short-term Study Abroad Scholarship ($500.00) 09/09 and 09/10
Phi Beta Delta Thailand Short-term Study Abroad Scholarship ($250.00) 03/10
Leon V. and Marion G. Pittman Science Scholarship ($527.00) 09-10
Association of Latino Faculty, Staff and Students Scholarship ($1,000.00) 09-10
Associated Students Incorporated Scholarship ($1,000.00) 08-09
Phi Beta Delta Korea Short-term Study Abroad Scholarship ($250.00) 03/09
Louis Stokes Alliance for Minority Participation Program Fellow 07-12
*California State University, San Bernardino*

## PRESENTATIONS, SEMINARS AND POSTER SESSIONS

1. **Guerrero-Juarez CF**, Astrowski AA, Murad R, Plikus MV. (2018). International Investigative Dermatology. *Orlando, FL, USA*. (Poster presentation).
2. **Guerrero-Juarez CF**. (2018). Math CEO Outreach Program. *UC Irvine, Irvine, CA, USA*. (Oral presentation).
3. Cho K, Mortazavi AS, **Guerrero-Juarez CF**. (2018). Developmental and Cell Biology Annual Retreat. *Costa Mesa, CA, USA*. (Oral presentation – co-presenter with Cho K, and Mortazavi AS).
4. **Guerrero-Juarez CF**. (2018). UC Irvine Skin Club. *Irvine, CA, USA*. (Oral presentation).
5. **Guerrero-Juarez CF**, MacLean A, Wang Y. (2018). Center for Complex Biological Systems Retreat. *Los Angeles, CA, USA*. (Oral presentation).
6. **Guerrero-Juarez CF**. (2017). DKFZ Postdoctoral Fellowship Symposium. *Deutsches Krebsforschungszentrum, Heidelberg, Germany*. (Oral presentation).
7. **Guerrero-Juarez CF**, Cotsarelis G, Plikus MV. (2017). IX Latin American Society for Developmental Biology Meeting. *Medellin, Colombia*. (Oral presentation).
8. **Guerrero-Juarez CF**, Cotsarelis G, Plikus MV. (2017). NSF-GRFP Research Symposium. *UC Irvine, Irvine, CA, USA*. (Poster presentation).
9. **Guerrero-Juarez CF**, Ito M, Zheng Y, Cotsarelis G, Plikus MV. (2017). Society for Investigative Dermatology 76th Annual Meeting. *Portland, Oregon, USA*. (Oral presentation).
10. **Guerrero-Juarez CF**, Plikus MV, Cotsarelis G. (2017). West Coast Developmental Meeting. *Tenaya Lodge, Yosemite National Park, CA, USA*. (Poster presentation).
11. **Guerrero-Juarez CF**, Plikus MV, Cotsarelis G. (2017). Dermatology Skin Symposium. *UC Irvine, Irvine, CA, USA*. (Poster presentation).
12. **Guerrero-Juarez CF**, Plikus MV, Cotsarelis G. (2016). Gordon Research Conferences – Tissue niches and resident stem cells in adult epithelia. The Hong Kong University of Science and Technology. *Hong Kong, People's Republic of China.* (Poster presentation).
13. **Guerrero-Juarez CF**. (2015). 6th Annual Graduate Summer Research Program. *Tsukuba University, Tsukuba, Japan*. (Oral presentation).
14. **Guerrero-Juarez CF**, Plikus MV, Gay DL. (2015). International Society for Stem Cell Research. *Stockholm, Sweden*. (Oral presentation – Gay DL *in lieu* of Guerrero-Juarez CF). Attended.
15. **Guerrero-Juarez CF**. (2015). 5th Annual Summit in Aesthetic Medicine. *Dana Point, CA, USA*. (Oral presentation – Guerrero-Juarez CF *in lieu* of Plikus MV).
16. **Guerrero-Juarez CF**. (2014). MARC/RISE Program Seminar Series. *CSU San Bernardino, San Bernardino, CA, USA*. (Oral presentation).

17. Sanchez A, **Guerrero-Juarez CF**, Newcomb LL. (2012). 111th American Society for Microbiology. *New Orleans, LA, USA*. (Poster presentation – co-presenter with Sanchez A.).

## SCHOLARLY ACTIVITIES

Dept. of Developmental and Cell Biology Graduate Representative 2017 Acad. Year
Dept. of Developmental and Cell Biology Speaker Committee Member 2017 Acad. Year
*University of California, Irvine*

MBRS-IMSD Programs 2012-2018
Drs. Luis Mota-Bravo and Marlene de la Cruz
2017 Minority Science Programs Journal Club Instructor – Incoming Doctoral/MARC Students
2017 Minority Science Programs Research Symposium Judge
2016 Minority Science Programs Journal Club Instructor – Bridges to Baccalaureate Students
2016 Minority Science Programs Research Symposium Judge
*University of California, Irvine*

6th Annual Graduate Summer Research Program 07/15
Dr. Akira Shibuya Laboratory
*University of Tsukuba, Tsukuba, Ibaraki, Japan*

Cancer Research Institute 2015 Summer Youth Science Fellowship Program 2015
Instructor/Mentor – Dr. Maksim V. Plikus Laboratory
*University of California, Irvine*

Summer Undergraduate Research Program 2014-2017
Undergraduate Research Opportunity Program 2015-2017
Instructor/Mentor – Dr. Maksim V. Plikus Laboratory
*University of California, Irvine*

Short-term Study Abroad Programs 09-12
Doing Business with the Middle East – Abu Dhabi University
Educational and Cultural Trip to Korea – Gwangju National University of Education
Doing Business with Asia: China and Taiwan – University of Beijing / Natl. Chung Cheng Univ.
Educational and Cultural Trip to Thailand – Chulalongkorn University
Academic and Cultural Trip to Korea – University of Incheon
*California State University, San Bernardino*

## TEACHING ASSISTANSHIP EXPERIENCE

Biology and Chemistry of Food and Cooking Winter 2018
Biology of Integrative Medicine Summer 2016
Biology of Oriental Medicine Summer 2016
Advances in Regenerative Medicine Spring 2014, 2015, 2016, 2017, 2018
Human and Eukaryotic Genetics Fall 2015, 2016
*University of California, Irvine*

## CORE COMPETENCIES

**Transferable:** Experimental design and conceptualization, Data analysis, Scientific writing (grants, technical reports, protocols, SOPs), Laboratory and project management, Public speaking, Teaching, Training, Laboratory safety.

**Technical:** Mouse genetics, Models of skin disease, Models of cutaneous wound healing and regeneration, Non-model organisms, Non-invasive mouse surgical procedures, Bacterial infection assays, Xenograft skin transplants, Tissue and cell culture, Basic bioinformatics, Standard molecular biology techniques, Viral vectors, Transfection, Transduction, Fluorescence and bright field microscopy, Bulk RNA-sequencing (SMART-seq2), Bulk ChIP-sequencing, Single cell RNA-sequencing (full length and 3'-end; Fluidigm/10X Genomics), *de novo* transcriptome assembly (basic), ATAC-sequencing, PCR/qPCR, FACS, Histology/Immunocytochemistry/Immunofluorescence staining, Chromatin/DNA/RNA/Protein purification, Western Blot, single cell Western Blot, UCSC Genome Browser, Broad Institute GSEA, Animal handling and husbandry (rodents).

**Computer:** Mac and Windows operating systems, Microsoft Office Suite, FlowJo (basic), ImageJ, GraphPad Prism, Adobe Photoshop, Adobe Illustrator, RStudio.

# ABSTRACT OF THE DISSERTATION


Delineating mechanisms of cutaneous wound healing and regeneration in adults

By

Christian Fernando Guerrero-Juarez

Doctor of Philosophy in Biological Sciences

University of California, Irvine, 2018

Assistant Professor Maksim V. Plikus, Chair

Regeneration of hair follicles (HFs) and dermal adipocytes (DAs) occurs in mouse skin wounds upon large excisional wounding. Although HF regeneration is observed in African spiny mice of the genus *Acomys* and northern elephant seals after apex predator-inflicted wounding, laboratory rats do not display such regenerative phenotype. Such regeneration defect was observed in large excisional wound healing models in several rat strains, which undergo otherwise normal wound re-epithelialization. Inter-species transcriptome analyses between laboratory mouse and rat wound tissues attributed such lack of HF regeneration to differences in expression of inflammation markers, epigenetic remodelers and pleiotropic signaling molecules, including *Satb1*, *Setd1b*, *Setdb1*, and *Whsc1l1*. In mice, the origin of *de novo* HF regeneration has been partially elucidated, whereas the origin of DAs, a complex tissue that proceeds HF regeneration, remained elusive. Functional lineage tracing revealed the origin of DAs to be myofibroblastic. Bulk RNA-sequencing of genetically-labeled, FACS-purified myofibroblasts across a wound healing time course identified *Zfp423* to be markedly up-regulated at a time-point coincident with initiation of DA regeneration. Pharmacological and genetic ablation/down-modulation of BMP signaling resulted in a significant DA regeneration defect. Because the origin of myofibroblasts appears to be tissue- and injury context-specific, the origin of

myofibroblasts that contribute to DA regeneration in skin wounds was interrogated. Droplet-enabled single cell transcriptome analyses on unsorted, viable cells from wound dermal tissues collected prior the onset of HF regeneration was performed. Dimensionality reduction analyses revealed a large degree of cellular heterogeneity in the dermal compartment of early stage wounds. Furthermore, sub-clustering of wound fibroblasts further revealed a large degree of fibroblast heterogeneity. Pseudotime analyses revealed a putative fibroblast-myofibroblast differentiation trajectory and identified genes, including transcription factors, that may be important in myofibroblast differentiation in skin wounds *in vivo*. A subset of myofibroblasts expressed hematopoetic markers, most notably *Lyz2*, suggesting a common monocytic-origin. Full-length single cell RNA-sequencing and immunoblotting analyses of genetically labeled myofibroblasts confirmed these *in silico* observations. Bone marrow transplantation and functional lineage tracing using pan-hematopoetic *Cre* drivers demonstrated labeling of DA in regenerated skin wounds, suggesting that a population of hematopoetic-derived myofibroblasts contributes to regeneration of mouse skin wounds.

# CHAPTER 1

## Introduction

Adapted and/or modified, in part, from:

Guerrero-Juarez CF, and Plikus MV. Emerging non-metabolic functions of skin fat. *Nat Rev Endocrinol*. (2018). Mar;14(3):163-173. PMID: 29327704.

Reprinted with permission from Nature Publishing Group.

# INTRODUCTION

## 1.1 THE SKIN

### THE ANATOMY OF SKIN

The skin is considered to be the largest organ in an organism's body. It covers approximately 25 $m^2$ of surface area in humans (Gallo, 2017) and it consists of multiple, organized layers that are further compartmentalized, housing distinct cell types, appendages and a diverse multitude of microorganisms that together form the so-called skin microbiome (Lange-Asschenfeldt et al., 2011). The first layer of the skin, the epidermis, forms the outermost layer and provides skin with its barrier function. It protects organisms against mechanical and physical insults, UV-exposure, and foreign pathogens and opportunistic microorganisms. The epidermis sub-divides into five distinct layers, each with its own characteristics and gene expression profile. The first layer is known as the *stratum basale*. This basal layer houses the interfollicular epidermal stem cells (Blanpain and Fuchs, 2009, Solanas and Benitah, 2013). Subsequently, these cells differentiate into supra-basal layers which ultimately form the *Stratum corneum*, a layer containing dead cells that eventually shed off the skin surface. The epidermis lies on top of the dermis, a heterogeneous structure composed mainly of fibroblasts, collagens and elastin fibers. The dermis sub-divides into upper papillary and lower reticular dermis (Harper and Grove, 1979, Woodley, 2017). Underlying the reticular dermis is the dermal white adipose tissue (dWAT) (Driskell et al., 2014, Festa et al., 2011, Schmidt and Horsley, 2012, Wojciechowicz et al., 2013). In mice, the dWAT is separated from the subcutaneous WAT (sWAT) by a later of striated muscle called the *panniculus carnosus*. In humans, however, this layer of muscle is rudimentary. In addition to HFs, skin contains sweat glands consisting of a straight duct and secretory coil nested in the dermis (Lobitz and Dobson, 1961, Lu et al., 2012) and sometimes, abuts dWAT (Kimani, 1983). While in humans sweat glands are distributed widely throughout the skin, in many other species, including mice, they are restricted to the paws (Lu et al., 2016, Montagna, 1984). (Figure 1.1).

## THE HAIR FOLLICLE AND ITS REGENERATIVE BEHAVIOR

Traversing through the skin are its ectodermal appendages – hair follicles (HFs), and sweat glands. HFs are stem cell-rich mini-organs that regenerate new hairs repetitively in a process known as the hair growth cycle. This regenerative cycle consists of three phases: active hair growth (anagen), regression (catagen), and rest (telogen) (Muller-Rover et al., 2001, Oh et al., 2016). HFs attain its largest size during anagen, when its proximal end, the hair bulb, extends deep into dWAT. Hair bulb harbors actively dividing epithelial matrix progenitors and specialized dermal papilla (DP) fibroblasts, that serve as the key signaling center of the HF (Morgan, 2014). Hair growth is sustained by proliferation and differentiation activities taking place in the hair matrix. Distally, above the dWAT, the HF houses its stem cells (Brownell et al., 2011, Jensen et al., 2009, Morris et al., 2004, Snippert et al., 2010), including the so-called bulge stem cells – the principal hair-fated, long-lasting progenitor cells (Cotsarelis et al., 1990, Morris et al., 2004). Above the bulge, HF contains sebaceous glands. Collectively, this structure is known as pilosebaceous unit. Connecting the bulge with the bulb is the outer root sheath (ORS). Hair growth termination during catagen is mediated by events of terminal differentiation, apoptosis, and phagocytosis (Foitzik et al., 2000, Lindner et al., 1997, Mesa et al., 2015). DP fibroblasts and some epithelial ORS cells survive catagen involution, move upwards toward the bulge, and constitute the lower portion of the resting telogen HF. Surviving ORS cells form the secondary hair germ (sHG) compartment. At the onset of new anagen, sHG progenitors respond to activating signals from DP, divide, and fuel rapid HF growth (Hsu et al., 2011, Panteleyev et al., 2001). Bulge progenitors divide with a delay and contribute progenies toward mature anagen HF (Hsu et al., 2011, Morris et al., 2004). This process occurs in cycles, allowing each HF to grow multiple rounds of hair shafts over the lifetime of the mouse. Furthermore, in many species thousands of neighboring HFs regenerate collectively as dynamic hair growth waves (Plikus et al., 2011, Plikus and Chuong, 2008, 2014, Plikus et al., 2008, Plikus et al., 2009, Wang Q. et al., 2017). Thus, their interactions with dWAT occur also at the collective level.

## DERMAL ADIPOCYTES

White adipose tissue (WAT) is a complex tissue with roles in energy balance and nutrient homeostasis (Rosen and Spiegelman, 2014). Anatomically, WAT is compartmentalized in various areas called depots that are conveniently allocated throughout the body. To-date, the most widely studied WAT depots include visceral (vWAT) – which extends within the body cavity and includes the epicardial, mesenteric, retroperitoneal, perirenal, omental and gonadal adipose tissues; and subcutaneous (sWAT) – which includes anterior, flank and the subcutaneous tissue below the skin. Each depot is characteristically different from each other in terms of the origin of their precursors, overall functionality, and their profound effects on pathophysiology. For example, vWAT is regarded as unfavorable due to its positive correlation with metabolic disease, whereas sWAT is considered beneficial because of its protective nature. Emerging evidence is now providing clues about the importance of other adipose tissue depots and their prominent roles in homeostasis and disease (Rivera-Gonzalez et al., 2014). Of these, dermal adipose tissue has recently gained broad interest as it has emerged as an important tissue with prominent roles in skin physiology, innate immunity and wound healing (Guerrero-Juarez and Plikus, 2018, Zwick et al., 2018).

Within the skin dermis lies a group of specialized unilocular, lipid-laden cells known as dermal/intradermal adipocytes (Driskell et al., 2014, Guerrero-Juarez and Plikus, 2018). Defined collectively as dermal white adipose tissue (dWAT), this highly dynamic, complex and heterogeneous tissue is geometrically arranged as a three-dimensional structure that is continuous throughout the dermis and is clearly demarcated from subcutaneous white adipose tissue (sWAT), which is physiologically and morphologically different, by a layer of striated muscle called the *panniculus carnosus*. In other species, such as rabbits, dWAT is non-continuous and, instead, forms complex clustered units with compound hair follicles (Guerrero-Juarez and Plikus, 2018). Human skin also harbors dWAT and is structured differently than that of mice. Indeed, the close spatial relationship between HFs and dWAT has been previously noted and their close association traced back to embryonic development. Spatio-temporal association studies between HFs and dWAT have been mainly conducted in pigs, and rats (Anderson et al., 1972, Hausman et al., 1981, Hausman and Kauffman, 1986, Hausman and Martin, 1981, 1982). Recently, however, owing to its wide usage in biomedical research, the association between dWAT and HFs was established in mice (Festa et al., 2011, Wojciechowicz et al., 2013, Zhang et al., 2016).

HAIR FOLLICLE AND DERMAL ADIPOCYTE SYMBIOSIS?

Although a close association between HFs and dermal adipocytes had been noted in the classic literature, recent advances in imaging, immunohistochemical and genetic approaches have shed light onto their closely related regulation and signaling crosstalk (Borodach and Montagna, 1956, Chase et al., 1953, Gipbs, 1941, Moffat, 1968). HF formation precedes dermal adipogenesis with the emergence of OilRedO-positive adipocytes at the base of growing HFs (Wojciechowicz et al., 2008). Rapid accumulation of lipid and subsequent enlargement of the firstly established multilocular intradermal adipocytes (Wojciechowicz et al., 2013) follows. The association between HFs and dWAT extends beyond embryonic and pre-natal days and is further exemplified during the HF cycle (Plikus et al., 2008, Zhang et al., 2016). HFs undergo cyclic regeneration throughout the life time of an organism and the mechanisms underlining this regenerative behavior have been widely studied in individual HF units (Plikus et al., 2008) and collectively as propagating HF waves (Plikus et al., 2011, Plikus and Chuong, 2008). The HF cycle can be divided into three functional states: anagen (growth), catagen (regression), and telogen (rest) (Muller-Rover et al., 2001). Indeed, novel genetic approaches, coupled with imaging, histochemical analyses and transplantation studies have confirmed previous observations that dWAT undergoes major changes in parallel with HF cycling, which include pre-adipocyte proliferation and hypertrophy of existing adipocytes, leading to approximately 20-40% contribution of new adipocytes during each hair cycle (Festa et al., 2011, Rivera-Gonzalez et al., 2016, Zhang et al., 2016). This parallel behavior appears to be a unique feature of dWAT as similar, intricate adipose tissue rearrangements have not been thoroughly described in other depots as an immediate consequence of changes in neighboring tissues. For example, bone marrow adipose tissue (BMAT) is encased and spatially constrained within a rigid bone structure – restricting a possible dynamicity (Zwick et al., 2018). Nonetheless, similar co-opted behaviors also occur during pre- and post-natal mammary gland development, although further investigation into the possible communication between mammary gland epithelium and adipose tissue is warranted. Hence, this sophisticated level of organized behavior between dWAT and HFs suggests a mutually inclusive, physiologically relevant relationship with possible functional roles in homeostasis, injury, and disease.

Can HFs influence dWAT to undergo rearrangement during cycling, and viceversa? Recent studies have shed light to the macro-environmental regulation of HF cycling (Plikus and Chuong, 2014); that is, cues emanating from surrounding tissues that directly or indirectly influence the hair cycle. Elevated expression of Bone Morphogenetic Protein (BMP) ligands – BMP2 and BMP4 in the dermis during the telogen stage (Plikus et al., 2008) suggested that BMPs expressed by mature intradermal adipocytes can modulate HF cycling by inhibitory expression areas, capable of maintaining HFs in a state of refractivity and preventing them from re-entering anagen after the first hair cycle. This level of regulation serves as one of the main regulators of the HF wave formation in mouse skin. A reciprocal, yet opposite effect where HFs direct regeneration of dWAT via canonical BMP signaling is observed during repair of large skin wounds. Large skin wound model differs greatly from the traditional, small excisional wound model. Adult mammals typically heal skin wounds with a scar devoid of HFs and dermal adipocytes. However, we and others identified that HFs can regenerate in the center of large excisional wounds in a phenomenon known as wound induced hair neogenesis (WIHN). Our most recent work uncovered that dermal adipocytes also form *de novo* in healing skin wounds via conversion of non-adipogenic wound bed myofibroblasts. This process is dependent on the ability of wounds to first regenerate HFs via WIHN, however, as hairless parts of skin wounds lack dermal adipocytes and cannot form adipocytes when cultured under conditions that promote adipocyte differentiation. Because HFs precede dermal adipocyte regeneration, it was postulated that hair follicles must therefore instruct myofibroblasts to reprogram into intradermal adipocytes (Plikus et al., 2017). Similarly, this HF-dermal adipocyte communication mechanism is also mediated by BMP signaling (Figure 1.2).

## DERMAL ADIPOCYTES AS A MODEL TO STUDY ADIPOSE LINEAGE DEVELOPMENT

The identification of skin pre-adipocytes, which share core signature genetic markers with sWAT and vWAT (Berry and Rodeheffer, 2013, Rodeheffer et al., 2008), enabled the identification of a putative role in HF cycling. For example, using several lipodistrophic mice models with known phenotypes in adipogenesis, Festa *et al* showed that intradermal pre-adipocytes begin to proliferate during late catagen and reach their apex during mid-anagen (Festa et al., 2011). This proliferative expansion of intradermal pre-adipocytes coincides with activation of HF cycling, which relies on activation of SCs in the HF bulge. A functional role of pre-adipocytes in HF cycling was established by careful analysis of histological sections at distinct timepoints between *WT, Ebf1*$^{-/-}$, which lack pre-adipocytes (Schmidt-Ott, 2014), and *Azip* mice (Kim et al., 2000). Additionally, by performing transplantation of WT pre-adipocyte cells into *Ebf1*$^{-/-}$ mice, and whole telogen skin allografts into the same recipient mice, it was determined that pre-adipocytes can initiate precocious HF SC activation. HF SC activation by pre-adipocytes was shown to be influenced in part by PDGF signaling (Rivera-Gonzalez et al., 2016). *Pdgfa* is expressed in pre-adipocytes while its receptor *Pdgfr* expression varies and is dependent on hair cycle stage. For instance, in anagen and telogen, it is expressed mainly in HF DP and bulge, while during anagen induction (AnaIII) it is found in the DP and matrix cells. Hence, it can be postulated that intradermal pre-adipocytes influence activity of HF SCs directly or indirectly via activation of PDGF signaling in DP or matrix cells, respectively.

Recently, a new study identified the precise molecular mechanism by which HF growth and expansion of the dWAT layer are coupled. The changes in the dWAT layer are directly attributed to SHH signaling by Transit-Amplifying Cells (matrix cells) in the hair follicle bulb (Zhang et al., 2016). This was discerned by cell-specific manipulations using distinct genetic tools. Specifically, the targeting of mature adipocytes with *Adipoq-CreER*$^{T2}$ for specific deletion of SHH ligand *Shh* and receptor *Smo*, in conjuction with their deletion in matrix cells by means of *K15-CrePR1* (a doxycycline-inducicle *Cre* line (Morris et al., 2004)) enabled the precise spatio-temporal regulation of an adipogenesis program in skin that is closely regulated by these cells. This level of regulation is intriguing, however, because it shows that matrix cells orchestrate not only regeneration of the HF, but also of the dWAT layer. Using a lineage tracing approach, it was observed that the newly infiltrated dermal adipocytes begin to influence the thickness of the skin during anagen III, a sub-level of anagen where fueling of matrix cells ensues. This level of lineage tracing was enabled by the ability to interrogate spatio-temporal regulation by means of inducible *Cre* activity. Similarly, in an experiment where anagen was induced via plucking of club hairs, similar results were observed in which dermal adipocytes begin to appear around a time when matrix cells form – further corroborating that dWAT expansion begins in anagen III and is coincidental with appearance of matrix cells in the regenerating hair follicle. Because Shh is a known factor solely secreted by matrix cells during anagen, it was postulated that it might play a role in directing adipocyte formation. This was interrogated using available *Cre* lines. For instance, when *Shh* is ablated specifically in matrix cells, dermal adipocyte formation is abrogated. However, this was not the case when *Smo*, a receptor of SHH signaling, was deleted in the same cells and mature adipocytes, as normal adipogenesis was observed, suggesting that activation of SHH signaling in mature cells and in matrix cells is not required for adipogenesis. These results suggest that the level of regulation lies in the ability of matrix cells to target and influence the behavior of adipocyte progenitors in skin. Indeed, when *Smo* is deleted in *Pdgfr-alpha*, which gives rise to the majority of skin dermal adipocytes, a defect in dermal adipogenesis was observed, exemplified by a thinner layer of adipocytes, despite normal hair growth. SHH is presumably required to 1) autonomously induce pre-adipocyte proliferation by regulating proliferation genes and subsequently 2) promote their differentiation into lipid-filled adipocytes by expression of *Ppar-gamma*. Indeed, when Shh is overexpressed in the vicinity of skin epidermis, skin dermis is thickened and is accompanied by an increase in mature adipocytes. The positive role in adipogenesis of SHH signaling in skin is intriguing, given that in other tissues it has been shown to have opposite roles.

## GENETIC TOOLS TO STUDY DERMAL ADIPOCYTE DEVELOPMENT

In skin, HFs and dWAT or its progenitors can act as reciprocal dominant signaling sources, depending on the signaling context. Other adipocyte depots in the body do not have such degree of separation between the signaling source and the target, making *in vivo* studies regulating the mechanisms of adipose lineage development challenging or unfeasible. To this end, the development of WAT-specific *Cre* lines has revolutionized the study of WAT development and regeneration *in vivo*. To-date, a multitude of *Cre* lines targeting WAT exist, but only a handful have proven effective for specific-labeling of pre- and mature adipocytes (Jeffery et al., 2014). Additionally, another consideration is the use of specific reporters. In this case, cytosolic reporters, such as *R26R-LacZ* and others, do not allow for effective quantification of individual adipose phenotypes. To mitigate these concerns, fluorescent membrane-bound reporters should be implemented instead. For example, the reporter of choice in WAT lineage tracing studies is the mTmG reporter strain (Muzumdar et al., 2007) which, upon activation of a tissue-specific *Cre*/*CreER$^{T2}$*, a permanent switch from the *tdTomato* fluorescent tag to *GFP* is achieved. Two constitutive *Cre* lines were generated under the Fatty acid binding protein 4 (Fabp4) promoter to specifically label mature WAT. Careful lineage tracing studies, however, have shown non-specific labeling of brown adipose tissue (BAT) and endothelial cells using these lines, coupled with a rather low recombination efficiency (Jeffery et al., 2014). Two other mouse lines, *Pdgfr-alpha-Cre* and *Pdgfr-alpha-CreER$^{T2}$*, are widely used to label adipocyte progenitors in skin and precursors within WAT SVF. Similarly, *Pdgfr-alpha-CreER$^{T2}$* mice efficiently label dWAT and fibroblast-like cells in skin, suggesting some dWAT cells derive from *Pdgfr-alpha$^{+}$* cells. Mature adipocytes can also be specifically labeled using constitutive and conditional *Cre* lines under the promoter of Adiponectin (Adipoq). These mouse lines do not mark pre-adipocytes in WAT SVF, suggesting high specificity to mature adipocytes. Using these lines, nearly all mature adipocytes within WAT, including idWAT, are labeled. Indeed, this is a *Cre* line employed in experiments described in Chapter 4.

One of the issues with studying vWAT and sWAT depots is the inability to conduct highly precise developmental studies. Skin, however, offers a solution to study the orderly progression of hair follicle and dermal adipocyte development in normal skin and their regeneration in skin wounds. To better understand the dynamics of adipocytes in different WAT depots, a novel doxycycline-inducible, mature adipocyte-specific *Cre* system was recently developed (Wang and Scherer, 2014, Wang et al., 2013). *Cre* expression in this *AdipoChaser* mouse is dependent on doxycycline treatment and is capable of labeling nearly all pre-existing mature adipocytes with an unpresented level of temporal resolution. Because the system is reversible, owing to the doxycycline-responsive *rtTA*-mediated expression of *Cre*, the rate of newly differentiated adipocytes can be assessed upon doxycycline removal. *AdipoChaser* is therefore a useful system for evaluating the rate of adipocyte formation during development and postnatally in response different challenges, including HFD, cold, and homeostatic turn-over rates. Because a large number of hair follicle-specific genetic tools already exist, the crossing of these tools with mice targeting pre-adipocytes and mature adipocytes in dWAT can serve as an attractive model system for studying mechanisms of adipose lineage development in response to hair follicle-derived signals.

NON-METABOLIC FUNCTIONS OF SKIN DERMAL ADIPOCYTES

Residing at the interface with the outside environment and in close association with hair follicles, dWAT evolved to play novel, non-traditional functions not readily observed by other depots. One of the main functions of dWAT mature adipocytes and its progenitors are to regulate HF cycling via BMP (Plikus et al., 2008) and PDGF signals (Rivera-Gonzalez et al., 2016), respectively. By doing so, they regulate activation of hair follicle stem cells and modulate the pace of hair growth during the lifetime of a mouse. Recently, the identification of how skin adipocyte stem cell self-renewal is regulated added yet another layer of complexity to the interplay between HFs and dWAT (REF). During aging, skin adipocyte stem cells, characterized by the signature marker $Lin^{-};Cd29^{+};Cd34^{+};Sca1^{+};Cd24^{+}$, become depleted with age or repeated depilation. The adipocyte stem cell pool appears to be maintained by *Pdgfa*, which, acting via PI3K/AKT signaling, regulates expression of proliferation and self-renewal genes. Maintenance of the skin adipocyte stem cell pool has implications in hair follicle cycling. For example, upon loss of the Cd24 mark, skin adipocyte stem cells give rise to a proliferative population of pre-adipocytes, which act to regulate both, directly and indirectly, hair follicle growth.

After skin injury, adipose progenitors activate and transiently populate early wounds, where they signal to facilitate efficient recruitment of fibroblasts, the key cellular building blocks of the scar tissue (Schmidt and Horsley, 2013) (Figure 1.3.B). By utilizing the lipodistrophic mouse model *Azip*, it was shown that they are defective in proper wound healing in a small skin wound injury model. To thie end, pre-adipocytes were shown to populate the wound bed by post-wounding day 5-7, directly after bypassing the preceding phases of inflammation and proliferation, characteristic of normal wound healing. Defective wound healing was associated with a reduced number of fibroblasts and myofibroblasts – in charge in contraction and remodeling of the wound bed. Indeed, these phenotypes were not due to improper macrophage recruitment and wound closure deficits associated with a diabetic phenotype. Hence, the results suggest a lack of mature adipocyte regeneration in the wounds of *Azip* mice as responsible for the wound healing defects. These results were further corroborated by pharmacological treatment with two distinct *Ppar-gamma* inhibitors during early and late stages of healing. These results suggest adipocytes are important in wound healing. In sharp contrast, dermal adipocytes regenerate in large excisional wounds via reprogramming of myofibroblasts (Figure 1.3.C).

Another role of dermal adipocytes is their ability to fight infection (Zhang et al., 2015). Upon infection of the skin with the opportunistic bacteria *S. aureus*, the dWAT layer expands in thickness in the next few days in an event similar to those observed as a result of hair follicle cycling. This expansion occurs via hypertrophy of pre-existing adipocytes and recruitment of pre-adipocytes via hyperplasia shown by an increase in proliferation in Pref1$^{+}$ and Zfp423$^{+}$ pre-adipocytes (Figure 1.3.A). Lipodistrophic mice lacking Zfp423 and WT mice treated with *Pparg* inhibitors showed increased infection area accompanied by septicemia. The ability of dWAT to kill *S. aureus* is dependent on expression of the antimicrobial peptide *Cathelicidin*. Indeed, *Camp* expression increase during pre-adipocyte differentiation relative to *alpha*- and *beta*- defensins and relative *Camp* mRNA expression increased nearly 20-fold when pre-adipocytes were differentiated in the presence of *S. aureus* conditioned media or UV-killed *S. aureus*. Similarly, *Zfp423* KO mice were more susceptible to bacterial infection and did not express *Camp* upon infection compared to controls. Hence, dWAT is an important component of the skin innate immune system.

## 1.2 SKIN WOUND HEALING

### SKIN WOUND HEALING AND REGENERATION

Wound healing of skin is a complex process that takes approximately 2-52 weeks to complete. It is divided into 3 distinct but overlapping phases –inflammation, tissue formation, and remodeling (Eming et al., 2014, Gurtner et al., 2008). Several mechanisms orchestrate the first stage of the wound healing response to prevent blood loss, remove dying cells, and prevent infection. First, the coagulation cascade plugs the wound to prevent blood loss (Versteeg et al., 2013). Immune cells, namely neutrophils, are recruited to degrade infiltrating bacteria (Wilgus et al., 2013). A few days later, macrophages appear in the wound to further modulate the wound healing response (Koh and DiPietro, 2011). The second stage of wound healing involves tissue formation, and it is characterized by proliferation and migration of cells into the wound bed. During this process, keratinocytes re-epithelialize the wound, angiogenesis and capillary sprouting occurs, and fibroblasts migrate to begin the formation of the granulation tissue. The differentiation of fibroblasts to alpha smooth muscle actin-expressing myofibroblasts also takes place during this stage. Myofibroblasts are in charge of wound contraction and collagen deposition (Gonzalez et al., 2016). During the remodeling stage, it is believed that cells present during the former two stages, including myofibroblasts, undergo cell death, or leave the wound (Gurtner et al., 2008). However, while this could hold, recent evidence suggests that myofibroblasts can attain a different fate and undergo reprogramming into dermal adipocytes during wound healing (Plikus et al., 2017). In the next few weeks, metalloproteins further remodel the wound bed in efforts to bringing the skin back to its original integrity.

The process of wound healing often culminates with the formation of a scar, a fibrous tissue devoid of appendages and dermal adipose tissue. These observations have been made in small wounds, which is the prevalent model of wound healing studies (Dunn et al., 2013). Recently, a new model of wound healing was established. In this model, large full-thickness squared (>1.0cm$^2$ or 2.25cm$^2$) wounds are inflicted in the lower dorsum of adult mice. These full-thickness wounds typically regenerate new hair follicles in their center. Interestingly, regeneration of hair follicles is age and strain dependent, but it doesn't gender and hair cycle (Nelson A. M. et al., 2015). This phenomenon was termed wound-induced hair neogenesis (WIHN) (Ito et al., 2007, Wang et al., 2015). Some of the cellular and molecular mechanisms for WIHN have elucidated (Ito et al., 2007, Snippert et al., 2010, Wang X. et al., 2017). Canonical WNT signaling (Gay et al., 2013, Ito et al., 2007, Myung et al., 2013) is important for WIHN, including dermal and epidermal ligands. A profound example is dermal WNT signaling. γδ T-cells migrate into the wound bed early during wound healing and secrete Fgf9, which acts on wound bed fibroblasts and amplifies a Wnt2a signal via a feed-forward positive loop (Gay et al., 2013). In the epidermal compartment, another signaling pathway also plays a prominent role in the establishment of WIHN. Toll-like receptor 3 (Tlr3) is activated by the double-stranded RNA released from damaged keratinocytes at the wound edge at the onset of wound healing. This signal promotes WIHN downstream of Il6/Stat3 signaling, which leads to up-regulation of Wnt/Shh and Edar signaling – leading to onset of HF regeneration (Nelson A. M. et al., 2015). WIHN is also modulated by macrophages via Tnfα signaling (Wang X. et al., 2017), and requires transient expression of the transcriptional regulator *Msx2* (Hughes et al., 2018). Further research into WIHN has also identified negative regulators of this regeneration phenomenon. For example, prostaglandin (Pdg2) signaling (Nelson A. M. et al., 2013), the transcriptional regulator Cxxc5 (Lee et al., 2017) and Msi2 RNA-binding protein (Ma et al., 2017) all have negative roles in WIHN.

WIHN has been definitely documented to take place in rabbits (Billingham and Russell, 1956, Breedis, 1954, Stenbäck et al., 1967). In sheep and humans, however, definitive assessment of WIHN efficiency remains fully inconclusive (Brook et al., 1960, Kligman, 1959). Recently, we reported the deficit of WIHN in laboratory rats (*Rattus norvegicus)* and how this process compares to that in mice using inter-species transcriptome analyses (Guerrero-Juarez et al., 2018). This study was conducted because of the contradicting reports in the classic literature on the outcomes of rat skin repair and regeneration following cryo-injury. For example, Taylor (1949) and Mikhail (1963) suggest that the skin of rats repairs with HF neogenesis after cryo injury. In sharp contrast, Stenbäck et al. (1967) failed to replicate such findings. We aimed to interrogate the potential of rat skin regeneration by inflicting large skin wounds in rats and asking whether they are capable of WIHN. Our results show that rats distinctly fail to regenerate new HFs in large full-thickness excisional wounds. ***These results are further explored and discussed in Chapter 2***.

## THE MYOFIBROBLAST

During wound healing, interstitial and peripherally-derived fibroblasts differentiate into contractile myofibroblasts, an alpha-smooth muscle actin-expressing cell with important roles in wound contraction and extracellular matrix (ECM) deposition. Myofibroblasts were first described in 1971 in the granulation tissue of healing wounds (Gabbiani et al., 1971). Myofibroblasts have a "hybrid" morphology – they appear to have fibroblastic spindle-like and smooth muscle cell-like features, contain bundles of actin microfilaments with associated contractile proteins, higher levels of ED-A splice variants, and are juxtaposed to one another via gap junctions (Tomasek et al., 2002). The latter suggests that a functional "myofibroblast unit" may be required for optimal force generation during late stages of wound healing.

Myofibroblasts are considered to be a terminally differentiated cell type. The process of fibroblast-to-myofibroblast differentiation begins after an injury has been inflicted, when fibroblasts begin to migrate into the wound bed via chemo-attraction by cytokines produced by inflammatory and other resident cells present in the wound bed (Gurtner et al., 2008, Werner and Grose, 2003). Once in the granulation tissue, tension generated at the wound bed leads to the formation of a proto-myofibroblast, a precursor cell type that forms cytoplasm-localized actin fibers and express and organize ED-A fibronectin splice variants. These characteristics enable proto-myofibroblasts to generate a weak contractile force. Subsequent TGF-beta expression leads to their differentiation into a mature, alpha-smooth muscle actin-expressing myofibroblast. Because this leads to the expression of more contractile proteins, enhanced focal adhesion sites, and higher collagen deposition and ED-A fibronectin splice variant expression, myofibroblasts can generate a higher contractile force with physiological relevance during wound healing (Tomasek et al., 2002). The source of the TGF-beta signal that stimulates differentiation of myofibroblasts (Vaughan et al., 2000) appears to be diverse within the context of wound healing. For example, it has been suggested that plaletes and immune cells produce TGF-beta and that this signaling is important for myofibroblast differentiation (Massague, 1998). Autocrine and paracrine TGF-beta signaling by fibroblasts and re-epithelializing keratinocytes, respectively, may also play a role (Yang et al., 2001). Indeed, inhibiting TGF-beta1 inhibits myofibroblast formation *in vivo* (Hinz et al., 2001).

## TRACING THE ORIGIN OF MYOFIBROBLASTS

Myofibroblasts can be regarded as "the culprit cell of fibrosis and scarring" – they are the main cell type that inflict a fibrotic and scarring phenotype. This is achieved in different organ systems including the heart, lung, kidney, bone marrow and skin after injury (Kramann et al., 2015, Schneider et al., 2017), and the role of myofibroblasts does not appear to be organ or tissue-specific. Similarly, myofibroblasts have also been regarded as important regulators of tumor stroma formation (Otranto et al., 2012). However, their origin appears to be highly heterogeneous; that it, it is largely tissue- and injury context-specific. ***The heterogeneous origin of myofibroblasts and their implications in skin wound healing and regeneration is further explored in Chapter 4***. For example, by using a GFP-labeling and FACS quantification approach, it was determined that approximately ~95% of all myofibroblasts present in liver after carbon tetrachloride or bile duct ligation were derived from hepatic stellate cells or portal fibroblasts, with a contribution of ~87% and ~70%, respectively (Iwaisako et al., 2014). Pericytes have also been suggested to give rise to myofibroblasts in kidney (LeBleu et al., 2013). Similarly, Henderson *et al*., showed that Pdgf-beta+ cells also give rise to myofibroblasts in lung, kidney and heart (Henderson et al., 2013). By implementing a completely different approach and experimental regimen, Kramann *et al*., showed that perivascular Gli1$^+$ cells from liver vasculature commit to a myofibroblast lineage in different organs. For example, after hepatotoxic injury, Gli1$^+$ cells contribute approximately to ~40% of the total myofibroblast pool (Kramann et al., 2015). In a myocardial infarction model, it was determined that approximately 60% of myofibroblasts in heart derived from Gli1$^+$ progenitors; whereas ~37% were Gli1-derived in a model of intratracheal bleomycin instillation in lung, and ~45% in kidney. Indeed, ablation of Gli1$^+$ cells using human diphtheria toxin receptor allele driven under Gli1-CreER driver ameliorated kidney fibrosis and reduced heart fibrosis. In myelofibrosis (fibrosis of the bone marrow), Gli1$^+$ cells also give rise to myofibroblasts. Indeed, myofibroblasts in myelofibrosis can be targeted using Gli1 inhibitors, ameliorating the condition (Guerrero-Juarez and Plikus, 2017, Schneider et al., 2017). These studies highlight the heterogeneity of origin of myofibroblasts and distinct ways in which they can be targeted for ablation and amelioration of tissue and organ fibrosis. Even though Gli1$^+$ cells do not appear to give rise to myofibroblasts in skin during wound healing or fibrosis, ADAM12$^+$ vascular pericytes can give rise to myofibroblasts in injured skin dermis, and theire ablation leads to reduced scarring (Dulauroy et al., 2012). A recent study suggest that cells developed from somites during embryonic development have important roles in collagen deposition during homeostasis, wound healing, and cancer stroma formation. Using lineage tracing with *En1-Cre*, Rinkevich et al. (2015) identified two major fibroblasts populations – En1-positive and negative populations, with the former making major contributors toward wound repair. These cells express Cd26/Ddp4. By using small molecule inhibitor against this molecule, they were able to reduce scarring of skin. A recent study also suggests that "engrailed 1-history-naïve" E1HP fibroblasts reduce in numbers during aging and their decline leads to scarring as "engrailed 1-history-positive" fibroblasts emerge. Accordingly, this can be reversed upon transplantation of E1HP fibroblasts (Jiang et al., 2018).

## REPROGRAMMING OF MYOFIBROBLASTS

The treatment of fibrotic conditions remains a great challenge and health disparities in today's society. It is estimated that ~600K patients in the United States alone are affected by liver fibrosis (Scaglione et al., 2015). In the case of liver fibrosis, liver transplant is the only option for most affected by this condition. In other cases, such as skin, aesthetic approaches are often undertaken (Monstrey et al., 2014). The identification of the origin of certain myofibroblast populations have led to the identification of novel treatment regimes, including the use of inhibitors, targeted deletion, and replacement therapy. However, this does not ablate all myofibroblasts, as extensive heterogeneity, acquired by their origin, exists. Recent studies have suggested yet a different approach. Various studies have proposed to reprogram the myofibroblast to change its fate and ameliorate fibrosis and scarring. Myofibroblasts from a $CCl_4$-induced fibrotic liver can be reprogrammed into induced hepatocytes (iHeps) using viral-mediated ectopic expression of the transcription factors *Foxa3*, *Gata4*, *Hnf1a*, and *Hnf4a*. The *in vivo* iHep reprogramming efficiency ranged from 0.2-1.2%. iHeps were functionally similar to normal hepatocytes in that they demonstrated albumin secretion, urea synthesis, ability to uptake indocyanine green, uptake OilRedO dye, store glycogen, and showed cytochrome activity (Song et al., 2016). Myofibroblasts can also be reprogrammed into iHeps in a cholestasis-induced liver fibrosis model. An independent study also showed that myofibroblasts in liver can be reprogrammed into hepatocyte-like cells using AAV vectors expressing the hepatic transcription factors Foxa1, Foxa2, Foxa3, Gata4, Hnf1a, or Hnf4a (Rezvani et al., 2016). In a hepatotoxic model of liver fibrosis, approximately 0.87% myofibroblast-iHep reprogramming took place, whereas cholestatic model of liver fibrosis was not evaluated. In a recent study by us, we showed that in skin wound healing, the myofibroblast can be influenced by hair follicles via Bmp ligands to change fate into dermal adipocytes via activation of white adipose transcriptional lineage program. The newly formed dermal adipocytes are reminiscent of those in peri-wound skin in terms of depth relative to skin surface, size and volume, uptake or OilRedO, and expression of certain adipokines (Plikus et al., 2017). ***A more detailed explanation and full characterization of myofibroblast reprogramming under natural conditions is explored in Chapter 3***. A recent study in lungs also showed a two-way reprogramming of myofibroblasts-lipogenic fibroblasts is possible under normal conditions or fibrosis and formation and its resolution (El Agha et al., 2017). These new methods of cellular reprogramming – using cell specific, ectopically expressed transcription factors, or under natural reprogramming conditions, pave the way to novel, targeted therapeutic approaches to treating fibrosis and scarring in distinct complex tissues and organs by specifically targeting the myofibroblast.

## 1.3 WOUND HEALING AND REGENERATION IN WILD ANIMALS

### EMERGING MODELS OF WOUND HEALING AND REGENERATION: SPINY MICE

Although some mammalian species are capable of regenerating complex tissues and mini-organs, other species can and do it more efficiently than others. For example, in comparison to humans and laboratory rats (Guerrero-Juarez et al., 2018), small rodent species, such the house mouse (*Mus musculus*), are capable of regenerating hair follicles (Ito et al., 2007) and dermal adipocytes (Plikus et al., 2017) post-injury. Careful lineage tracing analyses, coupled with genetic gain and loss-of-function studies suggest these depend on the re-activation of embryonic mechanisms, such as WNT and BMP signaling. In comparison to laboratory mice, wild African mice of the genus *Acomys* were shown to have evolved enhanced regeneration of skin in response to injury and have become an emerging model of wound healing and regeneration (Gawronska-Kozak et al., 2014, Pinheiro et al., 2018). *Acomys* can regenerate parts of skin following full-thickness excisional wounding in what was regarded as an autotomy-like mechanism. This phenomenon is believed to have evolved as a response to predation and also depends on activation of WNT and BMP signaling (Seifert et al., 2012). A recent study has also suggested that epimorphic regeneration of the *Acomys* ear is enhanced and dependent on presence of macrophages (Matias Santos et al., 2016, Simkin et al., 2017). Indeed, wild animals might be a good model organism to study enhanced regeneration and wound healing under non-traditional, non-sterile and stressful environments.

Although the first experiments on *Acomys* were carried in out in captivity using wild-caught mice in the African savanna, recent interest in their biology has led to the establishment of this animal as a laboratory animal. Recent documentation exists on their husbandry and establishment of viable colonies of *Acomys* in the laboratory (Haughton et al., 2016). Indeed, this is an advantage when identifying and establishing novel species as emerging models of wound healing and regeneration. Nonetheless, there are certain animal species that offer similar advantages to studying wound healing and regeneration but simply cannot be kept in a proper laboratory setting. To overcome issues like this, different approaches must be taken. For instance, studies must rely on using interval censored-sampling (Archie, 2013b). Similarly, the development of xenograft transplantation models can enable high resolution interrogation on the mechanisms regulating wound healing in these animals. These alternative approaches to wound healing can be interrogated when studying wound healing and regeneration in the northern elephant seal, *Mirounga angustirostris*. Their ability to heal infected wounds and regenerate skin and their appendages under stressful conditions is superb. ***The wound healing dynamics and the use of the aforementioned alternative studies to study them are presented in Appendix A.***

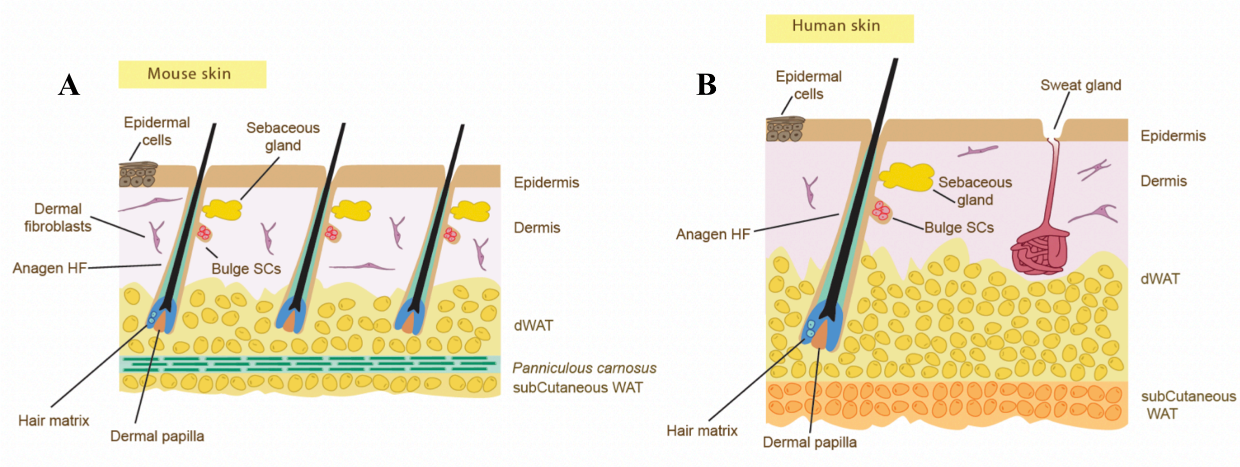


**Figure 1.1. Anatomy of mouse and human skin**. Intrinsic differences exist between human and mouse skin. Although both display stratification of epidermis residing on top of a heterogeneous collagen structure, in mouse skin, **(A)** dWAT is separated from sWAT via the striated muscle layer known as *panniculus carnosus*. **(B)** Human skin displays ectodermal-derived sweat glands. In mice, sweat glands are restricted to the paws. Unlike mice, no clear separation exists between dWAT and sWAT in humans.

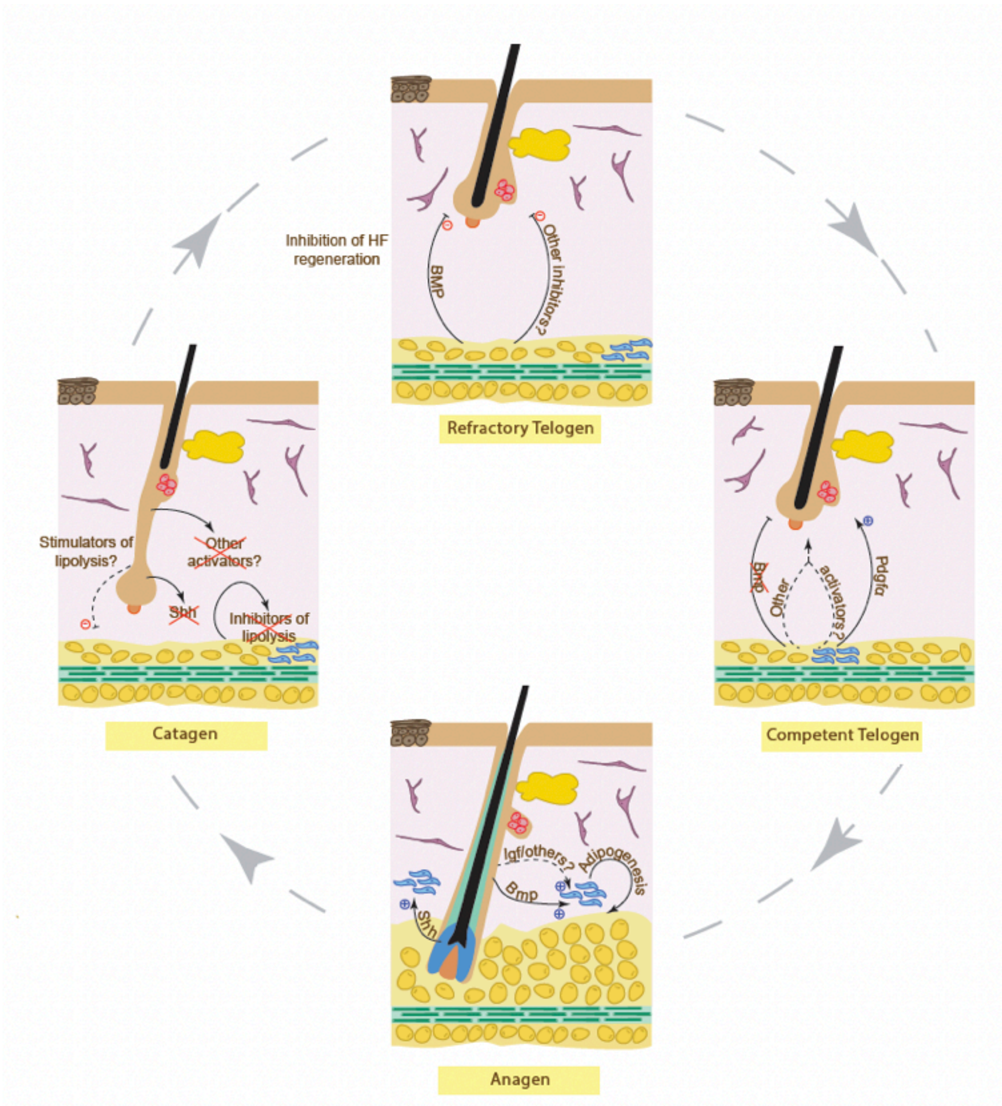


**Figure 1.2. Hair follicle-dermal adipocyte symbiosis**. The hair follicle is divided into active hair growth (anagen), involution (catagen), and rest (telogen). Dramatic changes in morphology and gene expression are observed in each of these stages. Concomitant with hair follicle cycle is the cycling of dWAT. Several mechanisms have been identified that suggest an intricate and functional relationship between them.

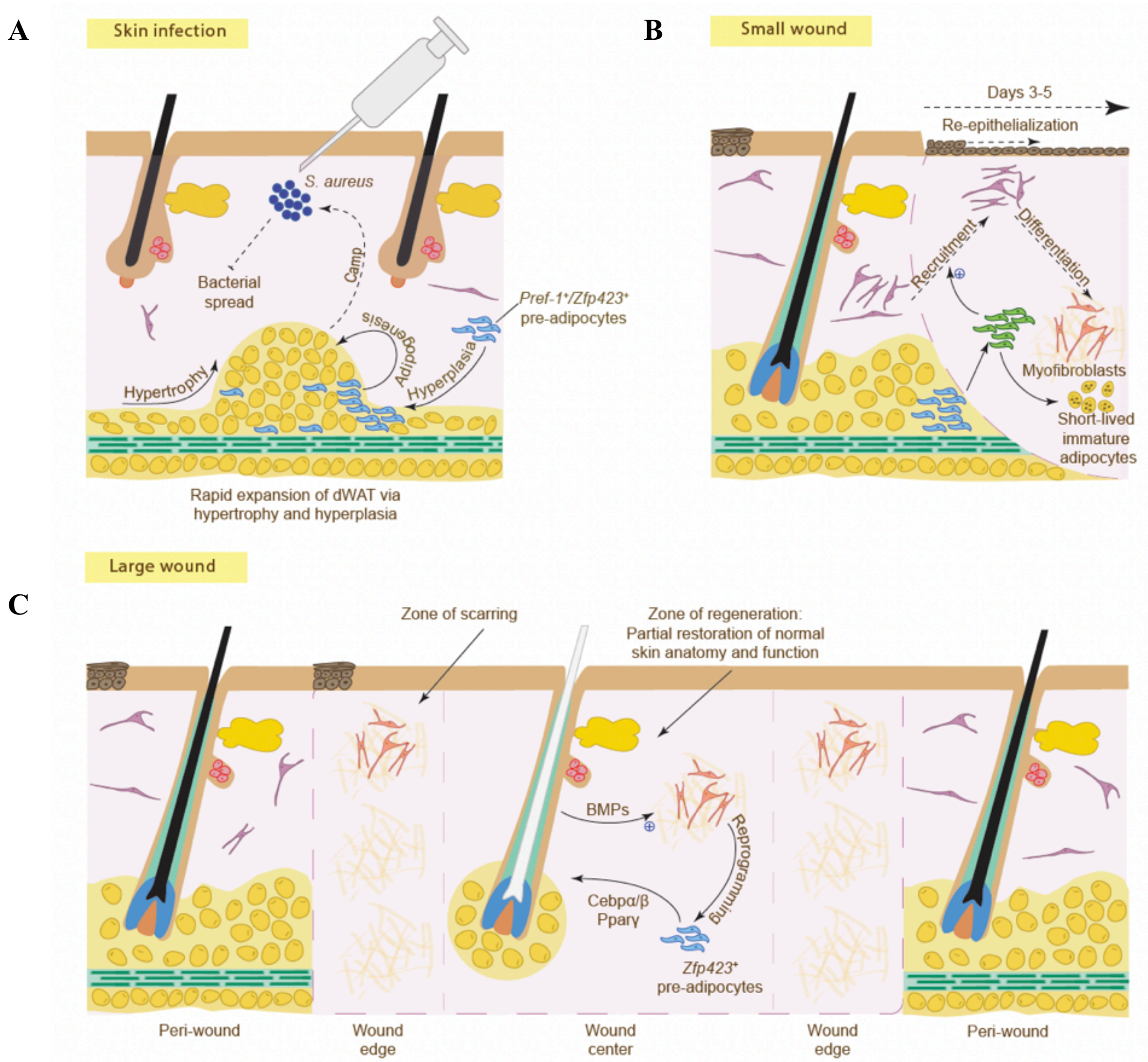


**Figure 1.3. Non-metabolic functions of skin dermal adipocytes**. Schematics showing the non-metabolic functions of dWAT. **(A)** dWAT has been shown to modulate innate immunity of skin upon infection with *S. aureus* via expression of *Cathelicidin*. Similarly, **(B)** dermal adipocytes have important roles in wound healing. Recently **(C)** dWAT has been shown to regenerate in large skin wounds. Regeneration of dWAT may have important roles in maintaining skin integrity.

# CHAPTER 2

## Wound regeneration deficit in rats correlates with low morphogenetic potential and distinct transcriptomic profile of epidermis

Reprinted from Wound regeneration deficit in rats correlates with low morphogenetic potential and distinct transcriptome profile of epidermis 138/6, Guerrero-Juarez, F. Christian, *et al.*, *Journal of Investigative Dermatology, /* Wound regeneration deficit in rats correlates with low morphogenetic potential and distinct transcriptome profile of epidermis, 1409-1419, 2018, with permission from Elsevier.

### Statement of contribution

In this study, I designed (in agreement with my thesis advisor Dr. Maksim V. Plikus) and performed experiments, analyzed data and interpreted results. My data contributes to Figures 2.1, 2.2, 2.3, 2.4. Dr. Chae Ho-Lim (New York University) contributed technically with whole-mount staining of mouse and rat skin wounds (Related to Fig. 2.2), Dr. Rabi Murad contributed technically with inter-species transcriptome analyses and visualization of data (Related to Fig. 2.3), Dr. Aliaksander A. Astrowski (Grodna State University) contributed technically with transplantation studies (Related to Fig. 2.5).

# ABSTRACT

Large excisional wounds in mice prominently regenerate new hair follicles (HFs) and dermal adipocytes. Currently, wound-induced regeneration, i.e. wound-induced hair neogenesis (WIHN), remains a clinically desirable, but poorly understood phenomenon. In this chapter, it is shown that large excisional wounding in rats, across seven different strains, fail to regenerate *de novo* HFs. To shed light on possible reasons of this regenerative failure program, the transcriptomes of mouse and rat wound tissues were resolved and compared against one another using inter-species transcriptome analyses. Wound tissues were collected at the time of scab detachment, which coincides with the onset of HF regeneration in mice. In both species, wound tissues shared core dermal and epidermal transcriptional programs, however, prominent inter-species differences were observed. For instance, rat epidermis expresses an array of distinct transcriptional and epigenetic factors, markers of epidermal repair, hyperplasia, and inflammation, and lower levels of the pleiotropic WNT signaling effectors and regulators. These findings help to establish rats as a potential non-regenerating rodent model for excisional wound healing that favors scarring over regeneration, and suggest that their associated transcriptional profile may contribute to such regenerative deficiency.

## INTRODUCTION

Full-thickness wounds in adult mammals typically repair with scarring. However, large wounds in laboratory mice *(Mus musculus)* regenerate new hair follicles in their center. This phenomenon, known as wound-induced hair neogenesis (WIHN), largely recapitulates embryonic HF morphogenesis programs (Ito et al., 2007, Wang et al., 2015). While the cellular sources for new HFs are poorly understood (Ito et al., 2007, Snippert et al., 2010, Wang X. et al., 2017), some of the signaling and epigenetic requirements for WIHN have been partially elucidated. Critical for WIHN is canonical WNT signaling (Gay et al., 2013, Ito et al., 2007, Myung et al., 2013). Physiologically, both dermal (Gay et al., 2013) and epidermal sources of WNT ligands (Myung et al., 2013) are important; however, they likely act at distinct phases of WIHN. Enhanced HF neogenesis in wounds of the African spiny (*Acomys*) is also positively correlated with high WNT activity (Seifert et al., 2012). Other signals also play a role in WIHN. For instance, dermal WNT signaling is driven by Fgf9, initially secreted by γδ T-cells (Gay et al., 2013). Also important for WIHN is Toll-like receptor 3 (Tlr3) signaling and its downstream effectors Il6 and Stat3 (Nelson A. M. et al., 2015). Tlr3 is activated by the double-stranded RNA released from damaged keratinocytes at the onset of wound healing. Promoting WIHN downstream of Il6/Stat3 signaling is TAp63, a p63 isoform (Nelson et al., 2016). WIHN efficiency is also negatively regulated by prostaglandin Pdg2 signaling (Nelson A. M. et al., 2013), Cxxc5 transcriptional regulator (Lee et al., 2017) and Msi2 RNA-binding protein (Ma et al., 2017), and modulated by the macrophage-derived Tnfα signaling via TNF/p-AKT/p-β-catenin pathway (Wang X. et al., 2017). Distinct from mice, definitive WIHN has been shown only in rabbits (Billingham and Russell, 1956, Breedis, 1954, Stenbäck et al., 1967). Although suggested to take place in sheep, the reported evidence for WIHN was inconclusive (Brook et al., 1960). In humans, Kligman A. M. and Strauss J. S. (1956) reported regeneration of sparse vellus HFs in the facial skin following partial freezing and dermabrasion. However, robust regeneration of new HFs in human wounds is generally not observed (Gay et al., 2013). In this study, it is interrogated whether WIHN occurs in laboratory rats (*Rattus norvegicus)* and how this process compares to that in mice. This inquiry was stimulated by the contradicting reports in the classic literature on the outcomes of rat skin repair following cryo-injury. While Taylor (1949) and Mikhail (1963) suggested that cryo-damaged skin in rats repairs with HF neogenesis, Stenbäck et al. (1967) failed to replicate these findings. In this chapter, it is shown that rats distinctly fail to regenerate new HFs in large full-thickness excisional wounds, and further explore non-regenerative wound healing in rats with means of inter-species comparative transcriptomic analyses and tissues recombination experiments.

## RESULTS

Large excisional skin wounds in adult mice regenerate new HFs soon after re-epithelialization, around post-wounding day (PWD) 15 (Gay et al., 2013, Ito et al., 2007), and new adipocytes surrounding neogenic HFs from PWD21 onward (Plikus et al., 2017) (Figure 2.1). Whether large excisional wounds in adult rats regenerate new HFs and dermal adipocytes similar to mice was interrogated. This was tested by inflicting large skin wounds (circular *d (diameter)* = 2.0 cm) in rats (outbred Sprague-Dawley strain), compared to mice (squared *s (side)* = 1.5 cm). Complete re-epithelialization in rats, as measured by the timing of scab detachment, took comparatively longer, 30.0+/-1.0 days; however, no neogenic HFs were observed in all animals when examined at PWD40 (n=5) (Figure 2.1.A, 2.1.B, Table 2.1). Because WIHN efficiency in mice can vary across strains (Nelson A. M. et al., 2013), wound repair outcomes across six other strains of rats were assessed. In addition to Sprague-Dawley, three other outbred strains were evaluated: CD IGS (n=5), Long-Evans (n=5), Wistar (n=5) and three inbred rats: F344 FISCH (n=5), Brown Norway (n=3), Buffalo (n=5). The timing of wound re-epithelialization varied significantly across the strains (*P*=0.0011) with a range of 25-33 days. Compared to mice (number of regenerated hair follicles=15±5.85), all rats studied consistently failed to undergo WIHN (*P*=0.0127). Absence of neogenic HFs in PWD40 wounds was further validated in Sprague-Dawley rats (n=4) by Krt17 and alkaline phosphatase whole-mount staining (Figure 2.2.B), and in several other rat strains by histology. Commonly, wound epidermis formed small peg-like projections, however these displayed clear epidermal, rather than HF, organization.

Next, it was considered that relatively large wounds, with their extended re-epithelialization dynamics, could be incompatible with WIHN. This possibility was assessed by studying repair outcomes of smaller squared $s$ = 1.5 cm and $s$ = 1.0 cm wounds in Sprague-Dawley (n=5 and n=4 respectively) and CD IGS rats (n=5 and n=5 respectively) (Table 2.2, 2.3). Surprisingly, generally slower wound re-epithelialization dynamics as compared to these in mice were observed, and all wounds studied failed to undergo WIHN by PWD40. Lack of neogenic HFs was further confirmed on Krt17 and alkaline phosphatase whole-mount staining. Consistent with a recent report in mice (Plikus et al., 2017), hairless wounds in rats failed to regenerate new adipocytes (Figure 2.2.C, 2.2.D). This is in contrast to mouse wounds (Table 2.4, 2.5). These observations suggest that rat is a suitable rodent model for studying non-regenerative healing of large excisional skin wounds.

To identify molecular signatures that underlie regenerative behavior differences between rats and mice, the transcriptomes of wound epidermis and dermis collected at the time of complete re-epithelialization were resolved. Inter-species transcriptome analysis was performed using mouse and rat one-to-one orthologs and principal component analysis (PCA) revealed significant separation between all tissue types, yet close clustering of biological replicates (Figure 2.3.A). To resolve the transcriptome of mouse *vs.* rat wound tissues, the Bioconductor package edgeR was utilized (Li and Dewey, 2011), which fits a generalized linear model to RNA-seq count data using a negative binomial distribution to model gene expression variance. Approximately 3,850 differentially expressed gene orthologs (DEGOs) (5% FDR level and minimum 4X-fold change) were identified, which grouped into eight distinct clusters (Figure 2.3.B). Clusters 1 and 2 include DEGOs upregulated in both species in wound epidermis and dermis, respectively (*aka* shared epidermal and dermal genes). Cluster 3 identifies mouse-specific and cluster 4 – rat-specific epidermal DEGOs, while clusters 5 and 6 identify mouse- and rat-specific dermal DEGOs, respectively. Finally, cluster 7 contains mouse-specific DEGOs upregulated both in epidermis and dermis, while cluster 8 contains rat-specific DEGOs.

The shared epidermal and dermal genes were assessed and whether these include multiple established markers of epidermal and dermal lineages was determined (Figure 2.3.C). On pathway analysis, epidermal cluster 1 is enriched for terms such as keratinocyte proliferation, keratinocyte differentiation, skin barrier, phospholipid metabolism and wound healing while dermal cluster 2 is enriched for terms such as extracellular matrix, cell-matrix adhesion, leukocyte migration, wound healing, WNT and BMP signaling. Rat and mouse wound epidermis share core transcriptional regulators of the epidermal lineage (*Cebpb, Gata3, Grhl2, Grhl3, Irf6, Klf4/5, Ovol1, Vdr, Zfp750*), key early epidermal differentiation markers (*Cnfn, Evpl, Krt1, Krt14, Krt15, Krt16, Tgm1, Tgm5*) and epidermal adhesion molecules (*Cdh1, Col17a1, Dsc1, Dsc3, Dsp, Epcam, Itga6, Lamb3, Ocln, Pkp1, Pkp3*). Rat and mouse wound dermis share multiple mesenchymal transcriptional regulators (*En1, Meox1, Meox2, Snai1, Tbx15*) and extracellular matrix proteins (*Col1a1, Col3a1, Col5a1, Col6a1*). At the same time, notable species-specific differences are present. Rat wound epidermal DEGOs include *Notch1, Krt17* and transcriptional regulators *Hopx, Hr, Id4, Sox9*. Hopx (Takeda et al., 2013) and Sox9 (Vidal et al., 2005) mark HF stem cells in unwounded mouse skin and given the non-regenerative characteristics of rat wounds, their elevated expression in rat epidermis, including on immunostaining, appears paradoxical. However, Hopx (Mariotto et al., 2016) and Sox9 (Shi et al., 2013) can also regulate epidermal lineage program in humans, and similar to Sox9 (Shi et al., 2013), elevated Krt17 (Depianto et al., 2010) and Notch1 expression (Li et al., 2016) correlate with epidermal repair, hyperplasia and inflammation. Mouse epidermal DEGOs include *Cebpa, Dlx3, Dlx5, Sox7* and *Tcf23*. Of these, Cebpa (Lopez et al., 2009) and Dlx3 (Hwang et al., 2011) reduce epidermal hyperplasia and inflammation, and promote differentiation. Consistently, on pathway analysis, rat wound epidermis is enriched for epithelial migration and proliferation terms, while mouse wound epidermis shows enrichment for lipid biosynthesis terms, including cholesterol synthesis typically associated with terminal differentiation. Therefore, these results suggest that, compared to mouse, rat wound epidermis is less mature at the time of scab detachment. Regarding the species-specific differences in wound dermis, rats express higher levels of transcriptional regulator *Runx2*, implicated in keloid scarring (Hsu et al., 2017), and extracellular matrix proteins *Col5a3, Des* and *Tnn*, while mice express higher levels of transcriptional regulators *Dnmt3a, Hdac7, Sox18,* contractile proteins *Acta2, Afap1* and collagens *Col26a1, Col27a1*.

The signaling activities implicated in HF development and regeneration were also evaluated in rat and mouse wounds. Prominently, we observe species-specific differences in canonical WNT signaling. While in both species, canonical WNT ligands *Wnt3, Wnt4* and *Wnt7b* are expressed in wound epidermis and soluble WNT inhibitors *Dkk3, Sfrp2* and *Sfrp4* in wound dermis, only mouse wounds (both epidermis and dermis) show high expression of *Axin2,* a direct WNT signaling target. Furthermore, compared to rats, mouse wound epidermis shows higher expression of the negative WNT signaling regulators, *Ctnnbip1* and *Kremen2.* In terms of BMP signaling, both species express *Bmp7* in wound epidermis, while wound dermis expresses BMP antagonists *Chrdl2, Grem1* and *Grem2*. Additionally, in rats, epidermis expresses the BMP antagonist *Sostdc1*, while mouse dermis expresses *Bmp4*. No prominent inter-species differences are seen for the FGF and SHH pathways. Among the pathways not implicated in HF development, mouse wounds show expression patterns consistent with higher IGF/insulin and TGFβ signaling, and distinct repertoire of immune cytokines.

Lastly, epigenetic factor differences were evaluated. Rat wounds overexpress chromatin modifiers regulating epidermal differentiation *Satb1* (Fessing et al., 2011), *Smarca4* (Mardaryev et al., 2014), and *Cbx2, Kdm8, Rbbp4, Setdb1*. Mouse wounds overexpress *Dnmt3a, Hdac4, Ing5, Kdm2a, Mysm1, Setd1b, Smyd4, Whsc1l1*. Select epigenetic factors were further validated by qRT-PCR (Rat/Mouse F.C., $P<0.05$) and immunostaining (Figure 2.4. A, 2.4.B, 2.4.C). These analyses suggest that despite sharing core transcriptional programs, wound epidermis in rats appears to be less mature, less WNT responsive, and potentially, less competent as compared to mice.

To further investigate if HF regeneration deficit in rat wounds relates to low epidermal competence, autologous tissue recombination assays were developed, in which inter-follicular epidermis (IFE) is co-transplanted with vibrissa dermal papillae (DPs) onto the surface of circular, $d$ = 2.0 cm wound (Figure 2.5). Briefly, in this assay a full-thickness wound is created on the dorsal skin inside of an isolating chamber. DPs are microdissected from vibrissae HFs and grafted onto the wound surface. Lastly, an intact sheet of IFE is isolated from the animal's flank using vacuum-suction and transferred in an unfolded state on top of the grafted DPs using adhesive semi-dissolvable carrier. This model enables studying regenerative responses of epidermis to hair-inducing DPs within wound settings.

The interaction outcomes between IFE and DPs were evaluated on post-grafting days 3, 5, 7, 10, 14 and 20 (n=5 per time point; ≥ 10 DP per experiment). Following grafting, IFE underwent transient hyperproliferation, increased in thickness and reformed the basal membrane (2.5.A, 2.5.B). By day 7, IFE formed prominent pocket-like invaginations surrounding DPs (2.5.C). However, no neogenic HFs formed even by day 20 (Figure 2.5. D). Because the hair-inducing properties of DPs may change with respect to the hair growth cycle, as previously shown in the vibrissa amputation model (Iida et al., 2007), DPs derived from eight different time points, comprehensively covering the entire vibrissa hair cycle, were used. Synchronized vibrissae were grafted as follow: post-plucking week 1 – latent period; weeks 2, 3 – early anagen; weeks 4, 5 – mid-anagen; week 6 – late anagen; week 7 – catagen/telogen and week 8 – second early anagen. The resulting morphogenetic interactions on day 10 (n=5 per time point; ≥ 10 DP per experiment) and day 20 (n=5 per time point; ≥ 10 DP per experiment) were evaluated. Upon evaluation of grafts, it was determined that transplanted DPs generally preserved their relative sizes, such that initially larger anagen DPs maintained greater volume as compared to initially smaller telogen DPs both on day 10 and day 20 (data not shown). Secondly, the extent of DP-IFE interactions changed as a function of hair cycle with a statistically larger portion of anagen DPs contacting IFE as compared to telogen DPs, both at day 10 ($P$=0.002) and day 20 ($P$=0.0039). Lastly, for all eight hair cycle time points tested, no morphologically recognizable neogenic HFs were induced at the sites of DP-IFE interactions. Despite failing to regenerate new

HFs, in rare instances DP-IFE interactions occurred some distance away from the surface and produced cup-like structures morphologically reminiscent of the hair peg stage of normal HF morphogenesis (data not shown). Taken together, it is shown that rat epidermis fails to regenerate new HFs or activate hair-specific differentiation program in response to DPs in this wound reconstitution assay. Considering that no HFs regenerate in rats spontaneously from wound epidermis or from wound-grafted IFE under the influence of DPs, their transcriptomes were compared. Expression differences are observed among transcriptional factors, with IFE upregulating *Foxo1/3, Klf2, Nfatc2, Rora, Rxra* and *Stat5a/5b* and wound epidermis upregulating *Cebpb, Fhl2, Foxp1, Nfkb1, Pitx1, Runx1, Sox9* and *Stat1*. Apart from *Wnt7b* in IFE, no substantial expression differences are observed for other canonical WNT ligands and antagonists; yet wound epidermis distinctly upregulates several non-canonical WNT pathway members, *Wnt4, Wnt11* and *Fzd6*. The latter also upregulates BMP antagonists *Fstl1* and *Sostdc1* and VEGF ligands *Vegfa, Vegfb*. Expression differences are also observed for some members of TGFβ pathway and immune cytokines, without clear epidermal type preferences. Together, albeit different in some respects, gene expression across the key pathways implicated in HF development is largely similar between the IFE and wound epidermis and the observed differences, including *Sox9*, *Wnt4* and *Wnt11* differences, do not positively correlate with the regenerative potential of epidermis.

## DISCUSSION

In mice, neogenesis of HFs (Ito et al., 2007) and adipocytes (Plikus et al., 2017) in large excisional wounds shifts the repair process away from scarring and toward embryonic-like regeneration. Unlike mice, however, humans rarely show signs of neogenesis (Kligman A. M. and Strauss J. S., 1956) and commonly heal with scarring (Gay et al., 2013, van den Broek et al., 2014). Therefore, regeneration of HFs and fat remains a desirable, yet clinically unmet outcome of wound repair and understanding the basis for WIHN and its failure constitutes an important research question. Non-regenerative healing in rats establishes a new paradigm for future WIHN studies through cross-species comparison with mice. This approach is facilitated by close evolutionary distance (Kimura et al., 2015) and similar skin anatomy between rats and mice. The analyses already show that transcriptomic profiles substantially differ between the two species at the time of complete wound re-epithelialization. Rat wound epidermis upregulates distinct transcriptional and epigenetic factors from that of mice. Rats also overexpress *Notch1* and *Krt17*. Considering the role of Sox9 (Shi et al., 2013), Krt17 (Depianto et al., 2010) and Notch1 (Li et al., 2016) in epidermal hyperplasia and inflammation, and that of Cebpa (Lopez et al., 2009) and Dlx3 (Hwang et al., 2011) in their reduction, we conclude that wound epidermis in rats is immature and, likely, not competent for HF neogenesis. The tissue reconstitution studies further support this notion. Future works will be required to explore the impact of inter-species differences in wound dermis. To this end, the transcriptomic data already points toward significant inter-species differences in the dermal wound compartment.

These findings are placed in the context of the classic works on wound healing and tissue recombination. These findings generally agree with these by Stenbäck et al. (1967) that full-thickness wounds in rats cannot regenerate new HFs, however, new inquiry into the cryo-injury wounding model is warranted. In terms of the reconstitution assays, new HFs were shown to form from non-hair fated adult epidermis (Jahoda, 1992, Jahoda et al., 1993, McElwee et al., 2003, Reynolds and Jahoda, 1992). Nonetheless, when tested in the context of well-controlled experimental conditions, HF-forming abilities of non-hair fated epidermis are on an order of magnitude lower than those of hair-fated epithelia (Ehama et al., 2007, Ferraris et al., 1997, Yang and Cotsarelis, 2010). This data reveals a general failure of adult rat IFE to reconstitute HFs in the presence of DPs, while vibrissa-like HFs are readily induced by the DPs from hair-fated epithelium. Reflecting on these differences with the classic literature, we note that our vacuum-assisted IFE isolation technique minimized contamination for HF epithelium, while prior experimental models contained endogenous HFs (ear pinna slit-wound model), or included hair-fated epithelial cells (enzymatically-digested newborn skin epithelium). In conclusion, the data presented in this chapter reveal an inability of excisional wounds in rats to undergo WIHN and implicate low epidermal competence and its associated gene expression signature as the possible contributing factors. Lastly, the non-regenerating rat *vs.* regenerating mouse wound comparison presented in this chapter can served as the new experimental paradigm for studying the basis for HF neogenesis across species.

## METHODS

**Rat strains.** The following rat strains were utilized in this study: Sprague-Dawley (Charles River Laboratories, strain code 400), Buffalo (strain code 281), Brown Norway (strain code 091), CD IGS (strain code 001), F344 FISCH (strain code 403), Long-Evans (strain code 006) and Wistar (strain code 003). Mixed background mice were used in this study.

**Wounding procedures**. All wounding experiments were carried out in accordance with corresponding IACUC guidelines. Briefly, hairs were clipped, skin site was disinfected and a single full thickness excisional wound was created on the dorsum of adult mice (squared $s$ = 1.5 cm) (Gay et al., 2013, Ito et al., 2007, Plikus et al., 2017) and rats (circular $d$ = 2.0 cm, squared $s$ = 1.5 cm and $s$ = 1.0 cm) using scissors. Following wounding, all animals were housed individually. Wounds were let to heal by secondary intention. No wound dressing was applied. Rats were approximately 150 g at the time of wounding, which corresponds to an age of approximately 5-7 weeks (as per Charles River's on-line growth chart). Mice were between 4-8 weeks of age. Animals were used as biological replicates. All animals were anesthetized with isoflurane and received acetaminophen for postoperative analgesia.

**Wound site preparation for autologous transplantation.** Autologous transplantation was performed in adult Wistar rats (100-150 g body weight). Recipient area was prepared twenty-four hours prior surgical procedure. Briefly, body hair was clipped and a circular incision ($d$ = 2.0 cm) was made in the interscapular area, resulting in a full-thickness excisional wound. A sterile, nonreactive ring chamber was then inserted and sewn to the edges of the skin to isolate the inside portion of the wound. The chamber was then covered with a lid to prevent desiccation. Synchronization of vibrissae hair follicles and microdissection of dermal papillae and isolation of interfollicular epidermis was performed as previously described (Guerrero-Juarez et al., 2018).

**Histology, immunohistochemistry and morphometric analysis.** Tissues were fixed in 4% paraformaldehyde, dehydrated, paraffin embedded, and sectioned at 7 μm or 10 μm thickness. Frozen tissues sectioned at 12 μm were also utilized. Tissue sections were stained with H&E. For immunohistochemistry, the following primary antibodies were used: mouse anti-PCNA (1:500; Millipore), rabbit anti-β-catenin (1:200; Sigma), rabbit anti-Krt14 (1:400; Berkeley Antibody Company), rabbit anti-Krt10 (1:200, Sigma), mouse AE13 and AE14 (Dr. Tung-Tien Sun, NYU), rabbit anti-Satb1 (1:200, Novus Biologicals), rabbit anti-Setdb1 (1:200, Cell Signaling), rabbit anti-Setd1b (1:200, Novo Pro), rabbit anti-Whsc1l1 (1:200, Novo Pro) and rabbit anti-Krt5 (1:200, BioLegend). Tissues were counterstained with Hoechst (1:200, Life Technologies). The AEC substrate kit was used for color development (Vector Laboratories). When necessary, antigen retrieval was performed by heating histological sections in citric buffer. Morphometric analyses were performed on serial H&E stained sections.

**Whole mount staining.** Whole-mount staining was performed as previously described (Guerrero-Juarez et al., 2018).

**Wound tissue processing and RNA isolation.** Fully re-epithelialized rat and mouse wounds were dissected from euthanized animals. Tissue was placed in a solution containing 0.2% Dispase (Roche) in RPMI medium (Gibco) and incubated overnight at 4°C or 0.33% Dispase in RPMI medium for 30-40 min at 37°C. Wound epidermis was then carefully separated from wound dermis using watch maker forceps. Following separation, wound epidermis and dermis were placed in cold RLT buffer containing 0.01% β-mercaptoethanol to preserve RNA integrity and homogenized using Precellys. Total RNA was isolated using the RNeasy Micro Kit protocol (Qiagen) as per manufacturer's instructions with minor modifications, including DNase I treatment to remove residual DNA. RNA samples with RIN scores higher than 8.5 were considered for library preparation.

**RNA sequencing.** cDNA libraries were prepared using the SMART-seq2 assay using total RNA as previously described with minor modifications (Picelli et al., 2013, Picelli et al., 2014). Briefly, 10 ng and 100 ng of total RNA was used for reverse transcription. The latter was performed using Super Script II as recommended per manufacturer with minor modifications. cDNA was pre-amplified for 12 and 10 cycles, respectively. Tagmentation was performed on 18 ng and 20 ng cDNA using the Nextera DNA Sample Preparation Kit (Illumina) at 55°C for 5 minutes. Tn5 was deactivated with PM buffer (Qiagen) and samples were purified using PCR Purification Kit (Qiagen). Adapter-ligated fragments were amplified for 8 continuous cycles using Phusion Polymerase (NEB) with unique barcodes (IDT). Amplified fragments were purified with AMPure XP beads (Beckman Coulter) at a 1:1 ratio and eluted with elution buffer (Qiagen). Final libraries were loaded on a High-Sensitivity DNA chip for quality control

(Agilent) and quantified using KAPA for Illumina Sequencing Platforms (Illumina). Libraries were multiplexed at a concentration of 2nM and sequenced as single-end 43 bp on a NextSeq 500 Illumina Sequencing Platform (Illumina).

**qRT-PCR analysis.** Total RNA was quantified using Qubit (ThermoFisher). 200 ng of total RNA was converted to cDNA using the SuperScript$^{TM}$ First-Strand Synthesis System for RT-PCR (Invitrogen) as per manufacturer's directions with minor modifications. cDNA was amplified using PerFecta SYBR Green MasterMix with ROX (Quantas) and the following validated mouse and rat-specific primers Genecopoeia were used: *SATB1* (rat catalog #RQP046263, mouse catalog #CS-MQP043505-1); *HDAC* (rat catalog #RQP085245; mouse catalog #MQP043505); *SETD1B* (rat catalog #CS-QP00830L, mouse catalog #MQP025449); *SETDB1* (rat catalog #RQP084673, mouse catalog #CS-KQP074457-01); *WHSC1L1* (rat catalog #RQP081826; mouse catalog #CS-MQP023522-01); *ACTB* (rat catalog #RQP051050; mouse catalog #MQP026493) in a C1000 Touch Thermocycler (BioRad). Transcripts from both species were normalized to corresponding *ACTB* transcripts. Relative fold change was computed using the $\Delta\Delta C_T$ method.

**Interspecies RNA-sequencing comparison.** Transcript alignment and quantification and inter-species transcriptome analyses was performed as previously described (Guerrero-Juarez et al., 2018).

**Statistics.** One-way ANOVA, two-tailed paired and unpaired *t*-tests were computed to determine statistically significant differences. $P<0.05$ was considered statistically significant. One-Way ANOVA with was performed using Prism, version 5.c for Mac OS X. For data representation, we used Prism's standard significance scheme.

**Table 2.1.** Quantification of scab detachment timing, hair follicle and dermal fat regeneration in circular wounds in different rat strains.

| Rat strain | Biological replicate (n) | Strain type | Scab detachment (avg. PWD ± S.E.M.) | *De novo* regeneration (on PWD40) | |
|---|---|---|---|---|---|
| | | | | Hair follicles | Dermal fat |
| F344 FISCH | 5 | Inbred | 25.0 ± 1.09 | No | No |
| Buffalo | 5 | Inbred | 25.8 ± 0.80 | No | No |
| Brown Norway | 3 | Inbred | 33.0 ± 0.00 | No | No |
| CD IGS | 5 | Outbred | 29.8 ± 1.49 | No | No |
| Sprague-Dawley | 5 | Outbred | 30.0 ± 1.0 | No | No |
| Long-Evans | 5 | Outbred | 28.2 ± 1.49 | No | No |
| Wistar | 5 | Outbred | 26.6 ± 0.75 | No | No |

**Table 2.2.** Quantification of scab detachment timing, hair follicle and dermal adipocyte regeneration in squared wounds in CD IGS and Sprague-Dawley rats.

| Rat strain | Biological replicate (n) | Scab detachment (avg. PWD ± S.E.M.) | *De novo* regeneration (on PWD40) | |
|---|---|---|---|---|
| | | | Hair follicles | Dermal fat |
| CD IGS | 5 | 23.4 ± 1.16 | No | No |
| Sprague-Dawley | 5 | 20.6 ± 0.245 | No | No |

**Table 2.3.** Quantification of scab detachment timing, hair follicle and dermal adipocyte regeneration in squared wounds in CD IGS and Sprague-Dawley rats.

| Rat strain | Biological replicate (n) | Scab detachment (avg. PWD ± S.E.M.) | *De novo* regeneration (on PWD40) | |
|---|---|---|---|---|
| | | | Hair follicles | Dermal fat |
| CD IGS | 5 | 20.2 ± 0.8 | No | No |
| Sprague-Dawley | 4 | 20.25 ± 0.25 | No | No |

**Table 2.4.** Assessment of hair follicle regeneration in squared wounds in mice.

| Mouse strain | Biological replicate (n) | Strain type | *De novo* regeneration (on PWD28) | |
|---|---|---|---|---|
| | | | No. of mice with hair follicle regeneration | No. of mice lacking hair follicle regeneration |
| *Mixed* | 5 | Outbred | 3 | 2 |

**Table 2.5.** Quantification of hair follicle regeneration in squared wounds in mice.

| Mouse strain | Biological replicate (n) | Strain type | No. of *de novo* hair follicles (on PWD28) | | |
|---|---|---|---|---|---|
| | | | Mouse 1 | Mouse 2 | Mouse 3 |
| *Mixed* | 3 | Outbred | 6 | 13 | 26 |

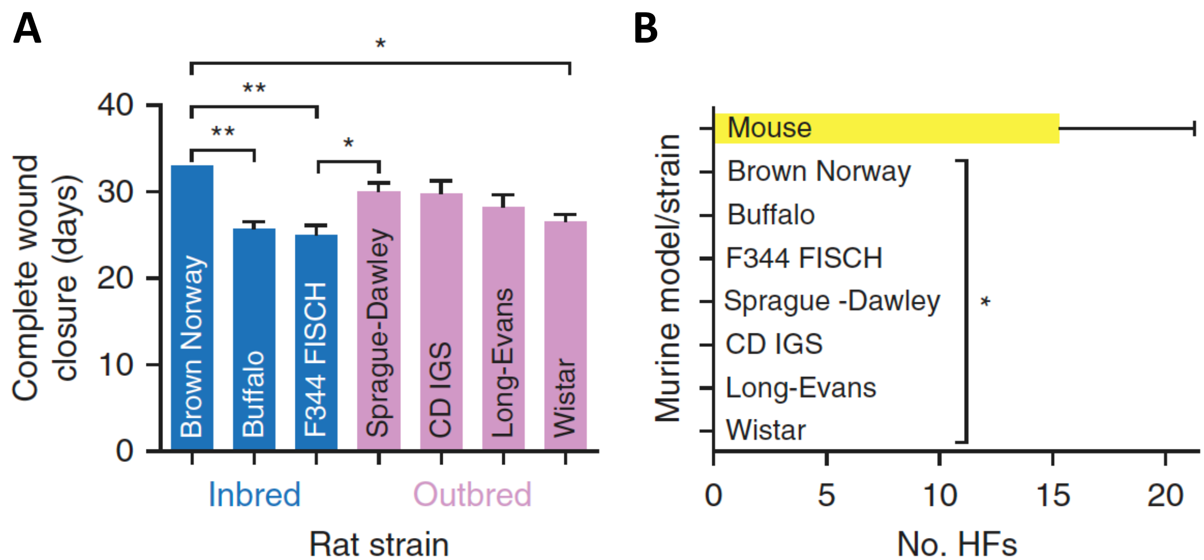


**Figure 2.1. Wound closure in laboratory rats**. **(A)** Timeline of full-thickness excisional wound healing in mice and rats. Despite their inability to regenerate, circular ($d$ = 2.0 cm) wounds in rats undergo complete re-epithelialization, ranging between 25-33 days depending on the strain. **(B)** Mouse wounds heal and regenerate new HFs and dermal adipocytes (DA), while rat wounds fail to regenerate. Values in the graphs on (b) and (c) are means ± S.E.M. One-way analysis of variance in **(A)**, $P < 0.05$; post hoc Tukey's multiple comparison test in **(A)**, $*P < 0.05$, $**P < 0.01$; two-tailed unpaired t-test in **(B)**, $*P = 0.0127$.

A B

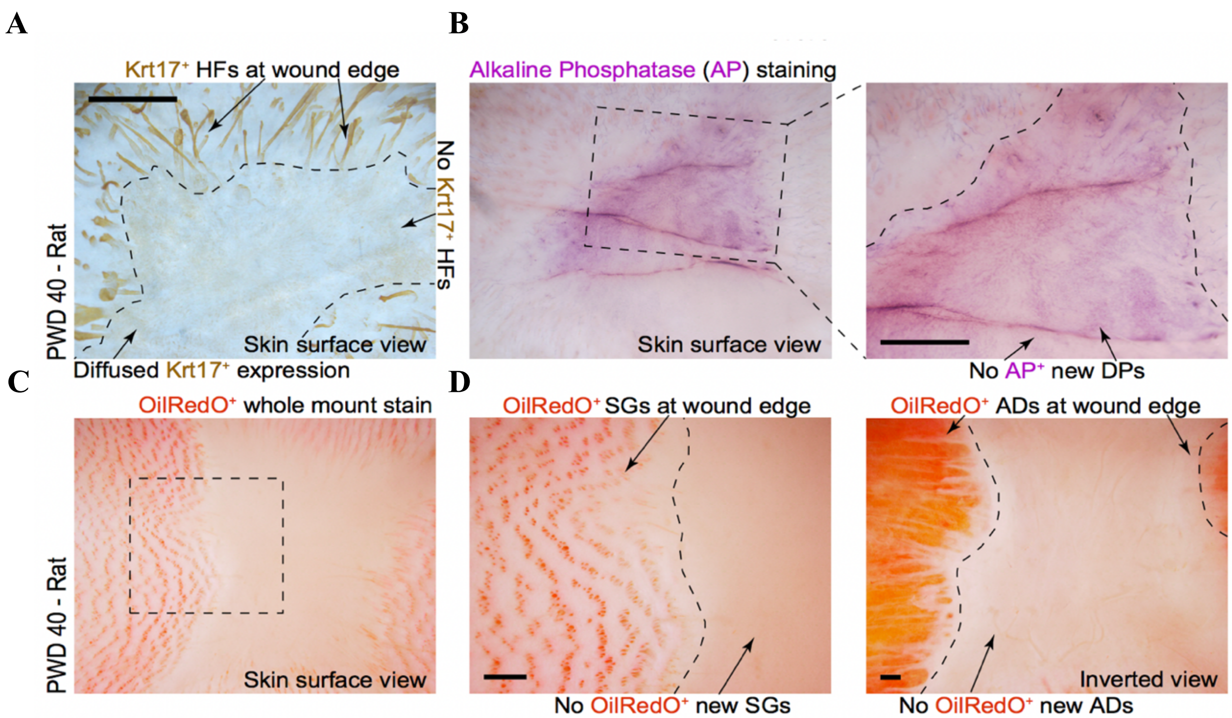


**Figure 2.2. Lack of appendage and fat regeneration in rats**. Circular $d$ = 2.0 cm wounds in all strains of rats (n=5 per strain) failed to regenerate new HFs and new DA. **(A)** Whole-mount Krt17 and **(B)** alkaline phosphatase (AP) staining revealed lack of new HFs in circular excisional wounds in rats at PWD40. **(C)** Whole-mount OilRedO staining confirms the absence of new HFs based on the lack of OilRedO$^{+}$ sebaceous glands (SGs) and **(D)** new DA in circular excisional wounds in rats. Size bars: A, B, D – 100 µm.

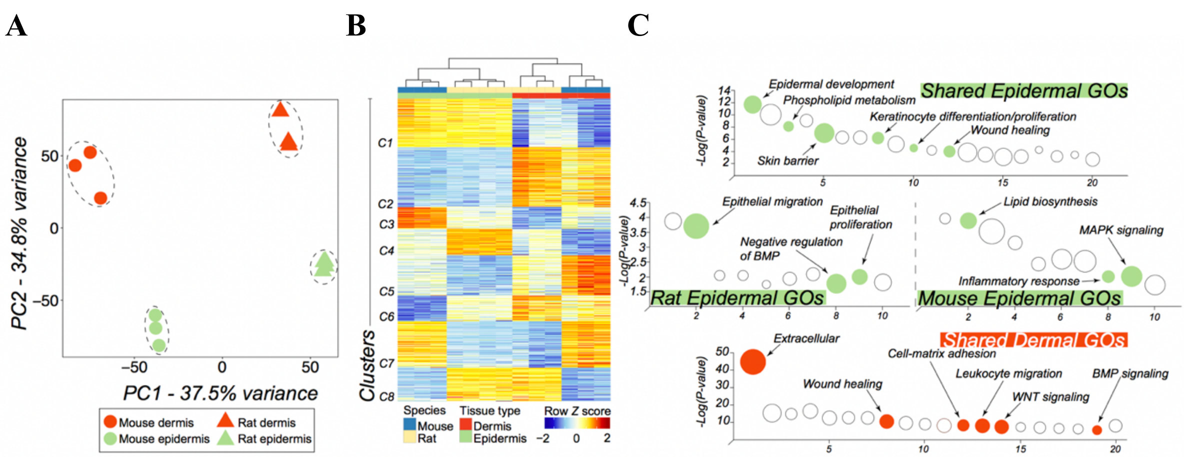


**Figure 2.3. Interspecies transcriptome analyses of wound tissues**. **(A)** Principal Component Analysis (PCA) reveals distinct separation between tissue types (wound epidermis and dermis) and between species (mouse *vs.* rat wound tissues). **(B)** Heat map representing 3,850 differentially expressed one-to-one gene orthologs between mouse and rat wound tissues grouped into eight different clusters. **(C)** Pathway analysis on gene clusters #1 (shared epidermal genes), #2 (shared dermal genes), #3 (mouse-specific epidermal genes) and #4 (rat-specific epidermal genes).

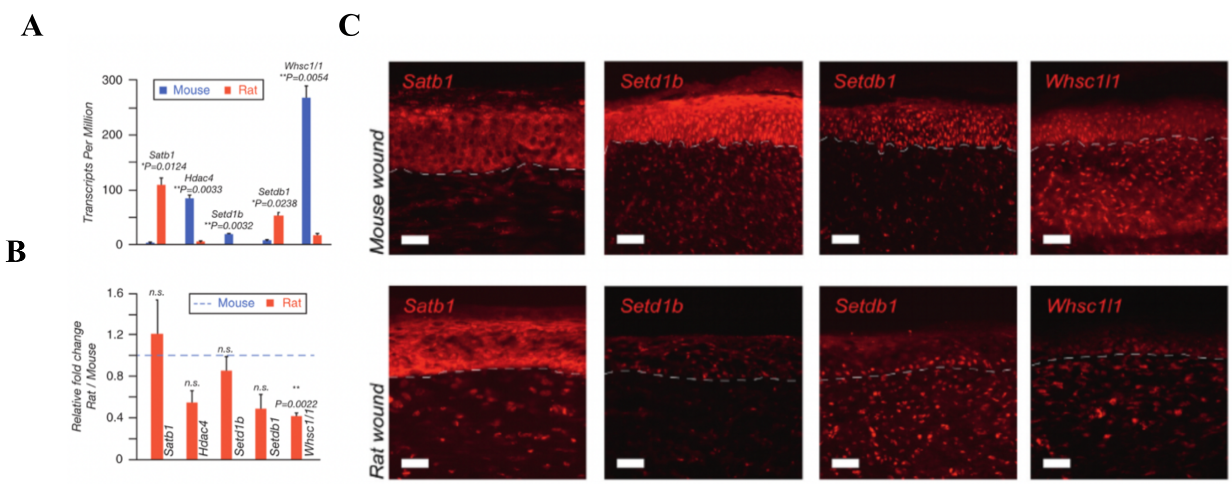


**Figure 2.4. Validation of epigenetic factors in mouse and rat wounds**. **(A)** Rat and mouse TPM values for select epigenetic factors from differentially expressed one-to-one gene orthologs. **(B)** qRT-PCR validation of select differentially expressed epigenetic factors between rat and mouse wound epidermis, including *Satb1, Hdac4, Setd1b, Setdb1* and *Whsc1l1*. **(C)** Immunostaining of mouse and rat wounds at the time of scab detachment for select epigenetic factors: Satb1, Setd1b, Setdb1 and Whsc1l1. Differential gene ortholog expression identification was performed at 5% FDR level and minimum 4X-fold change. Values in the graphs on **(A)** and **(B)** are means ± S.E.M. Two-tailed paired *t*-test in **(A)**, **P*=0.0124, ***P*=0.0033, ***P*=0.0032, **P*=0.0238, ***P*=0.0054; and in **(B)**, ***P*=0.0022. Size bars: C – 25 µm.

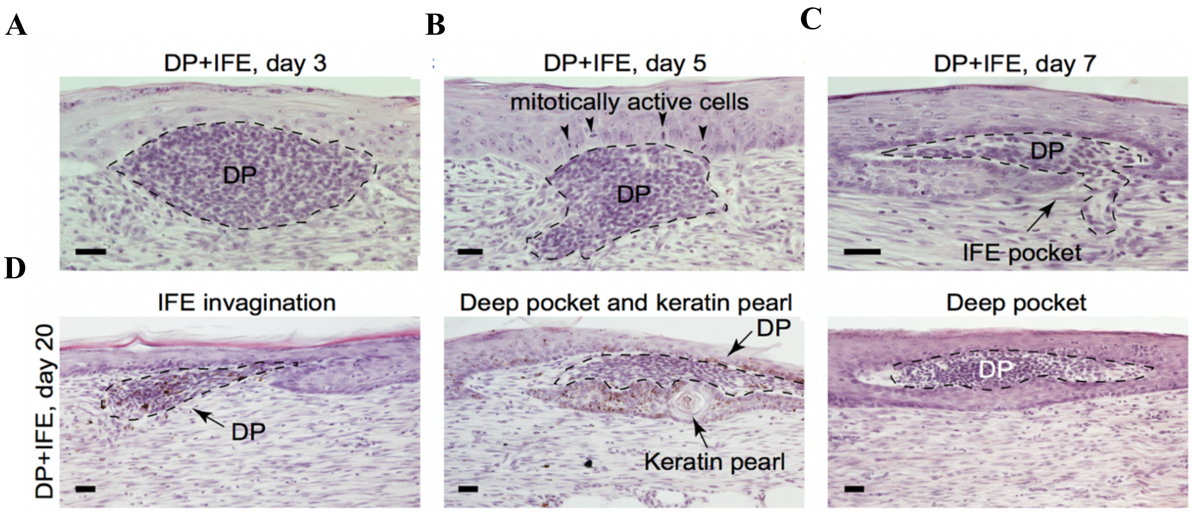


**Figure 2.5. Evaluation of IFE-DP interactions**. **(A-C)** Upon co-transplantation with IFE, DPs induce epidermal hyperplasia and rearrangements with complex DP-IFE structures forming as early as day 7 (n=5 per time point). **(D)** DPs and IFE often undergo extensive remodeling, with IFE forming pocket-like invaginations and with DPs assuming elongated, tongue-like shapes by day 20 (n=5 per time point). Representative images are shown. Size bars: A-D – 20 µm.

# CHAPTER 3

## Regeneration of fat cells from myofibroblasts during wound healing

From:

Plikus MV, Guerrero-Juarez CF, Ito M, *et al*, Regeneration. Regeneration of fat cells from myofibroblasts during wound healing. *Science*. (2017). Feb;17;355(6326):748-752. Reprinted with permission from AAAS.

**Statement of contribution**

In this study, I designed (in agreement with my thesis advisor Dr. Maksim V. Plikus) and performed experiments, analyzed data and interpreted results. My data contributes to Figures 3.2, 3.3, 3.4, 3.5, 3.6, 3.7, 3.8, 3.9, 3.10, and 3.11. Drs. Ricardo N. Ramirez and Rabi Murad aided and provided initial insight into the differential transcriptome analyses, including application and troubleshooting of MaSigPro/Next MaSigPro (Conesa et al., 2006, Nueda et al., 2014) (Related to Figs. 3.5 and 3.6).

## ABSTRACT

The skin of mice regenerates hair follicles after large excisional wounding. Dermal adipocytes, a lipid-laden cell in close association to hair follicles, also regenerate. These dermal adipocytes are very reminiscent of normal skin adipocytes and form only after hair follicles do. Lineage tracing suggests dermal adipocytes regenerate from myofibroblasts. Using bulk RNA-sequencing from genetically labeled myofibroblasts isolated from various time points during wound healing, it was established that up-regulation of Zfp423 occurs at the onset of dermal adipocyte regeneration. Indeed, using two independent approaches, Zfp423 was shown to be expressed in cells juxtaposed to hair follicles. In Zfp423 KO mice, dermal adipocyte regeneration fails to take place. BMP signaling acts upstream of Zfp423. LDN-193189 treatment of wounded mice leads to lack of Zfp423 activation and subsequent failure to regenerate dermal adipocytes, despite forming otherwise normal looking hair follicles. Overexpression of the BMP antagonist, Noggin, in epithelial cells, leads to failure to regenerate dermal adipocytes. Temporal deletion of the Bmp receptor 1a (Bmpr1a) in myofibroblasts phenocopies the former two Bmp signaling ablation conditions. *In vitro* differentiation of skin dermal cells into adipocytes isolated from early wounds is dependent on Bmp4 and 2. These results demonstrate that myofibroblasts are *bona fide* precursor cells of dermal adipocytes in adult cutaneous wounds and that the observed myofibroblast-adipocyte reprogramming phenomenon observed depends on Bmp-Zfp423 signaling.

## INTRODUCTION

Cutaneous wound healing in adult mammalian organisms has long been regarded as a process that culminates with the formation of a collagen-rich scar, devoid of appendages, elasticity – i.e. elastin fibers, and lack of overall physiological, mechanical and, possibly, immune integrity (Zhang et al., 2015). Previous studies, however, have shown that when adult mice are challenged with large excisional dorsum wounds (i.e. $\geq 1.0$ $cm^2$), fully functional *de novo* hair follicles (HFs) sporadically regenerate at the center of the healing skin – such phenomenon is regarded as Wound Induced Hair Neogenesis (WIHN) (Gay et al., 2013, Ito et al., 2007). We discovered that dermal adipocytes, a complex tissue intimately and physiologically associated with HFs within the dermal portion of the skin (Reviewed in Driskell et al., 2014, Guerrero-Juarez and Plikus, 2018, Zwick et al., 2018) also regenerate after wounding (Figure 3.1). Detailed histological and whole-mount analyses demonstrated that such dermal adipocytes begin to appear in the wound bed around post-wounding day (PWD) 24, and become fully mature lipid-laden adipocytes by PWD28. Closer characterization of such dermal adipocytes revealed that they are morphologically and biochemically similar to those in normal, unwounded adult skin. For example, they are similar in terms of depth relative to skin surface, cell size and volume, and expression of the hormones Adiponectin (Hu et al., 1996) and Resistin (Steppan et al., 2001). An interesting observation is that dermal adipocytes only form after *de novo* HFs have regenerated and reached anagen stage, suggesting that mature HFs are important for this regeneration event. The observation of HFs and its associated dermal adipocyte tissue suggests that restricted embryonic events, such as HF development and adipocyte lineage pre-determination (Guerrero-Juarez and Plikus, 2018, Hausman et al., 1981), can become reactivated in adults under normal, non-artificial conditions as part of a repair mechanism following injury.

Myofibroblasts are known as the "culprit cell of scarring". They are responsible for wound contraction, remodeling of the extra-cellular matrix and secretion of pro-inflammatory cytokines (Hinz et al., 2012). In addition to skin, they are "common" modulators of wound healing and fibrosis in many organs including lung, liver, heart, kidney, and bone marrow (Kramann et al., 2015, Schneider et al., 2017). Myofibroblasts follow a typical differentiation pathway, which begins with the formation of a proto-myofibroblast and is triggered by mechanical stress; and continues with the transformation into a mature, alpha-smooth muscle actin-expressing myofibroblasts, which is mediated by mechanical tension and TGF-beta signaling (Tomasek et al., 2002). In the WIHN model, myofibroblasts begin to appear in the wound bed 5 days post-wound infliction, and by PWD12 there is a large number of alpha-SMA$^+$ myofibroblasts covering the entire wound bed (Plikus et al., 2017). In agreement with previous literature, we observed that alpha-SMA expression disappears in the wound bed cells (i.e. myofibroblasts) but remains in peripheral blood vessel cells at the end of wound closure (i.e. re-epithelialization) (Darby et al., 1990, Gabbiani, 2003). This might be explained by the fact that granulation tissue, i.e. myofibroblasts, undergo cellular death via apoptosis. These observations have definitely been shown in small excisional wound models but not within the context of WIHN. Whether myofibroblasts undergo other processes is unknown – i.e. de-differentiation into a primitive fibroblast stage or trans-differentiation into a distinct cell lineage. We interrogated the origin and mechanism of regeneration of dermal adipocytes in the WIHN model. Because of the dynamics of myofibroblast differentiation in large wounds, and the activation of adipogenic markers observed after myofibroblasts cease to express alpha-SMA, we hypothesized that a subset of myofibroblasts can adopt an alternate adipogenic fate in regenerating skin.

## RESULTS

To address this hypothesis, lineage tracing using conditional *Cre*$^{ER}$-*loxP* technology (Kretzschmar and Watt, 2012) was performed. The contractile cell-specific, inducible *Sma-Cre*$^{ER}$ mouse strain (Wendling et al., 2009) was used. In this mouse model, tamoxifen-dependent activation of *Cre*$^{ER}$ strictly occurs in smooth muscle cells – including myofibroblasts, and crossed them with two independent reporter strains, *tdTomato*$^{STOP/loxP}$ (Madisen et al., 2010) and *R26R*$^{STOP/loxP}$ (Soriano, 1999). These reporters contain a STOP cassette flanked by *loxP* sites and, when crossed with a *Cre* transgenic strain, the STOP sequence is removed and the cell and their downstream progeny will be permanently labeled with that particular reporter system. Hence, this enabled us to reliably label myofibroblasts and their potential downstream progeny.

The efficiency and reliability of this reporter system to label myofibroblasts in regenerating wounds was tested (Fig. 3.2). To do this, two induction protocols were designed, one before (Fig. 3.2.A) and one after wounding (Fig. 3.2.B). In the first treatment regime, mice were induced two weeks prior wounding for five consecutive days. In the latter case, we created a 1.5 x 1.5 cm squared wound (2.25 cm$^2$) in the dorsum of adult mice and induced with tamoxifen at PWD 6-16. In both cases, wound tissues were collected at PWD28 for analyses. As expected, no labeling of myofibroblasts was observed when induced before wounding, but sporadic labeling of vascular smooth muscle cells in the wound became labeled with the reporter (van der Loop et al., 1997). On the contrary, the entire wound bed became labeled with the reporter when induced after wounding (Figure 3.2.A *vs.* 3.2.B). A similar wounding and induction protocol was performed and collected *Sma-Cre*$^{ER}$*;R26R* wounds (n=6), these were stained with X-gal and counter-stained with Oil Red O (OilRedO), a glycerol-based lipid dye specific to adipocytes (Mehlem et al., 2013), to analyze the number of reporter-labeled OilRedO-positive dermal adipocytes in regenerated skin wounds (Figure 3.3.A). Peri-lesional dermal adipocytes are not labeled by the reporter system (Fig. 3.3.B)

To further validate these initial lineage tracing studies and show a myofibroblastic origin of dermal adipocytes in cutaneous regeneration, peroxisome proliferator-activated receptor gamma (*Pparg*), a transcription factor important for maturation and lipid accumulation of pre-adipocytes (Siersbaek et al., 2010) was deleted. *Ppar-gamma*$^{loxP}$ mice (He et al., 2003) were crossed with conditional *Sma-Cre*$^{ERT2}$ mice to achieve specific *Ppar-gamma* deletion in myofibroblasts and their downstream progenies. The number of regenerated dermal adipocytes was quantified using a dermal adipocyte (DA) / hair follicle (HF) index ($I_{DA/\mathrm{HF}}$) (Plikus et al., 2017), which takes into account the number of dermal adipocytes relative to hair follicles in hair-bearing portions of the skin wound. This regeneration metric is reliable and easily quantifiable. By employing a similar induction protocol following wounding, it was shown that deletion of *Ppar-gamma* in myofibroblasts reduced the number of wound adipocytes compared to littermate controls ($I_{DA/HF}$ = 0.5 ± 0.07 vs. 22.7 ± 5.1, n=6; represented as avg ± s.e.m.) despite the formation of fully mature hair follicles (Figure 3.3.C). Taken together, these independent genetic lineages tracing and functional analyses suggested a myofibroblastic origin of dermal adipocytes in regenerating skin.

Next, the molecular mechanisms important for regeneration of dermal adipocytes from myofibroblasts during wound healing were determined. To do this, the transcriptome of myofibroblasts across wound healing was resolved. The dermal fraction from dorsal cutaneous wounds of adult *Sm22-Cre;tdTomato* mice was resected and viable myofibroblasts were FACS-sorted as *Zombie*$^{neg}$*;tdTomato*$^{hi}$ from four post-wounding time points which included: (1) PWD12 – which corresponds to initial wound closure and peak of myofibroblast presence, (2) PWD15 – which corresponds to active formation of new hair follicles, (3) PWD 21 – which corresponds to regeneration of dermal adipocytes, and (4) PWD26 – which corresponds to maturation of *de novo* dermal adipocytes (Fig. 3.4.A). SMART-seq2 (Picelli et al., 2013, Picelli et al., 2014) on whole RNAs isolated from viable, uncultured FACS-sorted *tdTomato*$^{hi}$ myofibroblasts was performed (Figure 3.4.B). Myofibroblasts displayed typical morphology in culture (Fig. 3.4.C). To identify unbiased gene expression profile changes in myofibroblasts across cutaneous wound healing, inferential statistical analyses using the two-step regression model algorithm *Next MaSigPro* was performed (Conesa et al., 2006, Nueda et al., 2014). *Next MaSigPro* identified 4,120 transcripts that showed statistically significant differential expression across all four time points analyzed ($P$<0.05) Principal component analysis (PCA) demonstrated that *Zombie*$^{NEG}$*;tdTomato*$^{hi}$ from individual wound healing time points clustered together (PC1 – 65.3% *vs*. PC2 – 18.0%), whether those from distinct time points did not, corroborating that pooled populations of myofibroblasts isolated across wound healing display unique and dynamic transcriptomic profiles (Figure 3.5, and 3.6). The expression patterns of all differentially expressed genes across wound healing was determined using *K*-means clustering and plotted on a heat map (Fig. 3.6.A). These differentially expressed transcripts were grouped into five distinct clusters: Cluster C1 contained 1,412 transcripts and displayed genes that were up-regulated on PWD12 and down-regulated by PWD21, (ii) Cluster C2 contained 1,244 transcripts that were up-regulated on PWD12 and 15 and down-regulated on PWD26, (iii) Cluster C3 displayed 379 transcripts in that displayed transient dynamics and appear up-regulated on PWD15 and 21 compared to PWD 12 and 26, (iv) Cluster C4 contained 688 transcripts up-regulated on PWD 21 and 26 and, lastly, (v) Cluster C5 contained 397 transcripts that were up-regulated on PWD26. These differentially expressed genes grouped into seven distinct gene ontologies (GOs) (Figure

3.6.B). Interestingly, the number of enriched cell cycle regulators significantly decreased during late post-wounding time points. Similar temporal gene dynamics (i.e. down-regulated gene categories on late PW time points) were observed for transcriptional regulators, epigenetic enzymes and inflammatory pathway genes. Contractile genes became down-regulated after PWD15, consistent with the shutdown of the active contractile state by myofibroblasts during late wound healing stages and preceding dermal adipocyte regeneration.

Signaling pathways were also identified to be differentially expressed across the time course (Fig, 3.6.C). WNT ligands, previously regarded as negative regulators of adipogenesis (Kennell and MacDougald, 2005, Kirton et al., 2007, Ross et al., 2000), were down-regulated in early stages of wound healing. Among the most significant ligands are *Wnt2b* (-3.8x), and *Wnt7b* (-1.2x). Conversely, WNT soluble antagonists were up-regulated in late stages of wound healing; these included *Dkk2* (+14.3x), *Wif1* (+32.5x) and *Sfrp4* (+2.3x) (Park et al., 2008). Members of the Bone Morphogenic Protein (BMP) pathway (Hata et al., 2003, Jin et al., 2006, Sottile and Seuwen, 2000) showed dynamic expression and appeared consistent with BMP activation at late post-wounding stages, merely on PWD21 and 26. BMP antagonists *Bambi (-1.6x)* and *Grem1 (-3.5x)* were down-regulated, while BMP ligands *Bmp4 (+5.0x)* and *Bmp7 (+7.4x)* became upregulated in late post-wounding time points. *Id1 (+2.0x)* and *Id2 (+1.7x)*, known direct BMP transcriptional targets, were also up-regulated on PWD26. BMP receptor 1a (*Bmpr1a*) was transiently up-regulated on PWD15 and 21. The dynamics in gene expression on BMP signaling members suggest that this signaling pathway may be important in regeneration of dermal adipocytes during wound healing.

Known modulators of adipogenesis, including negative regulators, such as *Nr2f6 (-1.4x)* (Pelaez-Garcia et al., 2015) and *E2f4 (-2.1x)* (Landsberg et al., 2003) were down-regulated, while *Zfp423 (+2.6x)* (Addison et al., 2014, Gupta et al., 2010, Gupta et al., 2012, Kang et al., 2012, Yun et al., 2015, Zhang et al., 2015), *Crebl2 (+1.9x)* (Ma et al., 2011), *Stat5b (+1.7x)* (Gao et al., 2015, Stephens et al., 1999, Wakao et al., 2011), and *Klf15 (+2.6x)* (Lee da et al., 2016, Mori et al., 2005) were upregulated. Other established and differentially expressed negative regulators of adipogenesis, including *Dlk1 (-10.5x)* (Lee et al., 2003, Mitterberger et al., 2012, Moon et al., 2002, Mortensen et al., 2012, Nueda et al., 2007, Smas et al., 1997, Smas and Sul, 1993) and *Mest (-23.9x) (Karbiener et al., 2015)*, were downregulated (early in time course), while *Agouti (+2.2x)* (Mynatt and Stephens, 2001, 2003), a known positive regulator, was up-regulated (late in time course). Interestingly, transcriptional regulators or chondrogenic and osteogenic lineages, including *Sox9* (-2.7x), and *Runx2* (-2.9x) (Ohba et al., 2015, Yoshida et al., 2002) were down-regulated in early stages of wound healing in myofibroblasts, suggesting that myofibroblasts reprogram into an adipocyte lineage rather than a osteo/chondrogenic one.

Of interest was the upregulation of *Zfp423*, a transcription factor with known roles in adipocyte lineage commitment *in vitro* (Gupta et al., 2010) (Fig. 3.6.C). Ii was hypothesized that Zfp423 could be important in initiation of adipogenesis in myofibroblasts. Indeed, analyses of PWD21 *Zfp423[XH542]* mouse wounds (Warming et al., 2006) show transactivation of Zfp423 (by means of LacZ activity) in areas of wound immediately adjacent to neogenic hair follicles. I then evaluated how whole-body knockout of Zfp423 would affect *de novo* dermal adipogenesis. Mice null for Zfp423 display ataxia, tremors and brain malformations associated with a proliferation and differentiation defect of neural precursor cells (Alcaraz et al., 2006). To determine whether Zfp423 is important for pre-adipocyte commitment of myofibroblasts in this *in vivo* model of dermal adipocyte regeneration, a *Zfp423* null mouse (*Zfp423[nur12]*) (Alcaraz et al., 2006) was used and its ability to form adipocytes following injury was interrogated. Few-to-none dermal adipocytes in the wound bed regenerated, despite the formation of normal hair follicles ($I_{DA/HF}$ = 0.07 ± 0.06 vs. 29.6 ± 5.4, n=9) (Figure 3.7). An interesting observation is that *Zfp423[nur12]* mice are not lipodistrophic, suggesting the presence of an alternate, surrogate mechanism driving adipogenesis during development. In contrast, *de novo* dermal adipocyte regeneration in the wound bed following injury seemed to be strictly dependent on expression of Zfp423, as *Zfp423[nur12]* mice do not readily regenerate dermal adipocytes post-injury.

*Zfp423* is known to contain Smad binding sitess the downstream effectors of BMP signaling (Rahman et al., 2015), which allow it to regulate expression of downstream target genes, including *Ppar-gamma* (Gupta et al., 2010, Hammarstedt et al., 2013). Hence, these observations suggest an interplay between *Zfp423* and BMP ligands that may regulate adipogenesis. Indeed, BMP signaling has been implicated in adipocyte differentiation *in vitro* (Jin et al., 2006, Wang et al., 1993). Next, it was determined whether BMP signaling may be an important regulator of dermal adipocyte regeneration in our *in vivo* model of skin regeneration and act via Zfp423 to induce dermal adipogenesis. To determine this possibility, BMP signaling was down-modulated in regenerating skin using three independent and distinct approaches. Previous studies identified Dorsomorphin as a compound with moderate inhibitory effects of BMP type I receptors ALK2, ALK3, and ALK6, allowing for blockage of BMP signaling activity by preventing phosphorylation of Smad1/5/8 and preventing translocation of the Smad/Co-Smad complexes into the nucleus and further preventing activation of BMP target genes. However, the inhibitory activity of Dorsomorphin proved only to be moderate and lacked metabolic stability *in vivo* (Yu et al., 2008b). In order to address these two issues, Cuny *et al.* conducted a structure-activity relationship study of Dorsomorphin and identified a superior compound capable of increased inhibitory activity and higher metabolic stability following intraperitoneal administration in rodents (Cuny et al., 2008). This compound, termed 4-[6-[4-(1-Piperazinyl)phenyl]pyrazolo[1,5-a]pyrimidin-3-yl]-quinole hydrochloride, commercially known as LDN-193189, was used to treat postnatal ossification in a mouse model of Fibrodysplasia Ossificans Progresiva (FOP) (Yu et al., 2008a), as well as prevention of the development of anemia in mice (Mayeur et al., 2015), showing its wide use *in vivo* and specificity towards blocking canonical BMP signaling. Hence, LDN-193189 was used to down-modulate BMP signaling activity in our *in vivo* model of skin regeneration.

Non-specific pharmacological ablation of BMP signaling activity in *Adipoq-Cre;R26R* mice using LDN-193189 at 2.0 mg/kg every 24 hours (Fig. 3.8). The treatment period ranged from PWD10-27. The efficacy of BMP down-modulation was determined by assessing the regeneration of fully matured lipid-laden dermal adipocytes based on OilRedO dye uptake at PWD28 (Fig. 3.8.B). Importantly, there was no adverse effects on rate of wound re-epithelialization and/or overall hair follicle regeneration (Lewis et al., 2014), rather, a reduced number of Zfp423-expressing dermal cells around neogenic hair follicles (Fig. 3.8.A) and dermal adipocytes (3.8.B) in LDN-193189-treated mice compared to vehicle-treated controls, despite the formation of normal neogenic hair follicles ($I_{DA/HF}$ = 0.58 ± 0.35 vs. 5.8 ± 1.4, n=7/4, respectively) was observed and further indicating a role for BMP signaling in expression of *Ppar-gamma* (Hammarstedt et al., 2013). Potential explanations for these phenotypic effects are 1) inhibition of Zfp423-mediated adipogenic pathway (prevention of entry to pre-adipocyte lineage), or 2) prevention of *Ppar-gamma* expression and subsequent differentiation.

To further interrogate the function of BMP signaling in dermal adipocyte regeneration, BMP signaling was down-modulated using two distinct mouse genetic models. In the first model, the soluble antagonist Noggin was up-regulated in basal keratinocytes of the interfollicular epidermis using *Krt14-Noggin* mice (Plikus et al., 2004) (Fig. 3.9.A). In this mouse model, up to four copies of Noggin are over-expressed under the endogenous Krt14 promoter. Hence, Noggin is specifically over-expressed in the basal epidermal layer of the inter-follicular epidermis and outer root sheath of hair follicles (Coulombe et al., 1989). A reduced number of dermal adipocytes in *Krt14-Noggin* mice compared to WT controls ($I_{DA/HF} = 0.2 \pm 0.1$ vs. $30.6 \pm 6.3$, n=10) was observed and further indicated a role for BMP signaling in expression of *Ppar-gamma* (Figure 3.9.B). *Krt14-Noggin;Zfp423[XH542]* mice showed a lack of Zfp423 transactivation in hair-bearing portions of the wound bed at PWD21 (data not shown), further suggesting that Noggin affects activation of Zfp423. Subsequently, these mice do not regenerate dermal adipocytes despite regenerating hair follicles. Indeed, the hair follicles look very similar to those already described (Botchkarev et al., 2001, Botchkarev and Sharov, 2004). Second, *Sma-Cre*$^{ER}$*;Bmpr1a*$^{floxf/lox}$ mice were generated to achieve ablation of *Bmpr1a* specifically in myofibroblasts. A tamoxifen-induction regime similar to the one previously stated was employed and evaluated dermal adipocyte regeneration at PWD28. A reduced number of dermal adipocytes in *Sma-Cre*$^{ER}$*;Bmpr1a*$^{floxf/lox}$ mice was observed compared to *Bmpr1a* controls ($I_{DA/HF} = 23.9 \pm 1.5$ vs. $0.38 \pm 0.36$, n=3/6, respectively) (Figure 3.10).

Lastly, *in toto* single cells were isolated from PWD15 dermal skin wounds of *Sm22-Cre;tdTomato* mice and treated them *in vitro* with Bmp ligands to further show that activation of BMP signaling can reprogram them into adipocytes. PWD15 dermal wound cells were cultured in three different conditions, including 1) commercially available adipogenic differentiation media, 2) growth media containing hBMP2, and 3) growth media containing hBMP4. Only the dermal skin wound cells cultured under the presence of Bmp2 and Bmp4 were able to reprogram them into adipocytes as confirmed by uptake of Bodipy® (Fig. 3.11.A). This was further confirmed by up-regulation of *Ppar-gamma* (+4.4x), *Adipoq* (+16x), and *Resistin* (+12.6) (Fig. 3.11.B). Taken together, this chapter describes the phenomenon that regenerated hair follicles in large skin wounds can reprogram myofibroblasts into adipocytes by activation of a BMP-Zfp423 axis.

## DISCUSSION

It has been well-documented that the regenerative potential of complex tissues and organs in response to injury varies greatly between distinct animal species, ranging from mammals to amphibians. In this regard, the animal with the most superb regeneration potential is the axolotl, *Ambystoma mexicanum*. Axolotls can regrow a multitude of organs and organ systems (Bryant et al., 2017), including spinal cord (Rost et al., 2016), brain (Amamoto et al., 2016), and limbs (Holder et al., 1980). Recently, important molecular mechanisms regulating limb regeneration in the axolotl have been described (Nacu et al., 2016, Roensch et al., 2013, Sugiura et al., 2016). Additionally, novel genomic and genetic techniques may pave the way to further identify genes important in regeneration (Khattak and Tanaka, 2015, Nowoshilow et al., 2018). An interesting aspect of axolotl limb regeneration is that this process replicates aspects of normal embryonic limb development. Traditionally, the final outcome of adult mammalian wound healing was considered to be scarring. This was considered the default repair pathway in most, if not all, types of injury. Recent advances in our understanding of lineage plasticity and the identification of novel models of wound healing and regeneration has led to identification of exceptions to this paradigm. Some examples include regeneration of digit tips (Johnston et al., 2016, Lehoczky et al., 2011, Rinkevich et al., 2011) and hair follicle neogenesis and dermal adipocyte regeneration in the skin of mice (Ito et al., 2007, Plikus et al., 2017). Lineage studies suggest the structures in the regenerated digit tip of mice arise from fate-restricted progenitor cells only; further pointing out that multipotent progenitor cells or lineage transdifferentiation events are not observed in this model. In contrast, large excisional wounds in adult mice demonstrate lineage plasticity toward regeneration of hair follicles and dermal adipocytes. For example, *de novo* hair follicles in the WIHN model regenerate via lineage commitment of non-hair fated wound epidermis cells. Lineage tracing suggests that peri-wound hair follicle bulge cells do not contribute to this *de novo* structures and other cell types contributing to re-epithelialization only transiently (Ito et al., 2007, Plikus et al., 2012). In this chapter, the regeneration of dermal adipocytes from non-adipogenic myofibroblasts is described. Lineage commitment of myofibroblasts to adipose lineage occurs via Bmp signaling. Neogenic hair follicles secrete Bmp ligands that instruct myofibroblasts to commit to an adipose lineage via activation of Zfp423, the master regulator of adipogenesis (Gupta et al., 2010). Hence, this suggests that, unlike regeneration of digit tip in adult mice, dermal adipocytes regenerate by lineage commitment of non-adipogenic wound myofibroblasts. It is possible that injury size could evoke regeneration via lineage commitment rather than from lineage restricted progenitor cells.

The current paradigm suggests that wounds in mammals heal by scarring. Although myofibroblasts are necessary to elicit a normal wound healing response; high number of myofibroblasts can lead to excessive scarring and modulation of fibrogenic potential. For example, wounds in fetal human embryos heal without scar – presumably because they lack myofibroblasts and prominent inflammatory pathways (Rowlatt, 1979). Similarly, myofibroblasts are largely absent in other tissues that heal without scars, including wounds in African spiny mice (Seifert et al., 2012). Contrary to these reports is the finding that myofibroblasts can induce regeneration of dermal adipocytes in large excisional skin wounds. This regenerative potential is driven, in large part, by other cell types that instruct myofibroblasts to acquire certain lineages (i.e. lineage determination). For example, early during the wound healing response, immune gamma delta T cells instruct myofibroblasts to initiate hair follicle neogenesis via Fgf9 signaling (Gay et al., 2013). Following regeneration of the hair follicle, myofibroblasts can become dermal adipocytes to reconstitute skin after injury.

The identification that skin injuries in adult mice can regenerate without scar formation debunks the long-lasting paradigm that adult skin healing culminates with formation of a scar. Additionally, the report in this chapter that myofibroblasts can be reprogrammed into distinct cell types opens up new venues for modulation of scarring and fibrogenic behavior, not only in skin, but also in other tissues and organs prone to such conditions.

## METHODS

**Mouse strains.** The following mice were used in this study: *Sm22-Cre* (Boucher et al., 2003); *SMA-CreER* (Wendling et al., 2009); *tdTomato* (Madisen et al., 2010); *Zfp423[XH542]* (Marshall et al., 1985); *Zfp423[nur12]* (Alcaraz et al., 2006); *Pparγ-flox* (He et al., 2003); and *WT Axin Negative* inbred mice. *SMA-CreER* mice were obtained via MTA. Mixed background mice were used in this study.

**Genotyping.** Genotyping was performed on genomic DNA isolated from tail or ear. Tissues were digested using proteinase-K. Different thermocycler programs were used for each individual strain. The following primers were used: ***Sm22-Cre, Adipoq-Cre*****:** Gnrc-Cre-F: GCGGTCTGGCAGTAAAAACTATC; Gnrc-Cre-R: GTGAAACAGCATTGCTGTCACTT; Gnrc-Cre-Ctr-F: CTAGGCCACAGAATTGAAAGATCT; Gnrc-Cre-Ctr-R: GTAGGTGGAAATTCTAGCATCATCC. Expected results: Internal control: ~324 bps, Mutant allele: ~100 bps. ***ROSA - R26R*****:** ROSA-Mut: GCGAAGAGTTTGTCCTCAACC; ROSA-F: 5'-AAAGTCGCTCTGAGTTGTTAT; ROSA-R: GGAGCGGGAGAAATGGATATG. Expected results: Mutant: 340 bps, Heterozygote: 340 bps and 650 bps, Wild-type: 650 bps. ***Zfp423[XH542]*:** bgeo1F (aka ZH542-F): CGGTCGCTACCATTACCAGT; bgeo1R (aka ZH542-R): TCGTCCTGCAGTTCATTCAG. Expected results: ~ 300 bp. ***Zfp423[nur12]*:** nur12-5'SNP-wt(3): GAGCTACTTGAAGAGGCATGAAC; nur12-5'SNP-mt(3): GAGCTACTTGAAGAGGCATGAAT; nur12-5'end: CTGCAGATGGTGATGACGAC; nur12-3'(1): 5'- GAGCTGGTGGAGGAGAAGC-3'. Expected results: Diagnostic band: ~200bps; Internal positive control: ~400bps. ***Bmpr1a*:** BmpR1a-Fx2: GCAGCTGCTGCTGCAGCCTCC; BmpR1a-Fx4: TGGCTACAATTTGTCTCATGC. Expected results: Wild type: 130 bps, Mutant 230 bps. ***tdTomato*:** TdTomato F: CGGATCCACCGGTCGCCACCATGGTGAGCAAGGGCGAGGAGGTC; TdTomato R: GAGCGGCCGCTTACTTGTACAGCTCGTCCATGCCGTACAG. Expected results: Mutant 200 bps, Wild type 300 bps.

**Wounding procedures.** All animal experiments were carried out in accordance with the guidelines of the IACUC of the University of California, Irvine. Full thickness 1.5 x 1.5 cm ($2.25cm^2$) excisional wounds were inflicted on the backs of three to eight week-old mice as previously described (Ito et al., 2007).

**Whole mount lacZ staining.** To detect lacZ activity, freshly isolated wound tissue samples were incubated with X-gal reagent in lacZ staining buffer as previously described (Ito et al., 2007, Plikus et al., 2017). Samples were post-fixed in 4% PFA.

**Whole mount OilRedO staining.** PFA-fixed wound tissue samples were pre-incubated in propylene glycol and then stained with OilRedO buffer for 20 minutes. Samples were then washed in propylene glycol and stored in 0.05% aqueous solution of sodium azide.

**RNA isolation and SMART-seq2.** Sorted, uncultured *Zombie*$^{neg}$*;tdTomato*$^{hi}$ myofibroblasts were re-suspended in RLT buffer supplemented with 1% beta-mercaptoethanol and homogenized with QIAshredder (Qiagen). Total RNA was isolated using the RNEasy Micro-Kit (Qiagen) as per manufacturer's protocol with minor modifications, including DNase I treatment (Qiagen). Optimal-quality RNAs were considered for cDNA library preparation (RIN>8.8). Full-length cDNA library amplification was performed as previously described (Picelli et al., 2013, Picelli et al., 2014). Briefly, 1ng total RNA was reversed-transcribed, and resulting cDNA was pre-amplified for 17 cycles. Tagmentation was carried out on 18ng cDNA using the Nextera DNA Sample Preparation Kit (Illumina). The tagmentation reaction was carried out at 55°C for 5 minutes and purified using PCR Purification Kit (Qiagen). Adapter-ligated fragments were amplified using limited cycle enrichment PCR with v2_Adx.x barcodes (IDT). Libraries were amplified for 7 continuous cycles and resulting libraries were purified with AMPure XP beads (Beckman Coulter). Library quantification was done using KAPA for Illumina Sequencing Platforms (Illumina). Libraries were multiplexed and sequenced as paired-end on an Illumina Next-Seq500 platform (Cluster density = 296K/mm2, Clusters PF = 71.2%, Q30 = 87.6%).

**Fluorescence-activated cell sorting.** Dorsal skin was collected from mice at different post-wounding time points. Scar tissue was micro-dissected, devoid of fascia and incubated in Dispase II solution (Sigma) to separate epidermis from dermis. Dermis was disaggregated into single cells with Collagenase IV (Sigma) at 37°C with constant rotation. Single cell fractions were stained with Zombie Violet™ (1:1000; BioLegend) and FACS-sorted as *Zombie*$^{neg}$*;tdTomato*$^{hi}$ using a BD FACSAria II flow cytometer (BD Biosciences).

**SMART-seq2 analyses.** Paired-end reads were aligned to the mouse genome (mm10/gencode.vM4) and quantified using the RNA-seq by Expectation-Maximization algorithm (RSEM) (version 1.2.12) with the following standard parameters: *rsem-calculate-*

*expression -p $CORES --paired-end* (Li and Dewey, 2011). Samples displaying >20,000,000 mapped reads and >75% mapping efficiency were considered for downstream analyses. Differential expression dynamics across our single time experimental series was identified using the two-step regression model algorithm MaSigPro with a P-value cutoff of 0.05 for multiple hypothesis testing and a false discovery control rate of 0.01 (Conesa et al., 2006, Nueda et al., 2014). Principle component analysis was performed using the R *ggbiplot* package.

**Primary mouse adipogenic cell culture.** Primary scar cells were isolated from day 15 wounds as previously described (Gay et al., 2013) with minor modifications. Single cell fractions were created and cultured to confluence in high-glucose DMEM (Gibco) supplemented with 10% FBS (Atlanta Biologicals) and 10,000 µl/ml Pen/Strep cocktail (Gibco). Upon confluency, cells were cultured in adipocyte differentiation media alone (Cell Solutions) or DMEM supplemented with 5µg/ml insulin (Sigma), and 1µM rosiglitazone (Sigma) with either 6ng/ml of recombinant hBMP4 (R&D Systems), or 25ng/ml of recombinant hBMP2 (R&D Systems), or differentiation media alone (Cell Solutions). After three days, cells differentiation media was switched to adipocyte maintenance media (Cell Solutions). Cells were cultured in a water-jacketed incubator at 37°C with 5% $CO_2$ output.

**Table 3.1.** Wound regeneration quantification.

| **Transgenic mouse line** | **Dermal adipocyte/hair follicle index** | ***P* value** | **Post-wounding day** | **N** |
|---|---|---|---|---|
| **Experiment: Inducible deletion of *Ppar-gamma* in myofibroblasts** | | | | |
| *Sma-Cre*$^{ER}$;*Ppar*$\gamma^{flox/flox}$ | 0.5 ± 0.07 | *P*<0.05 | Day 28 | 6 |
| *Sma-Cre*$^{ER}$;*Ppar*$\gamma^{flox/+}$ | 22.7 ± 5.1 | | Day 28 | 6 |
| **Experiment: Skin specific over-expression of soluble BMP antagonist Noggin** | | | | |
| *K14-Noggin* | 0.2 ± 0.1 | *P*<0.05 | Day 28 | 10 |
| WT | 30.6 ± 6.3 | | Day 28 | 10 |
| **Experiment: Inducible deletion of BMP receptor *Bmpr1a* in Myofibroblasts** | | | | |
| *Sma-Cre*$^{ER}$;*Bmpr1a*$^{flox/flox}$ | 0.38 ± 0.36 | *P*<0.05 | Day 28 | 6 |
| Tamoxifen treated control | 23.9 ± 1.5 | | Day 28 | 3 |
| **Experiment: Pharmacological treatment of mice with LDN-193189** | | | | |
| WT (LDN-193189 treated) | 0.58 ± 0.35 | *P*<0.05 | Day 28 | 7 |
| WT (Vehicle control) | 5.8 ± 1.4 | | Day 28 | 4 |

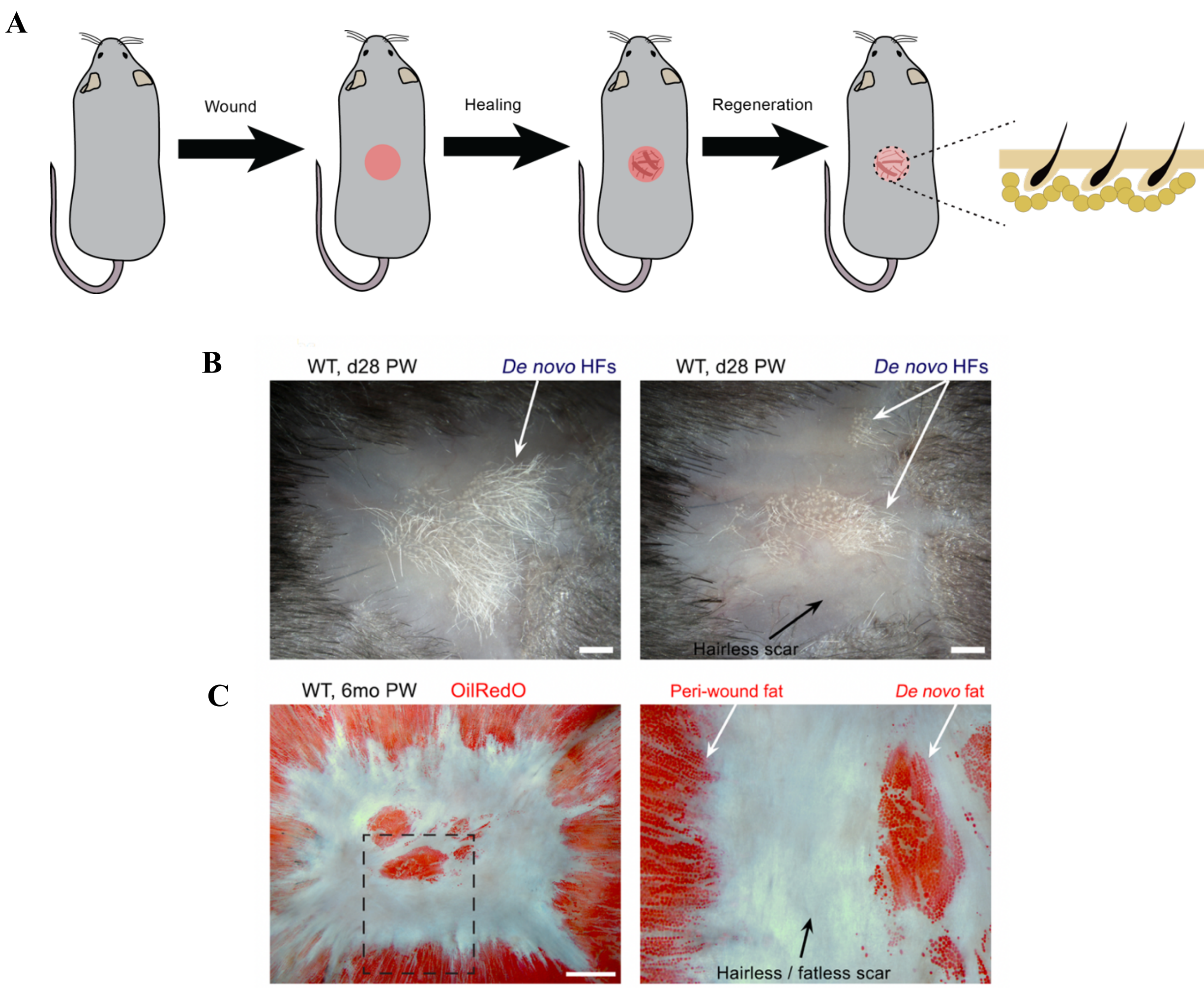


**Figure 3.1. Schematic of regeneration of hair follicles and fat in mouse wounds**. **(A)** In the model of Wound-Induced Hair Neogenesis (WIHN), adult mice are inflicted large excisional back skin wounds ($2.25cm^2$). 28 days post-wounding, mice regenerate **(B)** hair follicles and **(C)** dermal fat. Size bars: B-C – 1mm.

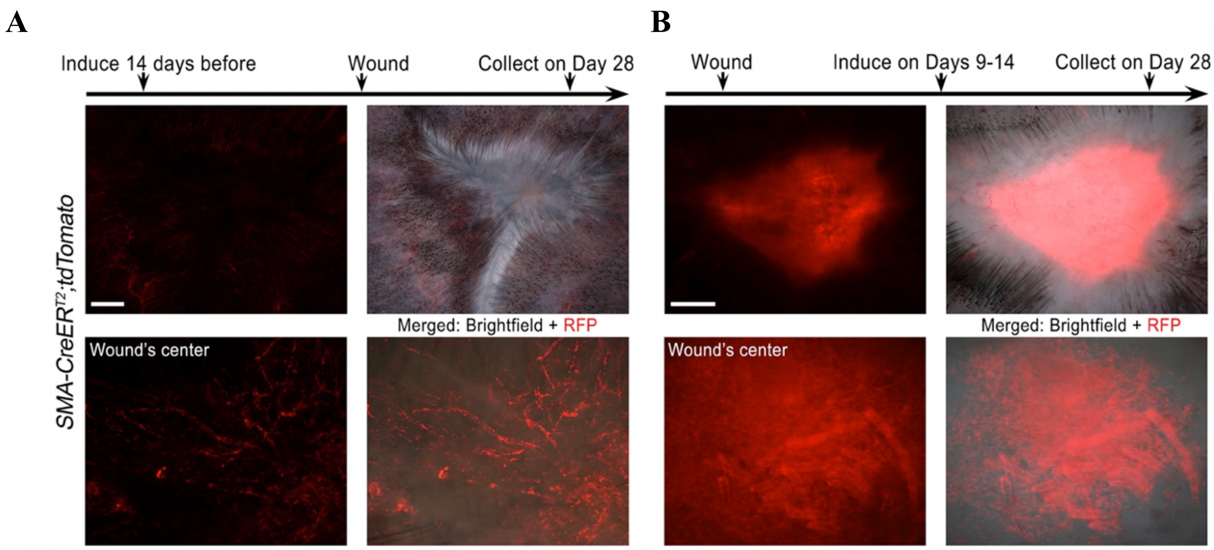


**Figure 3.2. Generation of *Sma-CreER;tdTomato* mice**. (A) Cre induction in *Sma-CreER;tdTomato* mice 14 days before wounding results in preferential labeling of vascular smooth muscle cells. In the second panel, (B) induction during days 9-14 after wounding results in labeling of myofibroblasts in the wound center. Size bars: A, B – 2mm.

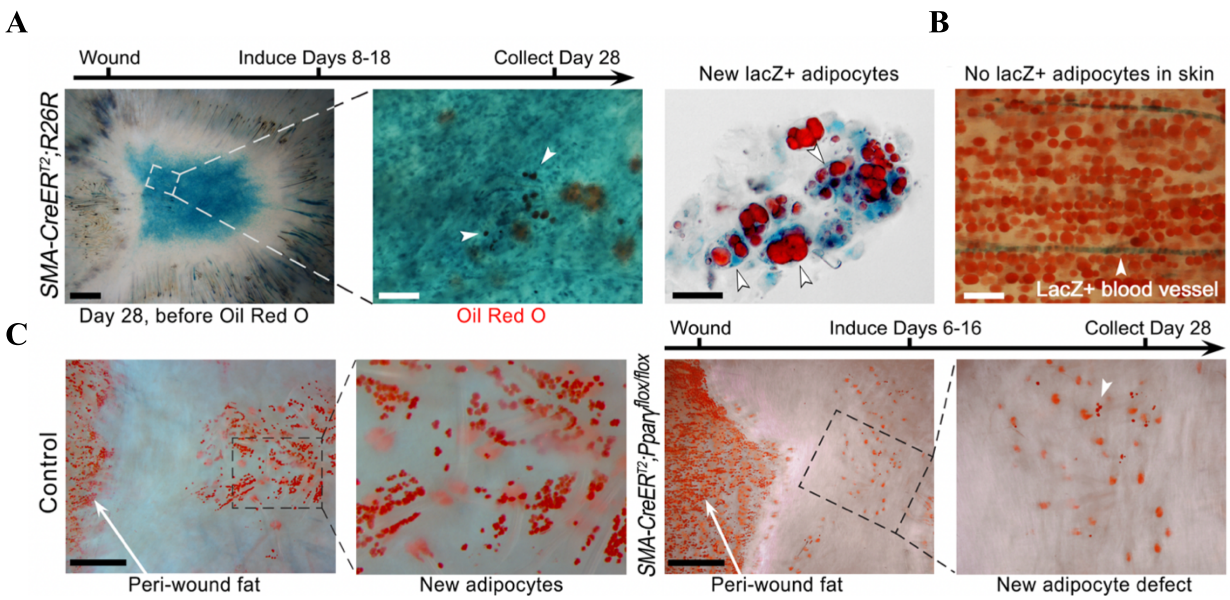


**Figure 3.3. Lineage tracing in mouse wounds**. **(A-C)** Functional lineage tracing identifies myofibroblasts as *bona fide* precursors of dermal adipocytes during wound healing. *Sma-CreER$^{T2}$;R26R* and *Sma-CreER$^{T2}$;Pparg$^{-/-}$* mice showed that **(A)** the origin of dermal adipocytes is myofibroblastic. **(B)** Dermal adipocytes in perilesional skin is not labeled by reporter. **(C)** Specific deletion of *Pparg* in myofibroblasts prevents differentiation into lipid laden adipocytes. Size bars: B (left), C – 1 mm; in A (center), 200 µm; in A (right), 50 µm; in C, 200 µm.

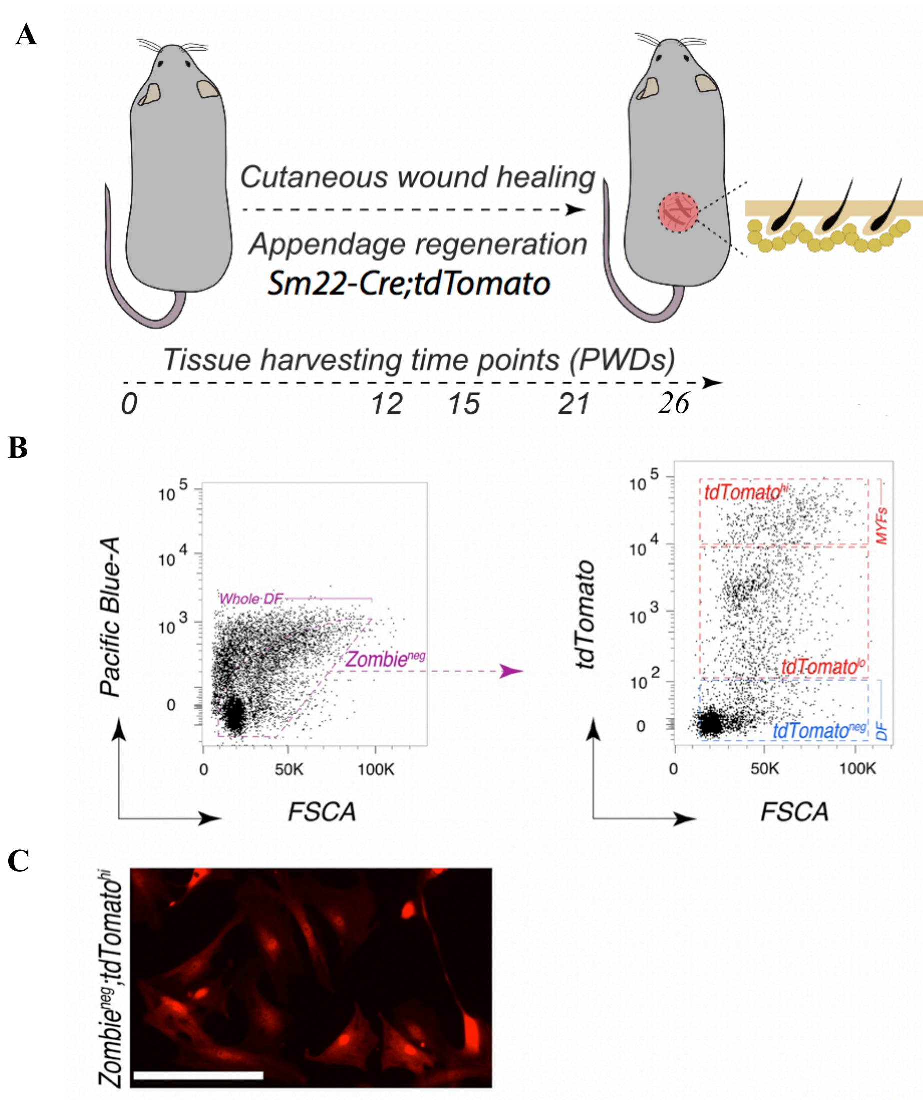


**Figure 3.4. Schematic of myofibroblast isolation and characterization**. **(A)** Myofibroblasts were isolated from various time points post-wounding, coincident with days were heightened myofibroblast presence is observed, hair follicle regeneration initiation, dermal fat regeneration initiation, and end of regeneration. **(B)** Viable myofibroblasts were isolated from cutaneous wounds from *Sm22-Cre;tdTomato* mice as *Zombie*$^{Neg}$*; tdTomato*$^{hi}$ across wound healing using fluorescent activated cell sorting (FACS). **(C)** Isolated myofibroblasts possess spindle shape-like morphology and express messenchymal genes, including *Vim,* and *Acta2*, and (data not shown). Size bars: C – 200µm.

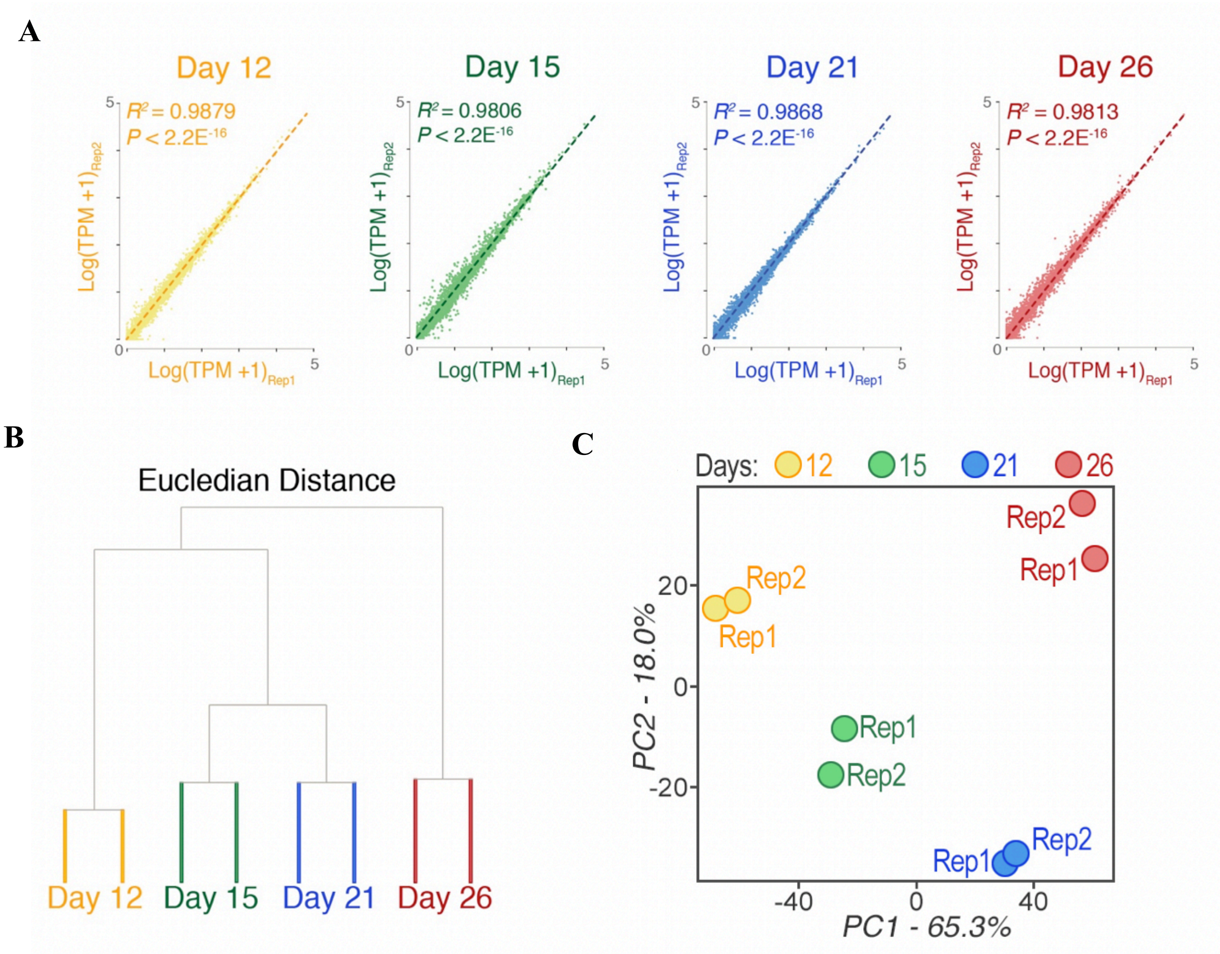


**Figure 3.5. PCA of myofibroblasts across wound healing**. SMART-seq2 was performed on freshly sorted, uncultured viable isolated myofibroblasts (sorted as *Zombie*$^{Neg}$*; tdTomato*$^{hi}$) across wound healing. **(A)** Biological replicates show strong Pearson correlation, suggesting high reproducibility and minimal technical variance. **(B)** Cladogram shows myofibroblasts from distinct post-wounding time points clustered together (biological replicates) and separately based on time point post-wounding from when they were isolated. **(C)** Myofibroblasts from distinct time points separate from each other (PC1 – 65.3% *vs.* PC2 – 18.0%).

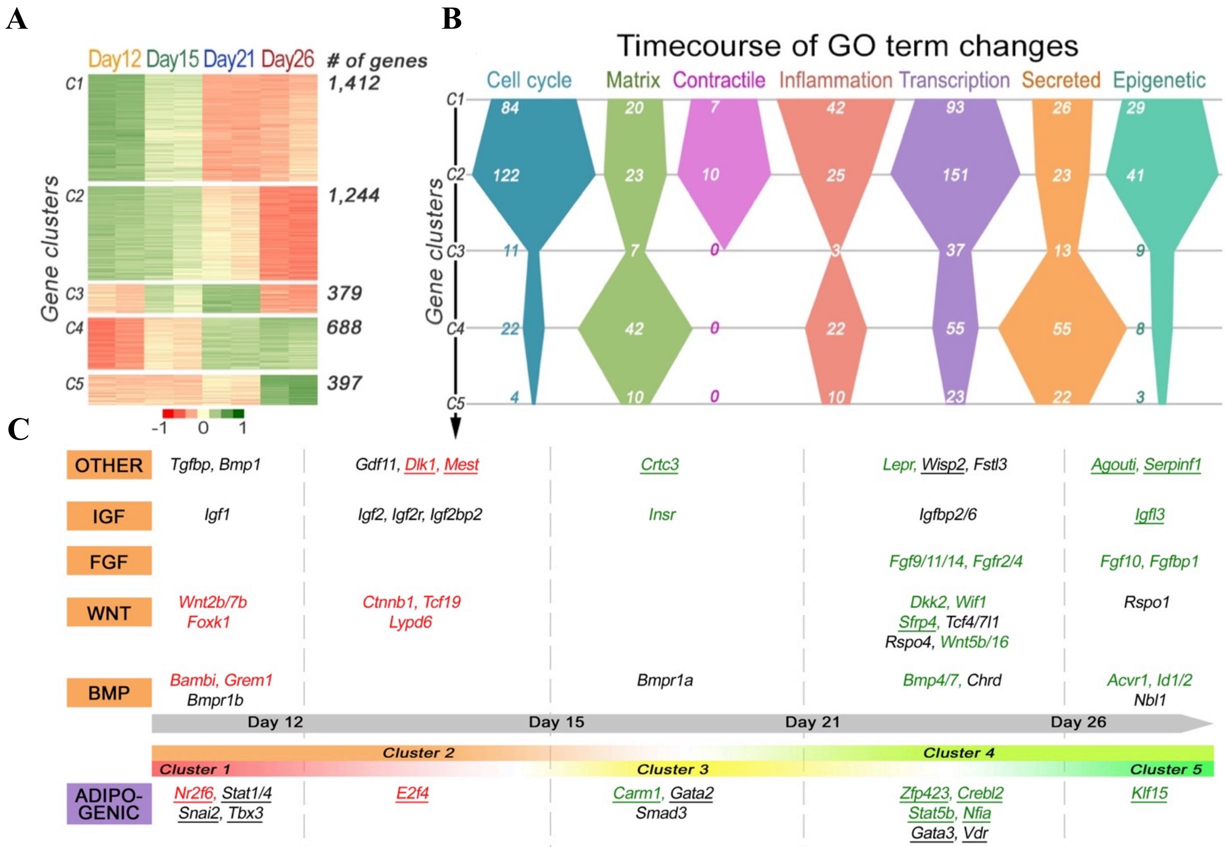


**Figure 3.6. Differential gene expression and distinct gene ontologies of myofibroblasts across wound healing**. **(A)** Inferential statistical analyses using Next MaSigPro identified 4,120 differentially expressed genes during wound healing ($P$<0.05) and form 5 distinct clusters (C1-C5) in heat map. **(B)** Gene Ontology (GO) terms identify significant changes in major pathways, including genes involved in cell cycle, matrix remodeling, contractile and epigenetic remodeling. **(C)** Gene scoring identified significant expression changes members of the IGF, FGF, WNT and BMP signaling pathways across wound healing. Zfp423 is shown to be differentially expressed at post wounding day 21.

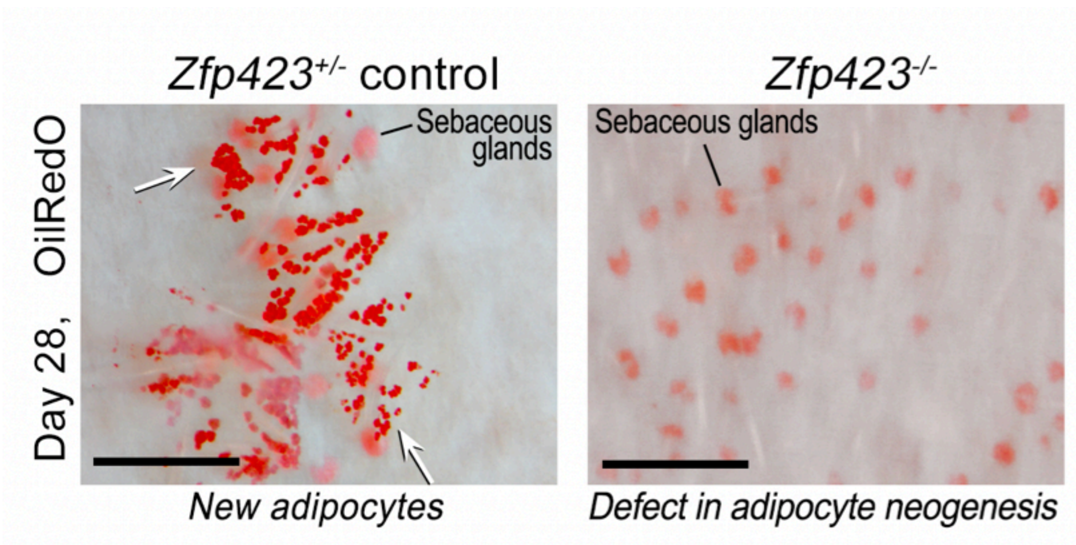


**Figure 3.7. Genetic ablation of Zfp423 leads to lack of dermal adipocyte regeneration in mouse wounds**. Whole body KO of Zfp423 leads lack of dermal adipocyte regeneration during wound healing, despite regeneration of hair follicles. Samples were collected 28 days post-wounding. Tissues were stained with OilRedO to visualize dermal adipocytes. Size bars: 100µm.

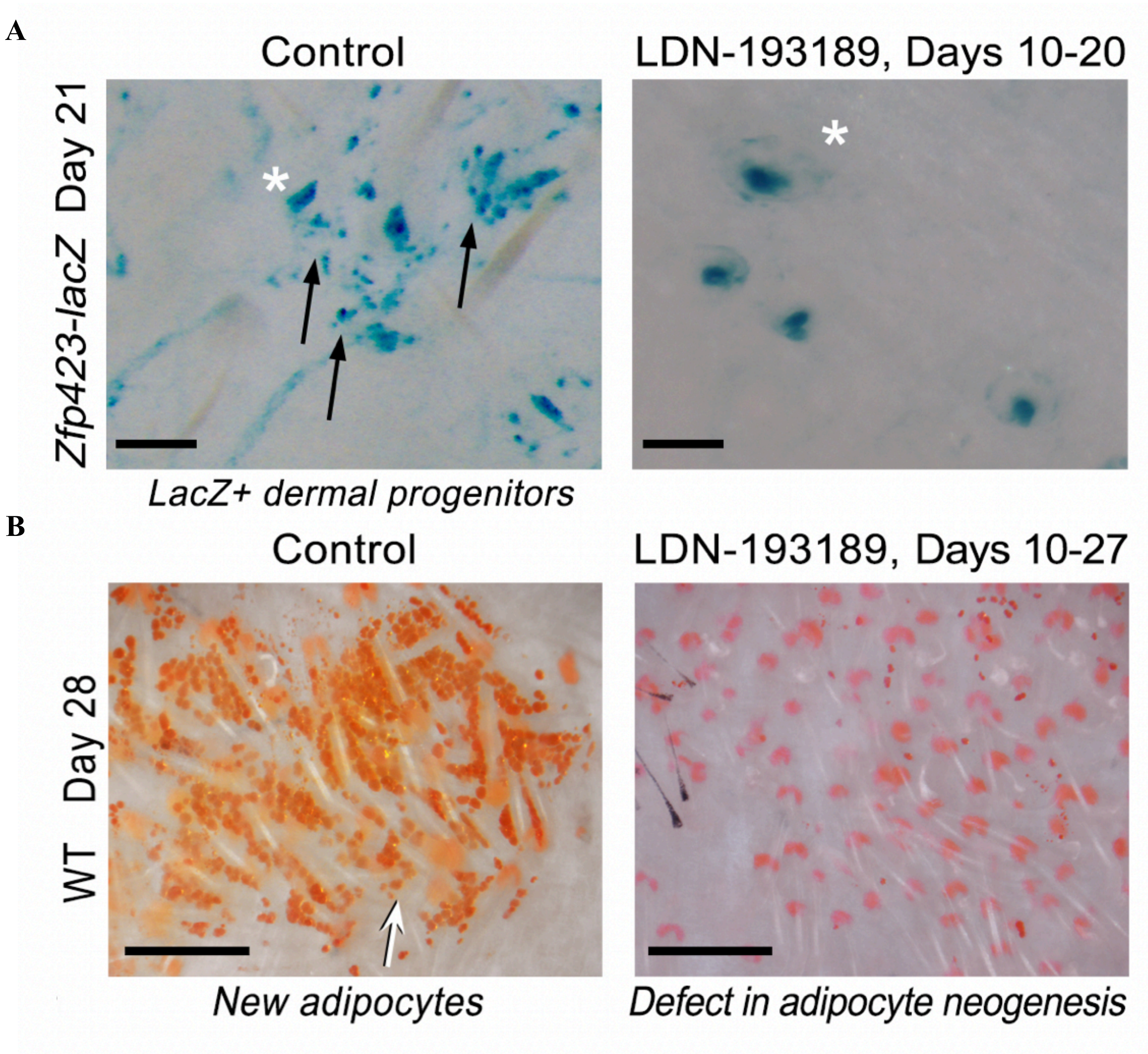


**Figure 3.8. Pharmacological downmodulation of BMP signaling in mouse wounds**. **(A)** Pharmacological inhibition of BMP signaling using LDN-193189 led to downregulation of Zfp423 expression in dermal cells juxtaposed to hair follicles and **(B)** ablation of dermal adipocyte regeneration despite the regeneration of otherwise normal looking hair follicles. Samples were collected 28 days post-wounding. Tissues were stained with OilRedO to visualize dermal adipocytes. Size bars: 100µm.

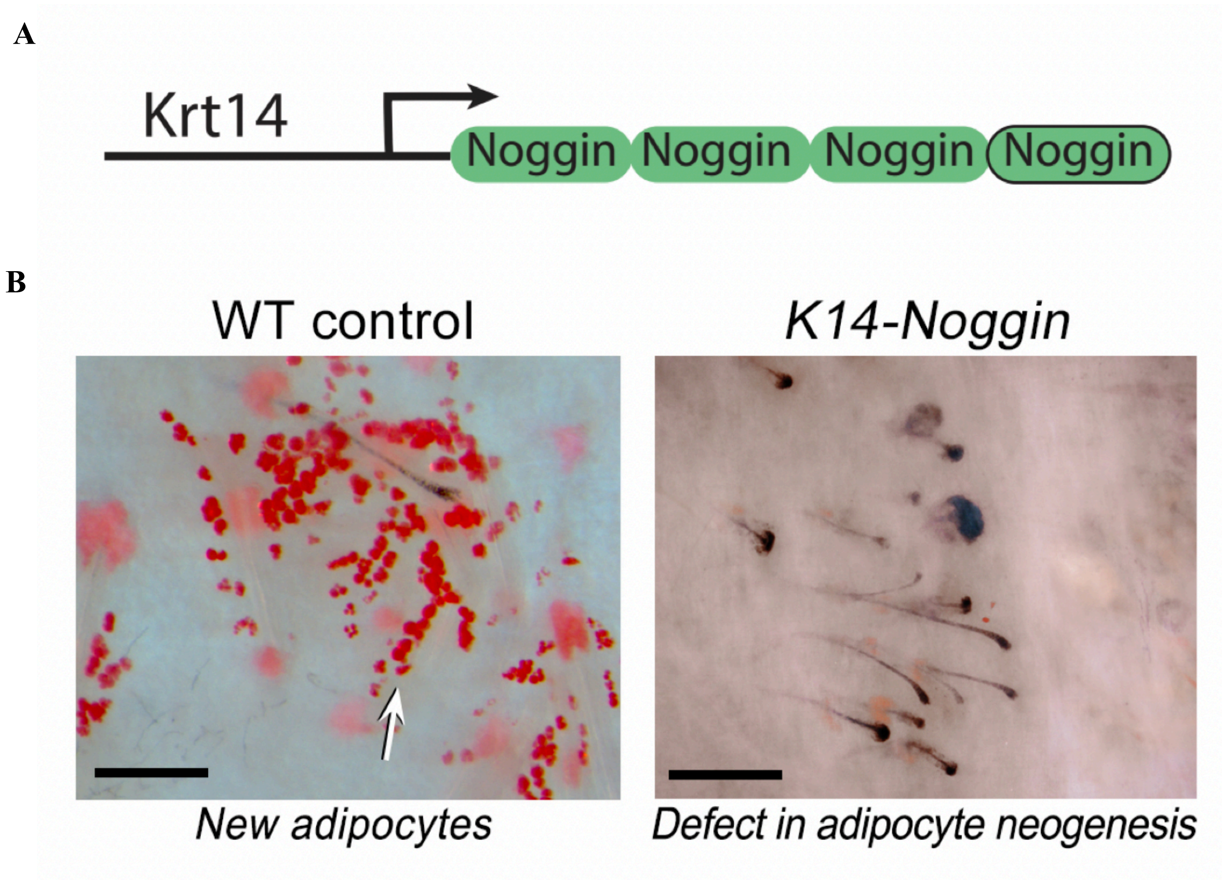


**Figure 3.9. Genetic downmodulation of BMP signaling in mouse wounds**. **(A)** Overexpression of Noggin in skin epithelium leads to **(B)** ablation of dermal adipocyte regeneration despite regeneration of hair follicles. Samples were collected 28 days post-wounding. Tissues were stained with OilRedO to visualize dermal adipocytes. Size bars: 100µm.

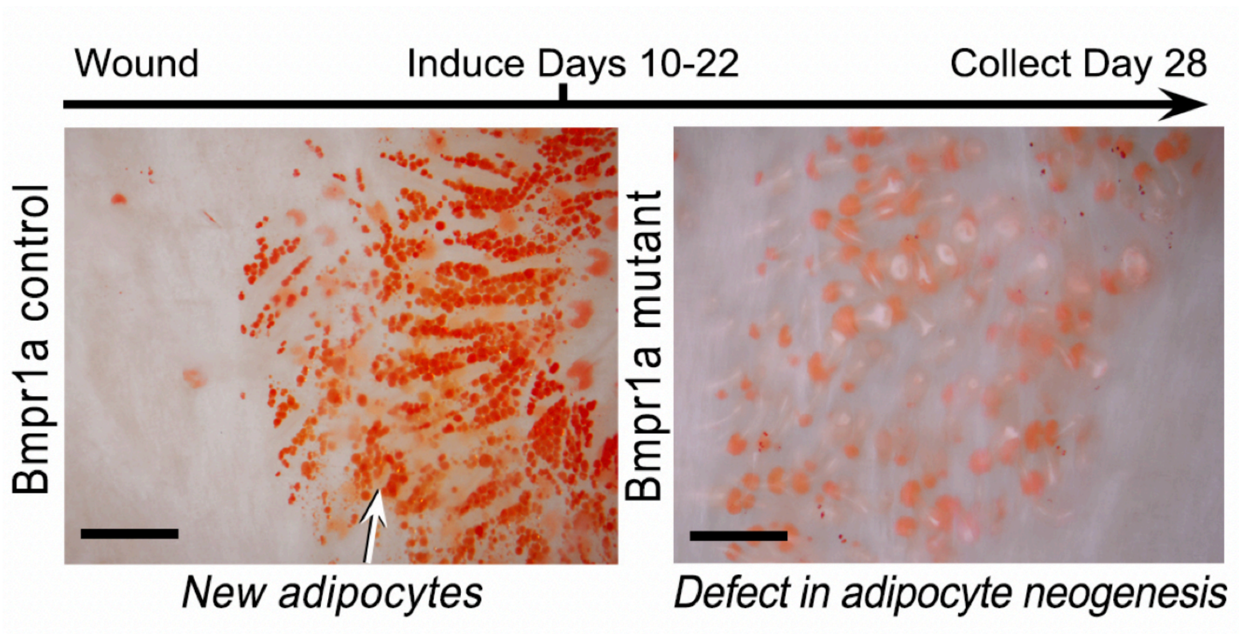


**Figure 3.10. Tissue specific ablation of BMP signaling in mouse wounds**. *Sma-CreER;Bmpr1a*$^{-/-}$ mice allowed to spatio-temporally ablate *Bmpr1a* specifically in myofibroblasts. BMPR1a deficient mice formed less adipocytes in the wound center. Samples were collected 28 days post-wounding. Tissues were stained with OilRedO to visualize dermal adipocytes. Size bars: 100µm.

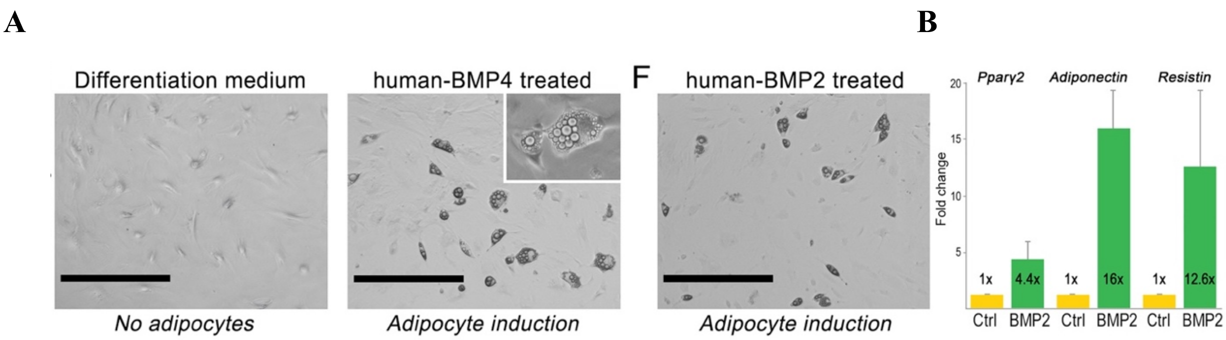


**Figure 3.11. Ectopic human BMP expression directs myofibroblasts to conversion into adipocytes *in vitro*. (A)** Total dermal cells isolated from early cutaneous wound tissues were cultured *ex vivo* in differentiation media or growth media supplemented with either hBMP4 or hBMP2. Only cells cultured in media supplemented with hBMPs differentiated into adipocytes. **(B)** qPCR analyses found white adipose-tissue gene expression up-regulation in hBMP-treated samples compared to differentiation medium only. Values in the graphs are represented as mean expression ± SEM. Size bars: A – 400µm. Values in graph are means ± SEM.

# CHAPTER 4

## Single cell transcriptomics reveals myofibroblast heterogeneity and hematopoetic-derived adipose progenitors during wound regeneration

### Statement of contribution

In this study, I designed (in agreement with my thesis advisor Dr. Maksim V. Plikus) and performed experiments, analyzed data and interpreted results. My data contributes to Figures 4.1, 4.2, 4.3, 4.4, 4.5, 4.6, 4.7, 4.8, 4.9, 4.10, and 4.11. I analyzed and interpreted data related to Fig. 4.12, 4.13, and 4.14. Dr. Suoqin Jin (University of California, Irvine) aided technically with single cell analyses and data visualization (Related to Figs. 4.2, 4.3, 4.4, 4.5, 4.6, 4.7, 4.8, 4.10, 4.11). Dr. Dennis Ma (University of California, Irvine) aided technically with single cell immunoblotting and its analyses (Related to Fig. 4.11). Dr. Priya Dedhia (University of Pennsylvania) aided technically with bone marrow transplantation (BMT) assays (Related to Fig. 4.11).

# ABSTRACT

During wound healing in adult mouse skin, hair follicles precede dermal adipocyte regeneration. Dermal adipocytes regenerate from contractile, mature myofibroblasts and is dependent on BMP-Zfp423 signaling. To interrogate the heterogeneity of fibroblasts in the wound, I used single-cell RNA-sequencing to profile skin wounds 12 days after wounding. This time coincides with the onset of appendage regeneration. Dimension reduction analyses clustered wound fibroblasts into twelve distinct groups – based on their unique mRNA signatures. Pseudotime analysis revealed that some of these clusters likely represent consecutive differentiation states, directed toward a contractile phenotype. Interestingly, one group of fibroblasts co-expressed contractile and myeloid markers, suggesting a putative hematopoietic origin. These findings were validated using single-cell western blot and full-length single-cell RNA-sequencing on FACS-purified, genetically labeled contractile wound cells. Using a series of bone marrow transplantation (BMT) experiments, it was confirmed that wounding recruits hematopoietic cells that give rise to myofibroblasts, which subsequently contribute to regeneration of new dermal adipocytes. Regenerated dermal adipocytes in wounds of BMT mice reconstituted with hematopoietic stem cells (HSCs) from fat-specific *Retn* reporter donors contained lacZ-positive dermal adipocytes. Furthermore, contribution of hematopoietic cells to regenerating dermal adipocytes was confirmed by lineage tracing in mice expressing the *R26R* reporter under the pan-hematopoietic *Cd45-Cre* and myeloid-specific *LysM-Cre* drivers. In conclusion, this chapter described that wounding induces a high degree of heterogeneity among wound fibroblasts and recruits highly plastic hematopoietic cells that contribute to dermal adipocyte regeneration.

# INTRODUCTION

Upon significant injury, such as full-thickness excisional wounding, skin undergoes extensive repair. While small skin wounds typically repair via re-epithelialization, significant contraction, and formation of scar tissue largely devoid of epidermal appendages and dermal adipocytes, large wounds can regenerate *de novo* hair follicles (Ito et al., 2007) and dermal adipocytes in their center (Plikus et al., 2017). Already noted in the classic literature (Billingham and Russell, 1956, Breedis, 1954, Brook et al., 1960, Stenbäck et al., 1967), this process of *de novo* hair follicle regeneration, now termed wound-induced hair neogenesis (WIHN), involves the reactivation of embryonic hair developmental programs within epidermal and dermal cells (Ito et al., 2007, Wang et al., 2015). Similarly, the process of *de novo* dermal adipocyte regeneration involves reactivation of an embryonic adipose lineage developmental program in myofibroblasts (Plikus et al., 2017). Beyond laboratory mice (Gay et al., 2013, Ito et al., 2007, Myung et al., 2013, Nelson Amanda M. et al., 2013, Nelson Amanda M. et al., 2015), WIHN has been definitively observed African spiny mice, member of the genus *Acomys* (Seifert et al., 2012), and in rabbits (Billingham and Russell, 1956, Breedis, 1954, Stenbäck et al., 1967). WIHN has also been documented in sheep (Brook et al., 1960) and in seldom occurs in humans (Gillman, 1955, Kligman Albert M. and Strauss John S., 1956, Muller, 1971) – where vellus hairs form after dermabrasion. However, WIHN appears lacking in the laboratory rat (Guerrero-Juarez et al., 2018).

Over the last decade, the signaling pathways for WIHN in mice have been partially elucidated. Activation of canonical WNT signaling in the center of the wound is necessary for WIHN (Gay et al., 2013, Ito et al., 2007, Myung et al., 2013) to take place, and both epidermal (Myung et al., 2013) and dermal wound cells secrete and respond to WNT ligands at distinct phases of regeneration (Gay et al., 2013). Production of WNT ligands by dermal wound cells is initiated by Fgf9, secreted by γδ T cells (Gay et al., 2013) and this positive forward feedback loop initiates regeneration of hair follicles. Macrophages also promote WIHN by secreting Tnfα, which, in turn, activates p-AKT/p-β-catenin signaling (Wang X. et al., 2017). Activation of Tlr3 signaling by double-stranded RNA released at the wound edge increases the production of Il6 and activates Stat3, both of which positively impact WIHN (Nelson Amanda M. et al., 2015). The pro-regenerative effect of Stat3 signaling in this context is mediated by TAp63 (Nelson et al., 2016). Contrary to Fgf9/WNT, TNF/p-AKT and Tlr3/Il6/Stat3 pathways, prostaglandin Pdg2 signaling inhibits *de novo* hair follicle regeneration in WIHN (Nelson Amanda M. et al., 2013). Furthermore, WIHN outcomes are prominently modulated by several transcriptional regulators, including the homeobox factor Msx2 (Hughes et al., 2018), zinc finger protein Cxxc5 (Lee et al., 2017) and RNA-binding protein Msi2 (Ma et al., 2017). *De novo* dermal adipocyte regeneration is activated by BMP ligands produced by growing neogenic hair follicles (Plikus et al., 2017). Wound myofibroblasts activate the transcription factor Zfp423, a transcriptional regulator that drives adipogenic lineage commitment (Gupta et al., 2010), leading to dermal adipocyte regeneration. Hair follicles are critical for dermal adipocyte, as no dermal adipocytes can regenerate in hairless wounds (Plikus et al., 2017).

While the signaling pathways for wound-induced hair follicle and dermal adipocyte regeneration have been partially elucidated, much less is known about the origin of both, the epithelial and mesenchymal cells competent for *de novo* regeneration (Plikus et al., 2012). Lineage tracing experiments by Ito et al. (2007) demonstrated that progeny of pre-existing Krt15-positive epithelial bulge stem cells from peri-lesional hair follicles do not give rise to *de novo* hair follicle components. Instead, lineage studies by Snippert et al. (2010) and Wang X. et al. (2017) suggest that progeny of non-bulge Lgr6-positive and Lgr5-positive epithelial stem cells can contribute to the generation of neogenic hair follicles. Furthermore, the origin of *de novo* dermal papillae, the principal mesenchymal component of neogenic hair follicles, remains elusive. Lineage studies on Cd133-positive dermal papillae cells of preexisting hair follicles indicate that they do not mobilize upon skin wounding (Kaushal et al., 2015). At the same time, recent lineage tracing studies suggest that multiple pre-existing skin fibroblast lineages contribute progeny toward the repair of small wounds and that their contribution is not equivalent. Using lineage tracing with *En1-Cre*, Rinkevich et al. (2015) identified En1-positive and En1-negative dermal fibroblast populations, with the former making major contributors toward wound repair. In an independent study and using different *Cre* lines, Driskell et al. (2013) demonstrated that distinct dermal fibroblast lineages contribute to repair of small wounds and this occurs in successive waves. For instance, the progeny of lower, reticular dermal fibroblasts are recruited early after wounding and constitute the reticular dermis, while the progeny of upper, papillary fibroblasts migrate into the wound with a significant delay and establish the papillary dermis. On this end, contribution from distinct dermal fibroblast lineages toward newly-formed dermal papillae in the context of WIHN model warrants further investigation. The diverse nature of dermal papillae cell types (Driskell et al., 2011) and the lack of clear dermal papilla lineage master-regulators complicates functional validation of their origin.

Unlike dermal papillae, the white adipose lineage with its well-established master-regulators, such as Zfp423 (Gupta et al., 2010), Cepbs and Pparγ (Cristancho and Lazar, 2011), provides a tractable model system for studying *de novo* cell type regeneration. Recently, it was showed that *de novo* adipocytes regenerate from Sm22/Sma-positive contractile wound myofibroblasts (Plikus et al., 2017). Myofibroblast-specific ablation of *Pparγ* or BMP receptor

1a *(Bmpr1a)* largely prevented adipocyte regeneration in otherwise hair-bearing wounds. However, it remained unclear to what degree wound myofibroblasts are heterogeneous and if only some or multiple types of myofibroblasts are competent for reprogramming into new adipocytes under the signaling effects of *de novo* hair follicles. While it is broadly accepted that skin fibroblasts are highly heterogeneous in terms of their plasticity and secretory profile in normal skin, its heterogeneity in wounds, how it changes across wound healing and its potential contribution to the regeneration of skin appendages remains profoundly elusive, mainly due to the lack of cell surface markers that would render enable high-resolution fibroblast sorting, transcriptomic, proteomic and functional studies. The advent of microfluidic and droplet-enabled single-cell RNA-sequencing (scRNA-seq) technologies (Macosko et al., 2015, Pollen et al., 2014) provides the ability to profile cellular heterogeneity in tissues with poorly characterized cell types and limited lineage-tracing tools. In fact, recent scRNA-seq studies performed on human skin demonstrates heterogeneity among dermal fibroblasts under homeostatic conditions (Philippeos et al., 2018a, Tabib et al., 2017). Similarly, scRNA-seq studies have also revealed a large degree of cellular heterogeneity in diseased (Filbin et al., 2018, Gaublomme et al., 2015, Puram et al., 2017, Stubbington et al., 2017, Tirosh et al., 2016a) and injured (Wurtzel et al., 2015)tissues. Using a scRNA-seq approach, I identified and characterized multiple distinct fibroblast populations in regenerating mouse wounds *in silico*, demonstrated that they co-exist in wounds across the time course of regeneration and using distinct functional approaches, demonstrated that a rare myeloid-derived subset of wound myofibroblasts is capable of contributing toward *de novo* dermal adipocyte regeneration.

## RESULTS

3-end scRNA-seq was performed on viable cells isolated *in toto* from PWD12 large excisional wounds isolated from *Sm22-Cre;tdTomato* mice (Fig. 4.1). This time point was chosen for several reasons. First, it coincides with completion of wound re-epithelialization. Second, precedes the onset of hair follicle neogenesis and lastly, this time point shows heightened presence of alpha-smooth muscle actin-expressing myofibroblasts (Plikus et al., 2017). Post capture in the droplet-enabled Chromium Platform, a total of approximately 22,322 cells were obtained. Out of these, approximately 21,819 cells met quality control metrics post initial processing using Cell Ranger and were used for downstream analyses (see Chapter 2 for quality control metrics, Figure 4.2). Unsupervised clustering analysis using t-distributed stochastic neighbor embedding (t-SNE) (van der Maaten and Hinton, 2008), which is a feature built in Seurat and the package used in this analyses (Satija et al., 2015), identified 13 distinct cell clusters that were grouped based on differentially expressed gene signatures (Fig. 4.3.A). This information was utilized to attribute their putative cell type identities *in silico* and their unique gene expression profiles (Fig. 4.3.B, 4.3.D, 4.3.E). Among the clusters, the most abundant of them, representing 15.3% of all cells, was cluster C3, which was enriched for cells expressing macrophage markers, including *C1qb, Cd14, Cd68, Lyz2, Mafb* and *Pf4* (Murray et al., 2014). Cluster C7 cells were classified as lymphocytes (representing approximately 4% of the total cell population) and they expressed *Cd3d, Cd52, Ccl5, Icos* and *Nkg7* markers. Cluster C8 cells were identified as B lymphocytes (3.1%), C10 cells as T lymphocytes (1.4%) (Raff, 1971, Tedder, 2015) and C12 as dendritic cells (0.8%) (Chu et al., 2011). Two other distinct cell clusters were C5 (9%) and C13 (0.6%). Cluster C5 cells were enriched for the endothelial markers *Cav1, Cd34, Cd93, Ly6e, Ly6c1* and *Pecam1* (Vecchi et al., 1994), while cluster C13 cells were classified as lymphatic endothelial cells based on their expression of *Ccl21a, Lyve1,* *Pdpn* and *Prox1* (Kong et al., 2017). The remaining five cell clusters – C1, C2, C4, C6 and C9, representing approximately 64.6% of all wound cells analyzed and based on marker expression, were collectively characterized as wound fibroblasts. These five cell clusters were highly enriched for the expression of the collagens *Col1a1* (Sokolov et al., 1995), *Col3a1* (Le Goff et al., 2006), *Col5a1, Col12a1* and the extracellular matrix proteins *Dcn (Decorin)* (Asano et al., 2009) and *Fbln2 (Fibulin 2)* (Sicot et al., 2008). Many of putative fibroblasts also showed high expression levels of contractile proteins implicated in a myofibroblast-like phenotype acquisition, including *Cald1 (Caldesmon 1), Acta2 (aka Sma)* and *Tagln (aka Sm22)* (Hinz et al., 2007).

In order to learn more about the distinct fibroblast sub-populations/states that may be present in the wound, unsupervised clustering analysis (Satija et al., 2015) on all wound fibroblasts (those expressing the genes aforementioned and belonging to clusters C1, 2, 4, 6 and 9) and observed further heterogeneity, which included 12 sub-clusters termed sC1-sC12 (Fig. 4.4). Each sub-cluster contained unique marker gene profile signatures that may represent unique wound fibroblast sub-populations/states (Fig. 4.4.B, 4.4.C). Considering that transcription factors (TFs) commonly regulate cellular characteristics and fates (Iwafuchi-Doi and Zaret, 2016), the TF expression patterns of these putative distinct fibroblasts were examined. All fibroblast sub-clusters shared expression of the following twenty TFs: *Cebpb, Egr1, Fosb, Fosl2, Hif1a, Klf2, Klf4, Klf6, Klf9, Nfat5, Nfatc1, Nfkb1, Nr4a1, Nr4a2, Pbx1, Prrx1, Runx1, Stat3, Tcf4 and Zeb2.* Collectively, these TFs can be defined as a common wound fibroblast TF signature. Notably, among these signature factors, Runx1 (Kim et al., 2014), Tcf4 (Noizet et al., 2016) and Zeb2 (Cunnington et al., 2014) were recently shown to regulate a contractile fibroblast differentiation program. Additionally, prominent sub-cluster specific TF signatures in sC3, sC9 and sC11 were characterized by $Ebf1^{high}$/$Id3^{high}$/$Zeb2^{high}$/$En1^{low}$/$Nfix^{low}$/$Prrx2^{low}$/$Sox9^{off}$. Intriguingly, En1 (Engrailed 1) was shown to mark a major pro-fibrotic population of skin fibroblasts, while selective enrichment of wounds for En1-negative fibroblasts via ablation of *En1-Cre* expressing cells, led to reduced scarring (Rinkevich et al., 2015). This suggests that cells present in sC3, sC9 and sC11 sub-clusters might be developmentally related to an *En1* negative fibroblast lineage, although further lineage tracing and functional analyses might be needed to further validate these claims. Among the remaining nine $En1^{high}$ sub-clusters, fibroblasts in six sub-clusters, namely sC1 and sC4-sC8, displayed low expression of *Id2* and *Id3* – direct targets of BMP signaling (Balemans and Van Hul, 2002). Among these six $En1^{high}$/$Id2^{low}$/$Id3^{low}$ sub-clusters, sC4 was $Sox11^{high}$, sC5 – $Twist2^{high}$, sC7 – $Twist1^{high}$/$Twist2^{high}$/$Foxp1^{low}$ and sC8 – $Nfia^{high}$. Other $En1^{high}$ sub-clusters also displayed their own, albeit complex TF expression signatures. Lineage tracing studies, coupled with functional tissue-specific deletion experiments will be required to conclusively delineate the contribution of such fibroblasts in the acquisition of a scarring *vs*. regeneration phenotype after wounding.

The expression of signaling pathway markers, secreted ligands and receptors of these putative fibroblast sub-populations/states was then determined. Three of the afore-mentioned $En1^{low}$ sub-clusters displayed the following receptor expression signature: $Mcam^{high}$/$Pdgfrb^{high}$/$Fgfr1^{low}$/$Tgfbr2^{low}$/$Tgfbr3^{low}$/$Ncam1^{off}$/$Pdgfra^{off}$, and ligand expression signature: $Il6^{high}$/$Pdgfa^{high}$/$Igf1^{low}$/$Igfbp3^{low}$/$Mdk^{low}$/$Dkk3^{off}$. Nine $En1^{high}$ sub-clusters were primarily differentiated from $En1^{low}$ sub-clusters on the basis of their expression of PDGF receptor alpha (*Pdgfra*), while displaying low *Il6, Pdgfa*, *Pdgfrb*, high *Igf1, Mdk, Tgfbr2* and *Tgfbr3* expression. Additionally, among $En1^{high}$ sub-clusters, fibroblasts in sC2 were $Angptl^{high}$, sC5 – $Ccl8^{high}$/$Cxcl5^{high}$/$Grem1^{high}$/$Spp1^{high}$, sC6 – $Il1b^{high}$, sC7 – $Ccl8^{high}$/$Igfbp3^{low}$, sC10 –

*Angptl1*$^{high}$/*Il1b*$^{high}$/*Pf4*$^{high}$ and sC12 – *Angptl1*$^{high}$/*Fst*$^{high}$. Fibroblast sub-clusters were also profiled based on their cell cycle state (Scialdone et al., 2015, Tirosh et al., 2016b). Intriguingly, *En1*$^{high}$ sC4 and *En1*$^{low}$ sC11 sub-clusters were prominently enriched for G2/M cell cycle markers, suggesting these cells represent an actively highly cycling population. (Figure 4.5) Taken together, this scRNA-seq analyses suggests that, upon completion of re-epithelialization on PWD12, large skin wounds may contain two major fibroblast populations (Fig. 4.3.C). One population, representing 23.6% of wound fibroblasts, consists of three sub-clusters sC3, sC9 and sC11, which express low levels of *En1*, low levels of TGFβ receptors *Tgfbr2, Tgfbr3,* high levels of PDGF receptor *Pdgfrb*, but not *Pdgfra.* The second and more heterogeneous population, representing 76.4% of all wound fibroblasts, consists of nine *En1*$^{high}$ sub-clusters and expresses intermediate to high levels of TGFβ receptors *Tgfbr2, Tgfbr3,* high levels of PDGF receptor *Pdgfra*, but not *Pdgfrb.* Compared to *En1*$^{low}$ cells, the *En1*$^{high}$ population also expresses higher levels of extracellular matrix genes, including *Col1a1* and *Col3a1*, but significantly fewer contractile factor genes, such as *Acta2* and *Tagln*. The existence of two major wound fibroblast populations differentiated by their *En1* expression is consistent with the report by Rinkevich et al. (2015), which identified two distinct contributions of *En1*-positive/negative cells to fibrosis. Notably, the *En1*$^{high}$ population also expresses high levels of *Pdgfra*, and previous studies implicated activation of Pdgfra signaling as the driver of fibrosis in the context of multiple tissues (Olson and Soriano, 2009), including adipose tissue (Iwayama et al., 2015) and skeletal muscle (Mueller et al., 2016). The *En1*$^{high}$ population also expresses higher levels of receptors for the TGFβ pathway, another well-established driver of fibrosis (Branton and Kopp, 1999). At the same time, the *En1*$^{low}$ population expressed high levels of *Pdgfrb*. In line with this observation, a recent study identified Pdgfrb-expressing perivascular cells as the precursors for new adipocyte regeneration in visceral white adipose tissue (WAT) depots in obesity (Shao et al., 2018). Similarly, this scRNA-seq analyses identified a high level of previously unappreciated heterogeneity within both fibroblast populations. Future studies will be necessary to definitely establish the role of each fibroblast sub-population in scar formation, wound contraction, as well as *de novo* hair follicle and dermal adipocyte regeneration.

While t-SNE analysis helped to reveal a high degree of cellular heterogeneity among wound cells as well as fibroblasts, I was interested in determining whether fibroblasts shared a common, interconnected differentiation trajectory and could be revealed using an unsupervised algorithm for ordering cells based on their differential gene expression profiles. Indeed, in response to wounding, many fibroblasts undergo a differentiation program (Qiu et al., 2017a, Qiu et al., 2017b, Trapnell et al., 2014) into mature, alpha-smooth muscle actin expressing contractile myofibroblasts (Hinz et al., 2007, Tomasek et al., 2002). Importantly, in large wounds, myofibroblasts serve as the principal progenitors for *de novo* dermal adipocyte regeneration (Plikus et al., 2017). Wound fibroblasts were ordered in pseudotime using Monocle 2, which performs pseudo-temporal ordering of cells based on differential gene expression profile and places cells along a putative differentiation trajectory (Qiu et al., 2017a, Qiu et al., 2017b, Trapnell et al., 2014) (Fig. 4.6). Indeed, unbiased Monocle 2 analyses arranged most of wound fibroblasts into a major putative differentiation trajectory. Indeed, Monocle 2 placed cells expressing contractile factors *Acta2* and *Tagln* toward the right end of the trajectory along Component 1, while cells expressing mature extracellular matrix genes *Eln and Fn1*, characterizing undifferentiated fibroblasts, preferentially distributed at the beginning of the pseudotime trajectory along Component 2 (Fig. 4.6.A). This analyses parallels the tSNE analyses performed on fibroblasts. This pseudotime analyses along Path 1 may represent a putative fibroblast-to-myofibroblast differentiation trajectory. To interrogate the genes involved in this putative developmental trajectory scEpath was utilized (Jin et al., 2018). scEpath is a broadly unsupervised probabilistic method directed to reconstruct developmental trajectories *in silico*. scEpath revealed five pseudo-temporal "rolling wave" clusters of genes, which represent gene sets up- or down-regulated on different time scales across pseudotime (Fig. 4.6.B). Independent gene scoring analyses of these "rolling wave" clusters revealed multiple secreted signaling factors and TFs differentially expressed across pseudotime (Fig. 4.7.A, 4.7.B). Among the identified factors, expression of the signaling ligands *Pdgfa* (Bostrom et al., 1996)*, Tgfb1, Tgfb2* (Thannickal et al., 2003) and TF *Zeb2* (Cunnington et al., 2014), previously implicated in myofibroblast differentiation, preferentially distributed in the same pseudotime scale as *Acta2* and *Tagln* (Fig. 4.6.C). Taken together, unsupervised pseudotime analysis establishes a basis for exploring new signaling and transcriptional regulators of a wound fibroblast-myofibroblast differentiation program *in vivo*.

Attention was turned to the fact that, in *in silico* data, many wound fibroblasts across all twelve sub-clusters expressed pan-hematopoietic markers (Fig. 4.8). Specifically, many fibroblasts expressed the myeloid-specific marker *Lyz2* (*Lysozyme 2*) (Clausen et al., 1999) (Fig. 4.8.A, 4.8.B). t-SNE analyses revealed fibroblasts that co-expressed *Lyz2* with collagen *Col12a1* and the contractile markers *Acta2* and *Tagln*, hence, identifying $Lyz2^{+}/Acta2^{+}/Tagln^{+}/Col12a1^{+}$ quadruple-positive wound myofibroblasts. These *Lyz2*-expressing myofibroblasts represented 11.3% of all wound fibroblasts and were present as puncta in all fibroblasts sub-clusters (Fig. 4.8.C). Following these findings, and to corroborate that these quadruple-positive cells do not represent duplets/multiplets, a common technical feature of droplet-enabled scRNA-seq, mRNA and protein of single cell analyses was performed on genetically labeled myofibroblasts (Fig.

4.9). Full length scRNA-seq (Pollen et al., 2014) (Fig. 4.9.A) was performed on *tdTomato*$^{hi}$ cells isolated from *Sm22-Cre;tdTomato* wounds at PWD12 (Plikus et al., 2017). Due to the low yield of capture in Fluidigm IFCs, 3 individual experiments were performed (Figure 4.10.A). Gene sets were normalized using SCnorm (Bacher et al., 2017). Post quality control assessment, a total of 166 cells were used in downstream analyses (Figure 4.11.A, 4.11.B, 4.11.C). t-SNE analyses revealed *tdTomato*$^{hi}$ myofibroblasts clustered into 3 distinct clades (fC1-3), with fC3 showing a subset of cells expressing *Lyz2* (Fig. 4.11.B). Indeed, cells in this clade also expressed *Acta2*, *Talgn*, and *Ptprc* (Bryder et al., 2006) (Fig. 4.11.C). In parallel, single cell immunoblotting (Hughes et al., 2014) was performed on cells isolated *in toto* from wounds of *Sm22-Cre;tdTomato* mice (Fig. 4.9.C). Blots were probed with mCherry and LYZ antibodies to detect tdTomato$^{+}$/Lyz2$^{+}$ cells. Indeed, a total of X cells were tdTomato$^{+}$ and approximately Y cells were Lyz2$^{+}$ cells (Fig. 4.11.D, 4.11.E). Taken together, 3'-end droplet-enabled scRNA-seq analyses, with further corroboration and characterization using full length scRNA-seq and single cell immunoblotting, identified a population of wound myofibroblasts with hematopoietic features that could contribute to wound remodeling and regeneration.

Previous work indicates that circulating hematopoietic cells can convert into myofibroblasts at sites of injury (Ogawa et al., 2006), and that the extent and significance of this conversion tends to be organ and injury context-specific (Badiavas et al., 2003, Barbosa et al., 2010, Fathke et al., 2004, Ishii et al., 2005, Opalenik and Davidson, 2005, Roufosse et al., 2006, Sinha et al., 2018, Suga et al., 2014, van Amerongen et al., 2008). Considering that in large excisional wounds *de novo* dermal adipocytes originate predominantly from myofibroblasts (Plikus et al., 2017), the extent to which hematopoetic cells contribute to wound remodeling and regeneration of dermal adipocytes was determined. First, bone marrow transplantation (BMT) mouse models (Duran-Struuck and Dysko, 2009) were utilized to interrogate the hematopoetic contribution to large wound repair and regeneration. In some BMT models, lethally-irradiated mice were reconstituted with GFP-expressing hematopoetic stem cells. In others, bone marrow was reconstituted with cells expressing lacZ under the control of various lineage specific promoters. Peripheral blood chimerism was determined to assess bone marrow reconstitution. Hematopoietic lineage specificity in these experiments was determined by generating BMT mice using multipotent hematopoietic stem cells (HSCs) purified based on the described SLAM marker signature: $Lineage^{neg}, Sca1^{+}, c\text{-}kit^{+}, Cd150^{+}, Cd48^{neg}$ (Yilmaz et al., 2006). Between 2,300 and 4,400 HSCs were transplanted per recipient mouse and in all cases achieved successful reconstitution of the hematopoietic lineage, which was confirmed by high levels of peripheral blood chimerism and bone marrow fluorescence. Following large excisional wounding, healed tissue in $GFP^{+}$ HSC BMT mice showed consistently high contribution from hematopoietic lineage on PWD28, with many $GFP^{+}$ cells surrounding neogenic hair follicles (n=18). Flow cytometry analysis of wound tissue confirmed that long-term contribution from the hematopoietic lineage constituted approximately 30% at both PWD28 (n=3) and 2 months PW (n=3). In contrast, BMT mice that received $GFP^{+}$ $Cd45^{neg}$ non-hematopoietic bone marrow fraction had no $GFP^{+}$ contribution to the wound. Wounding in BMT mice reconstituted with *Sm22-Cre;R26R* HSCs was performed whether LacZ marked hematopoietic-derived contractile cells in the wound bed. Indeed, consistent with the possibility of hematopoietic contribution to wound myofibroblasts, many lacZ positive cells in the wound tissue of *Sm22-Cre;R26R* HSCs BMT mice (n=9) were observed, suggesting they can graft in the wound for long term (Fig. 4.12.A).

Because fibroblast and white adipose lineages are closely related, it was hypothesized that some hematopoietic cells that initially convert into wound myofibroblasts might then become *de novo* dermal adipocytes. Although contested (Berry and Rodeheffer, 2013, Koh et al., 2007, Tomiyama et al., 2008), several studies report that, in principle, hematopoietic cells can convert into adipocytes upon integration into pre-existing white adipose tissue depots (Crossno et al., 2006, Majka et al., 2010, Sera et al., 2009) under normal conditions. Contribution of hematopoietic cells toward adipose depots appears to be variable, and largely depends on gender and anatomical site (Majka et al., 2010). To evaluate the possibility of hematopoietic contribution toward *de novo* dermal adipogenesis in the wound, BMT and non-BMT mouse models were interrogated (Fig. 4.12.B, 4.13.B). Indeed, wounds in $GFP^{+}$ HSC BMT mice contained many $GFP^{+}$ cells that co-stained for the adipocyte marker FabP4 (Shan et al., 2013) in the areas surrounding neogenic hair follicles, but not in the hairless portions of the scar. Importantly, further BMT assays determined that hematopoietic to dermal adipose conversion, rather than cell fusion, takes place during *de novo* dermal adipocyte regeneration in large wounds (data not shown).

Functional lineage tracing using *Cd45-Cre;R26R* mice further verified that hematopoietic cells contribute to *de novo* dermal adipocyte regeneration under physiological conditions, and not only in the context of BMT models (Fig. 4.14.A). In these mice, where *Cre* recombinase activity is restricted to the hematopoietic lineage (Yang et al., 2008), consistent, albeit occasional formation of lacZ positive *de novo* dermal adipocytes (n=9) was observed. Similarly, lacZ positive dermal adipocytes formed in the wounds of *LysM-Cre;R26R* mice (n=12) (Clausen et al., 1999) (Fig. 4.14.B), suggesting that hematopoietic contribution to dermal adipocyte regeneration is mediated, at least in part, via myeloid progenitors. Consistent with occasional distribution patterns of lacZ positive adipocytes in *LysM-Cre;R26R* mice, as well as the small percentage of *Talgn/Lyz2*, *Acta2/Lyz2*, or quadrupled-positive cells, *LysM-Cre;Pparγ*$^{-/-}$ mutants did not have a significant *de novo* dermal adipocyte defect (n=20), unlike that observed in constitutive *Sm22-Cre;Pparγ*$^{-/-}$ or conditional *Sma-CreER;Pparγ*$^{-/-}$ mice described before (Plikus et al., 2017) (Fig. 4.11.C). Of interest, in both mouse models, occasional formation of neogenic hair follicles with lacZ positive dermal papillae and dermal sheath were observed, suggesting that the lineage plasticity repertoire of hematopoietic cells during wound regeneration might extend beyond dermal adipogenesis. Taken together, functional BMT and lineage tracing studies help to establish the role of hematopoietic cells as a source of dermal adipogenic progenitors during wound healing.

## DISCUSSION

Traditionally, adult mammals are considered to have limited regenerative abilities and scarring is thought to be the default repair response in most types of injuries. The notable exceptions to this rule are digit tip regeneration after amputation (Johnston et al., 2016, Lehoczky et al., 2011, Rinkevich et al., 2011, Takeo et al., 2013), pancreatic islet (Thorel et al., 2010), lung alveoli (Jain et al., 2015), stomach epithelium (Stange et al., 2013), biliary system (Schaub et al., 2018), and neogenesis of hair follicles (Billingham and Russell, 1956, Breedis, 1954, Brook et al., 1960, Gay et al., 2013, Ito et al., 2007, Myung et al., 2013, Nelson Amanda M. et al., 2013, Nelson Amanda M. et al., 2015, Stenbäck et al., 1967) and dermal adipocytes (Plikus et al., 2017) in large excisional skin wounds. Intriguingly, lineage studies reveal important differences in the regenerative strategies between these systems, including regeneration from fate-restricted progenitors, lineage reprogramming and transdifferentiation.

A remaining question that stands in the field is whether all wound myofibroblasts are identical or heterogeneous in terms of their origin (Mack and Yanagita, 2015), properties and morphogenetic competence (i.e. scarring *vs*. regeneration-prone)? Indeed, myofibroblast origin has been determined to be tissue and injury-context specific, with Gli1$^+$ perivascular cells giving rise to myofibroblasts in kidney, lung, liver, heart (Kramann et al., 2015) and bone marrow (Schneider et al., 2017). While studying the cellular pedigree of cells requires specific genetic fate mapping strategies and assessment of morphogenetic competence using functional studies, scRNA-seq analyses enables large-scale profiling of cellular properties in complex tissues. Indeed, scRNA-seq has been successfully applied to studying cellular heterogeneity in skin, including epithelial cells of mouse hair follicles (Joost et al., 2016, Yang et al., 2017), and immune cells (Ahn et al., 2017) and fibroblasts of human dermis (Philippeos et al., 2018b, Tabib et al., 2017). Tabib et al. (2017) identified two major populations of human dermal fibroblasts, characterized by co-expression of *SFRP2*$^+$/*DPP4*$^+$ and *FMO1*$^+$/*LSP1*$^+$ markers, respectively. These further subdivide into several sub-populations, each with unique differentially expressed gene sets. Philippeos et al. (2018b) on the other hand, identified five fibroblast populations: corresponding to upper (papillary) and lower (reticular) dermal fibroblasts, pericytes, and two as of yet uncharacterized populations. scRNA-seq has also been used to study heterogeneity of disease-associated fibroblasts in the synovial tissue upon rheumatoid arthritis (Mizoguchi et al., 2018, Stephenson et al., 2018).

In this chapter, a description of a scRNA-seq study aimed at identification of heterogeneity of wound fibroblasts in the mouse model for injury-induced skin regeneration is presented. Data shows that fibroblasts can be broadly classified into two major populations on the basis of their *En1* and PDGF receptor expression patterns. Indeed, previous work showed that

*En1* differentiates between two major mouse skin fibroblast populations and that *En1-Cre* expressing cells dominate during fibrotic repair of small skin wounds (Rinkevich et al., 2015). *En1*$^{high}$ wound fibroblasts in our analyses also expressed high levels of *Pdgfra*, a known signaling driver of tissue fibrosis (Iwayama et al., 2015, Mueller et al., 2016, Olson and Soriano, 2009). In the wound model employed, *En1*$^{low}$/*Pdgfra*$^{low}$ cell clusters constituted 23.6% of all wound fibroblasts. In the future, it will be important to examine if these cells preferentially contribute toward newly regenerating dermal adipocytes as compared to *En1*$^{high}$/*Pdgfra*$^{high}$ fibroblasts. Future work will be required to understand the functional significance of this heterogeneity in the context of regeneration and to lineage trace their origin to distinct skin fibroblast populations in unwounded skin (Driskell et al., 2013, Lesko et al., 2013, Philippeos et al., 2018a, Rinkevich et al., 2015, Rivera-Gonzalez et al., 2016, Schmidt and Horsley, 2013).

BM-derived progenitors, including circulating HSCs, fibrocytes, endothelial progenitors and mesenchymal stem cells can contribute progenies toward injured tissues in various organs. For instance, scar tissue in heart following myocardial infarction (van Amerongen et al., 2008), cornea following keratectomy (Barbosa et al., 2010) and lung in pulmonary fibrosis (Ishida et al., 2007, Schmidt et al., 2003) contains many BM-derived collagen-producing myofibroblasts. In skin, many studies have documented BM giving rise to fibroblasts at the sites of injury, such as in wounds (Badiavas et al., 2003, Chen et al., 2017, Ding et al., 2011, Fathke et al., 2004, Ishii et al., 2005, Maan et al., 2015, Oh et al., 2011, Opalenik and Davidson, 2005, Ou et al., 2015, Sinha et al., 2018, Suga et al., 2014, Sun et al., 2018, Yang et al., 2005). Despite the vast majority of works describing these findings, some studies, however, report this contribution to be minimal (Barisic-Dujmovic et al., 2010, Higashiyama et al., 2011). Such a discrepancy is likely attributed to several factors, including the type and extent of injury and experimental timing. The contribution from BM progenitors toward repairing tissues was shown to increase with the extent of injury (Ishii et al., 2005, Mansilla et al., 2006, Yamaguchi et al., 2007), yet most of the previous studies were performed on small wounds. In addition, many previous studies failed to evaluate long-term BM contribution to the wound.

This data from large excisional wounds shows that the contribution from hematopoietic cells to the scar tissue one month after wounding is significant, and that at least a portion of these cells can convert into *de novo* dermal adipocytes around neogenic hair follicles. Previously, adipogenic conversion of hematopoietic cells has been shown both *in vitro* (Eto et al., 2013, Gavin et al., 2017, Hong et al., 2007, Hong et al., 2005) and *in vivo* in major adipose depots, such as in inguinal fat (Crossno et al., 2006, Gavin et al., 2016, Majka et al., 2010, Sera et al., 2009). Most recently, approximately 10% of adipocytes were shown to form from hematopoietic progenitors in human subjects undergoing BMT treatment (Ryden, 2016, Ryden et al., 2015), while in another human BMT study, up to 35% of adipocytes were traced to transplanted BM source (Gavin et al., 2016). Overall, the findings presented here illustrate the dynamic nature of fibroblast identities during wound healing, and the powerful wound induced plasticity of hematopoietic derived cells. scRNA-seq its subsequent analysis inferred three main results. First, it revealed a previously unappreciated degree of cellular heterogeneity in healing large skin wounds, composed of large subsets of immune, endothelial and fibroblast cells. Second, sub-clustering of fibroblasts and unsupervised pseudotime analyses revealed a putative fibroblast-myofibroblast differentiation trajectory and identified putative TFs involved in this process. Lastly, it revealed a high degree of myofibroblast heterogeneity and identified a hematopoetic-derived sub-population of myofibroblasts that contribute to wound healing long-term and undergo reprogramming toward a dermal adipocyte fate. This intimate relationship between the hematopoietic derived cells and dermal adipogenesis suggests further characterization of the factors influencing plasticity and lineage switching in skin wounds and could help uncover potential novel therapeutic approaches to the treatment of wounds and scars.

## METHODS

**Mouse strains.** The following transgenic mouse models were used in this study: *Retn-lacZ* (Banerjee et al., 2004), *Sm22-Cre* (JAX stock 004746), *Cd45-Cre* (Yang et al., 2008), *LysM-Cre* (Clausen et al., 1999), *FabP4-Cre* (JAX stock 005069), *Pparγ-flox* (JAX stock 004584), *R26R* (JAX stock 003474), *tdTomato* (JAX stock 007909), GFP (*UBC-GFP*; JAX stock 004353), *RFP* (*ACTB-DsRed.MST*; JAX stock 006051), *Rag1*$^{-/-}$ (JAX stock 002216). Mixed background mice were used in this study.

**Genotyping.** Genotyping was performed on genomic DNA isolated from tail or ear. Tissues were digested using proteinase-K. Different thermocycler programs were used for each individual strain. The following primers were used: ***Cd45-Cre, Sm22-Cre, Adipoq-Cre*:** Gnrc-Cre-F: GCGGTCTGGCAGTAAAAACTATC; Gnrc-Cre-R: GTGAAACAGCATTGCTGTCACTT; Gnrc-Cre-Ctr-F: CTAGGCCACAGAATTGAAAGATCT; Gnrc-Cre-Ctr-R: GTAGGTGGAAATTCTAGCATCATCC. Expected results: Internal control: ~324 bps, Mutant allele: ~100 bps. ***ROSA - R26R*:** ROSA-Mut: GCGAAGAGTTTGTCCTCAACC; ROSA-F: 5'-AAAGTCGCTCTGAGTTGTTAT; ROSA-R: GGAGCGGGAGAAATGGATATG. Expected results: Mutant: 340 bps, Heterozygote: 340 bps and 650 bps, Wild-type: 650 bps. ***tdTomato*:** TdTomato F: CGGATCCACCGGTCGCCACCATGGTGAGCAAGGGCGAGGAGGTC; TdTomato R: GAGCGGCCGCTTACTTGTACAGCTCGTCCATGCCGTACAG. Expected results: Mutant 200 bps, Wild type 300 bps.

**Wounding procedures.** All animal experiments were carried out in accordance with the guidelines of the Institutional Animal Care and Use Committee of the University of California, Irvine. Animals were anesthetized with isoflurane, hairs were clipped, skin site was disinfected and a single full thickness excisional wound was created on their dorsum using scissors (squared $s$ = 1.5 cm) (Gay et al., 2013, Ito et al., 2007, Plikus et al., 2017). Following wounding, all animals were housed individually. Wounds were let to heal by secondary intention. No wound dressing was applied. Animals were used as biological replicates.

**Histology and immunohistochemistry.** Tissues were fixed in 4% PFA, dehydrated, paraffin embedded, and sectioned at 7 µm thickness. Frozen tissues were sectioned at 12 µm. Immunostaining was performed both on frozen and paraffin sections. Heat-based antigen retrieval was performed when necessary. The primary antibodies used were goat anti-FabP4 (1:200; R&D Systems), rabbit anti-Sma (1:200; Abcam), rabbit anti-Krt5 (1:250; BioLegend).

**3'-end single cell RNA-sequencing.** Pooled skin wound tissues (n=12 animals) were collected from *Sm22-Cre;tdTomato* mice on day 12 PW. Wound tissues were micro-dissected and incubated in a Dispase II/Collagenase IV/Liberase solution for 60 minutes with constant rotation. Post-incubation, cell aggregates were mechanically dissociated using GentleMACS (MACS). Single cell suspensions were treated with 1X RBC lysis buffer, washed, and re-suspended in 0.04% UltraPure BSA (Biolegend). Dead cells were removed using the MS columns of the Dead Cell Removal Kit (MACS) as per manufacturer's directions. Live cells were resuspended in 0.04% UltraPure BSA and counted using the automated cell counter Countess (Thermo). Single cells were captured using the Chromium® Platform (10X Genomics) and libraries were generated using Single Cell 3' v2 chemistry, which is related to Drop-seq technology (Macosko et al., 2015). Library metrics were as follow: 550.19 pg/µl with an avg. size ~454 bps. Libraries were sequenced on an Illumina Next-Seq4000 platform (Illumina) (one lane, 100 PE). Cell counting, capture, chemistries, library preparation, quality control and sequencing was performed at the Genomics High Throughput Sequencing facility at the University of California, Irvine.

**Full length single cell RNA-sequencing.** Pooled skin wound tissues (n=2 to 3 animals) were collected from *Sm22-Cre;tdTomato* mice on days 12, 15 and 21 PW. Cells were collected and sorted as previously described (Plikus et al., 2017). Pre-sorted, viable *tdTomato*$^{hi}$ single cells were re-suspended at appropriate concentrations in DMEM supplemented with 10% FBS, antibiotics and antifungals, diluted with suspension reagent for attribution of optimal buoyancy, and loaded onto a large 17-25µm 96-well microfluidic IFC (Fluidigm) for single cell capture in the automated C1® system for single-cell genomics (Fluidigm) (Pollen et al., 2014). Capture efficiency was assessed using bright field/fluorescent microscopy. Only cells captured singly (singlets) per micro-well were considered for downstream purposes. Double (doublets) and multiple (multiplets) cells captured per well were excluded. Lysis, RT and cDNA pre-amplification were performed *in loco* (protocol 1.773x) with ultra-low input RNA reagents as suggested per manufacturer (Clonetech). RNA spike-in controls were omitted. cDNA concentrations were estimated using Qubit 2.0 (Thermo) and cDNAs with concentration ≥ 1.0 ng/µl were used for downstream library preparation. Libraries were amplified using the Nextera XT v2 Index Kit (Illumina). Quality control on multiplexed libraries was performed using the Agilent Bioanalyzer and quantification was performed using KAPA for Illumina Sequencing Platforms (Illumina). Multiplexed libraries were sequenced as paired-end on an Illumina Next-Seq500 platform (Illumina).

**Data processing for 3'-end single cell RNA transcripts.** Transcripts were mapped to the mm10 reference genome (GRCm38.91) using Cell Ranger Version 2.1.0. Sequencing metrics:

~308,471,010 total number of reads, ~98.5% valid barcodes; Mapping metrics: ~90.4% reads mapped to genome, ~85.5% reads mapped confidently to genome, ~65.9% reads mapped confidently to transcriptome. Cell metrics: ~22,322 estimated number of cells, ~84.2% fraction reads in cells, ~13,819 mean reads per cell, ~1,101 median genes per cell, ~19,070 total genes detected, ~2,448 median UMI counts per cell. Quality control metrics for 3'-end transcripts, downstream analyses of 3'-end transcripts were performed using Seurat (Satija et al., 2015). Cell-cycle discrimination analyses were performed as described in (Tirosh et al., 2016a). All details pertaining to these analyses are described in Guerrero-Juarez et al., In Review. Differential gene expression across pseudotime was performed using Monocle 2 (Qiu et al., 2017a, Qiu et al., 2017b, Trapnell et al., 2014). Identification of differentially expressed gene clusters across pseudotime, as well as rolling wave plots were generated using scEPath package (Jin et al., 2018).

**Full length single cell RNA transcript alignment and quantification.** Demultiplexed, paired-end FASTQs were aligned to the mouse genome (mm10/gencode.Mv13) using Bowtie (version 1.0.0) with the following standard parameters: *rsem-prepare-reference --bowtie --gtf* and quantified using the RNA-seq by Expectation-Maximization algorithm (RSEM) (version 1.2.31) (Li and Dewey, 2011) with the following standard parameters: *rsem-calculate-expression -p $CORES --paired-end*. Samples displaying ≥ 159,000 aligned reads were considered for downstream quality control filtering. All details pertaining to these analyes are described in Guerrero-Juarez et al., In Review.

**Single cell immunoblotting.** All details pertaining to these analyes are described in Guerrero-Juarez et al., In Review.

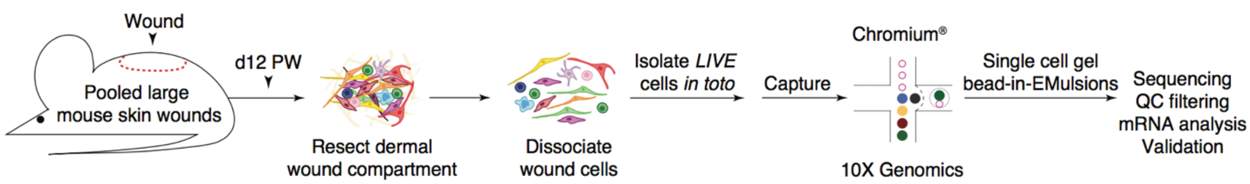


**Figure 4.1. Schematic of single cell RNA-seq on early mouse wounds.** Schematic of cell isolation from day 12 wounds, cell processing, capture by droplet-enabled device (Chromium® - 10X Genomics), sequencing and downstream analysis.

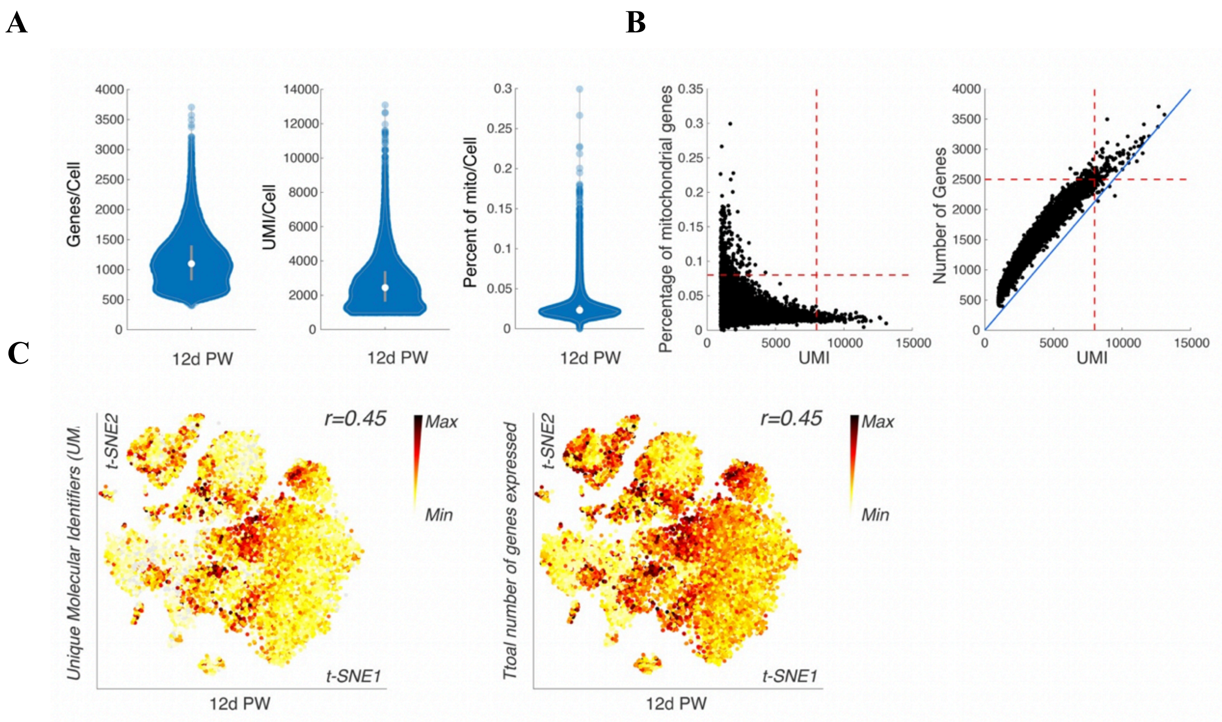


**Figure 4.2. Quality control metrics of 3'-end single cell data. (A, B)** Genes/Cell, unique molecular identifiers (UMI)/Cell, and ratio of mitochondrial (mito)/Cell genes are shown. **(C)** t-SNE plot with color-coded UMIs per cell is shown. Cells with the highest UMI are colored black. t-SNE plot with color-coded number of expressed genes per cell is shown. Cells with the lowest number of genes are colored in light yellow and highest number of expressed genes are colored black.

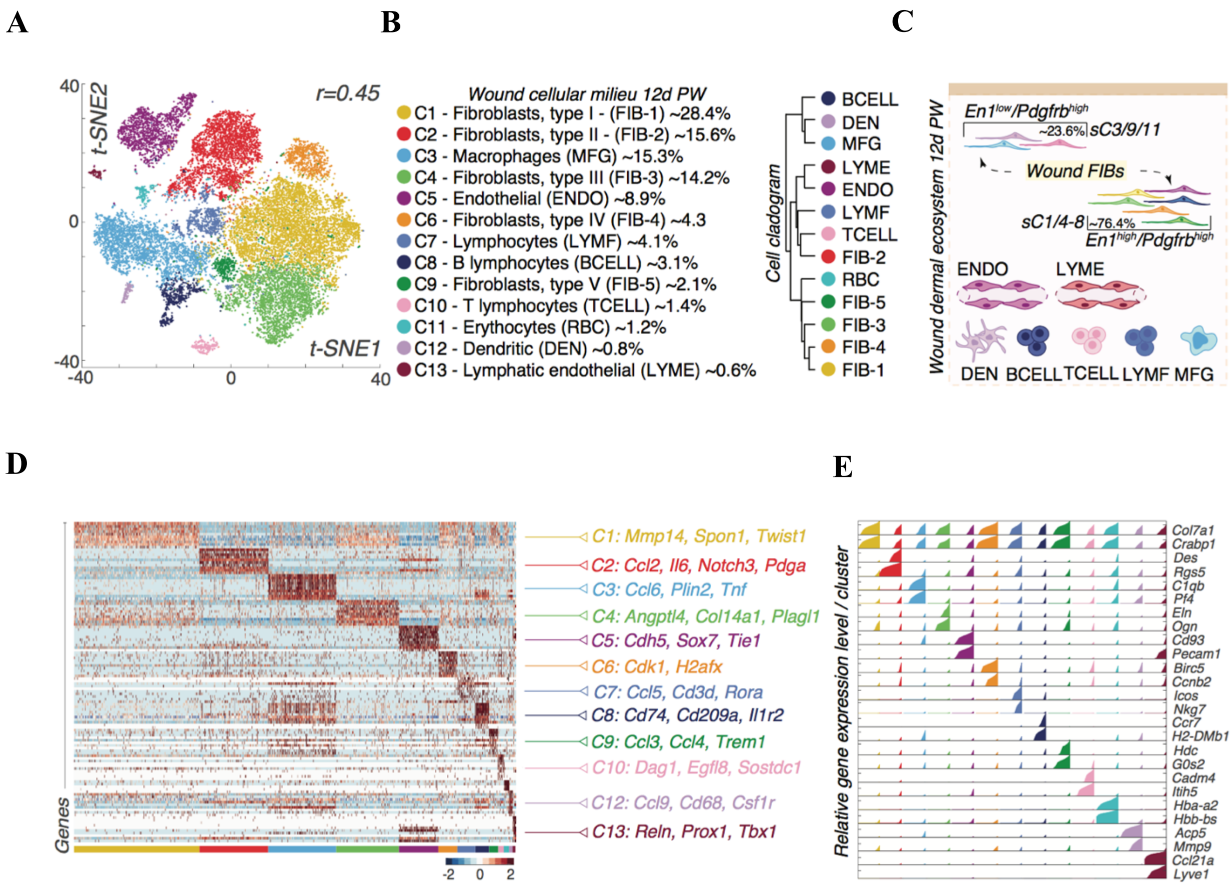


**Figure 4.3. Identification of the cellular ecosystem of early mouse skin wounds. (A, B)** t-SNE plot reveals cellular heterogeneity in post-wounding day 12 skin wounds. 13 distinct cellular clusters are identified and color-coded with hierarchical clustering of sequenced cells. **(C)** Wound schematic showing cellular repertoire in day 12 wounds. **(D)** Different cell types, as identified on scRNA-seq, are color-coded to match cell cluster colors. Heatmap of differentially expressed genes. **(E)** Relative expression of select cluster-specific genes in all sequenced wound cells is shown. Two differentially expressed genes are shown per cluster.

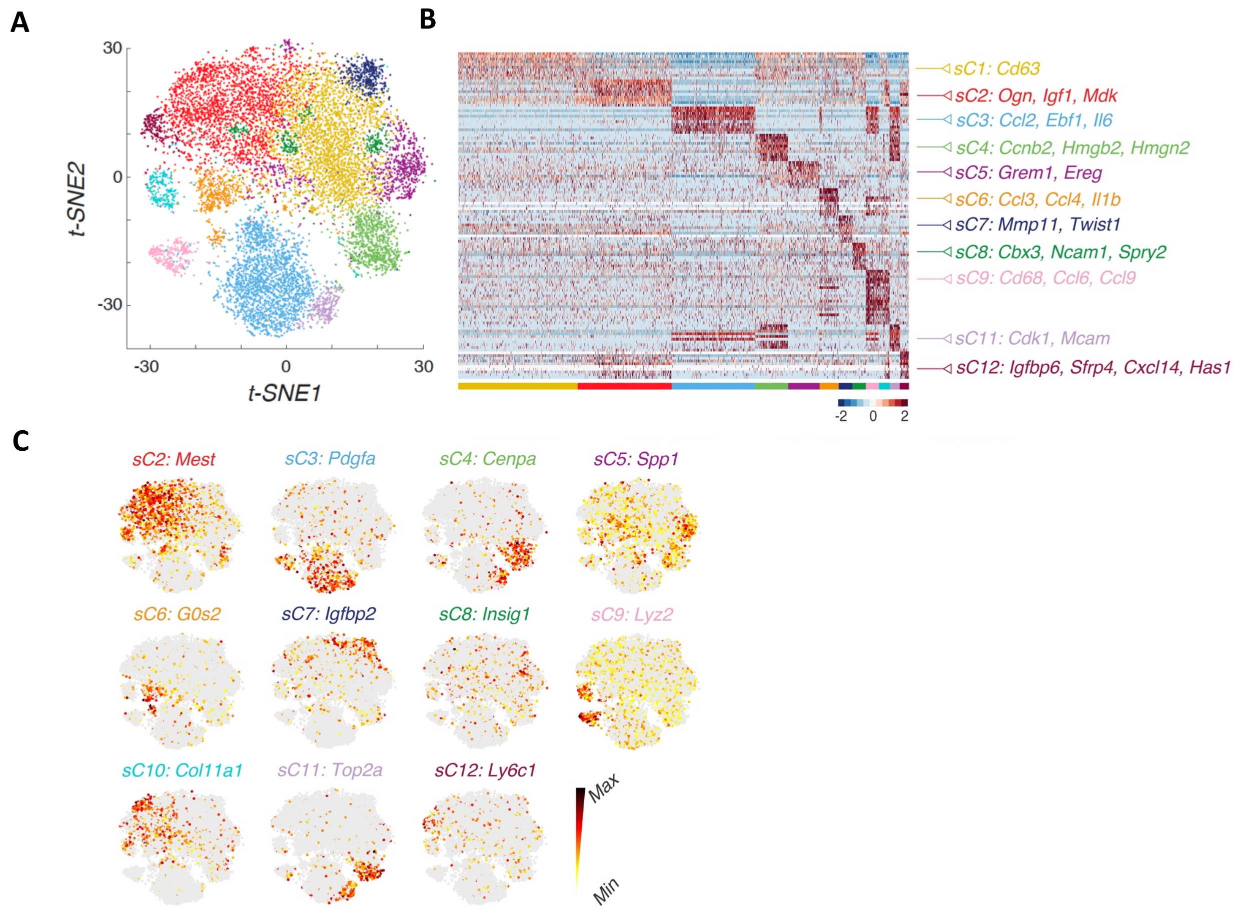


**Figure 4.4. Sub-clustering of wound fibroblast. (A, B)** Sub-clustering of wound fibroblasts identified twelve sub-clusters with distinct gene expression profiles. **(C)** t-SNE plots of select cluster-specific genes. Expression levels for each cell are color-coded and overlaid onto the t-SNE plot. Cells with the lowest number of genes are colored in light yellow and highest number of expressed genes are colored black.

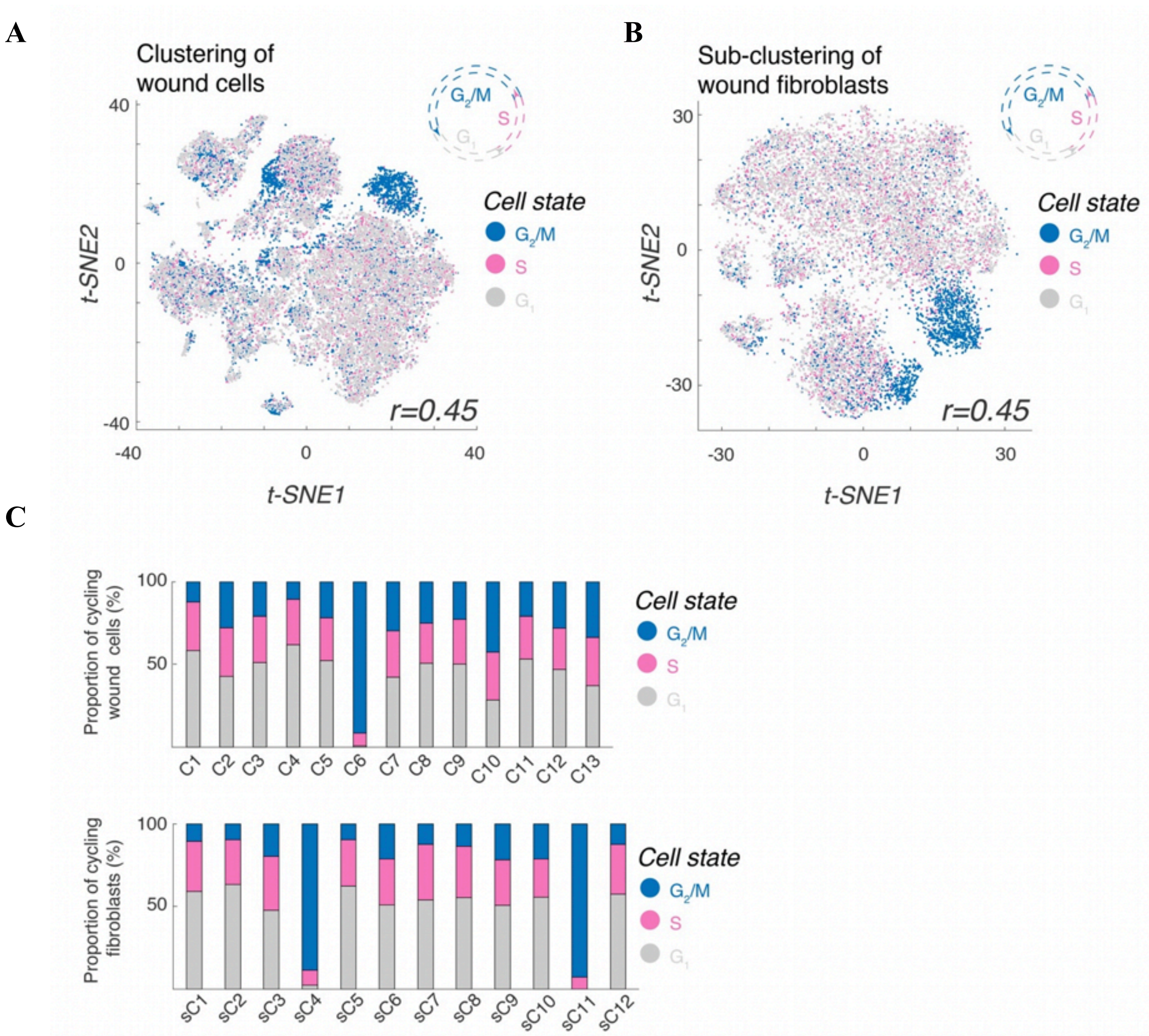


**Figure 4.5. Cell cycle analyses. (A)** t-SNE plot of assigned cycling score on total wound cells. Cells in S phase are colored pink, G2/M phase – blue and G1 phase – grey. **(B)** t-SNE plot of assigned cycling score on wound fibroblasts. **(C)** Proportion of hair cycle stages per cluster.

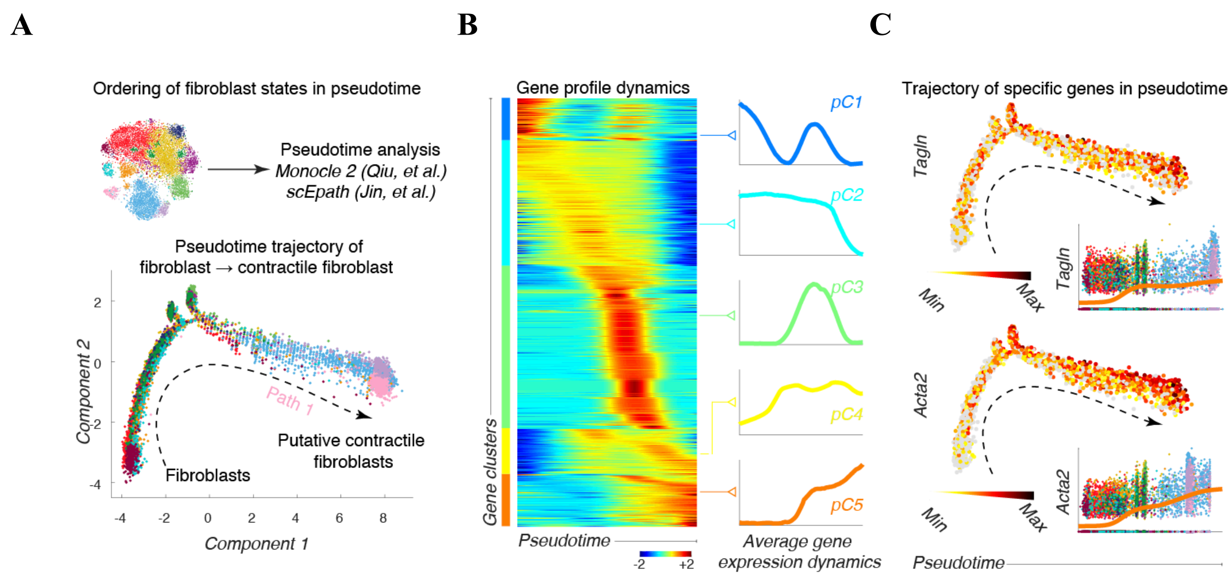


**Figure 4.6. Pseudotime analyses of wound fibroblasts**. **(A)** Unbiased pseudotime analysis on wound fibroblasts reveals putative fibroblast lineage trajectories. Putative fibroblast differentiation trajectory (Path 1) is marked. **(B)** scEpath analysis performed on Path 1 wound fibroblasts identifies five gene clusters (pC1 through pC5) of differentially expressed genes. "Rolling wave" plot of the expression levels for all differentially expressed genes in wound fibroblasts. **(C)** Expression levels of contractile markers *Tagln* (top) and *Acta2* (bottom) overlaid onto the pseudotime trajectory of wound fibroblasts.

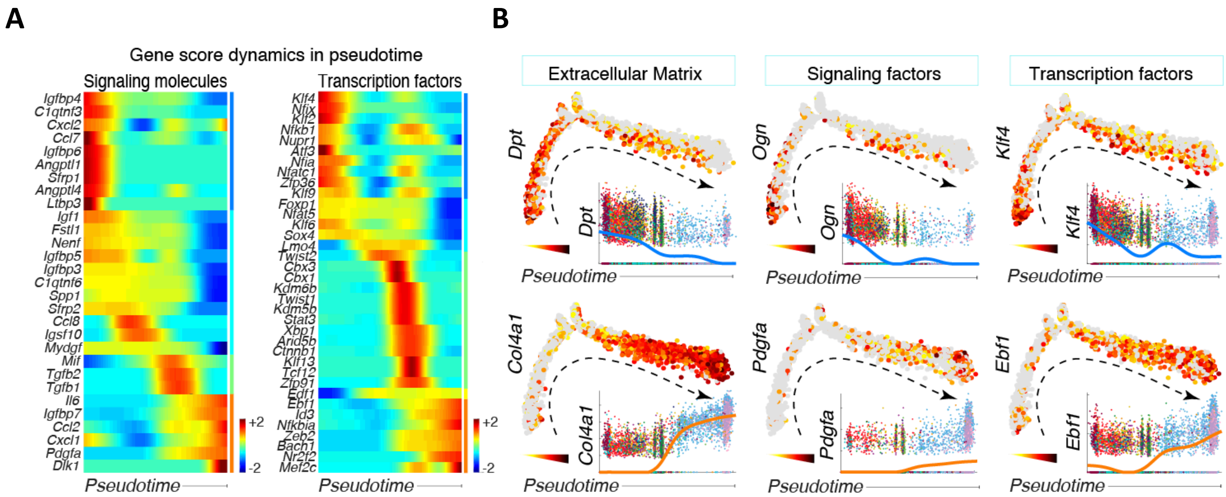


**Figure 4.7. Rolling wave plots and gene expression dynamics across pseudotime. (A)** Rolling wave plots for select signaling molecules (left) and transcription factors (right) identified as differentially expressed in wound fibroblasts from Path 1 pseudotime trajectory. **(B)** Pseudotime analyses of select extracellular matrix genes, signaling factors, and transcription factors.

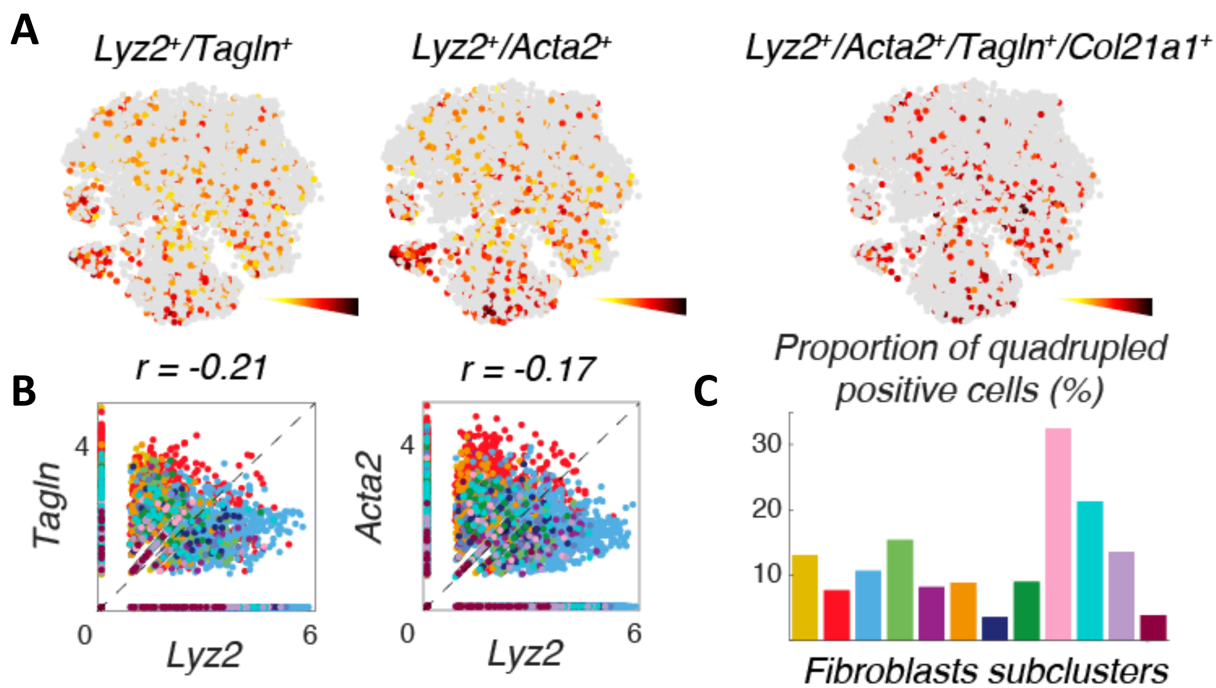


**Figure 4.8. Identification of rare hematopoietic-derived wound myofibroblasts *in silico*. (A)** Overlay of *Lyz2, Tagln* and *Acta2* expression onto t-SNE space reveals *Lyz2/Tagln* and *Lyz2/Acta2* double-positive cells among wound fibroblasts. Similarly, quadruple-positive cells distribute throughout all wound fibroblast subclusters, similar as double-positive cells. **(B)** Correlation plots of *Lyz2 vs Tagln* or *Lyz2 vs. Acta2*. **(C)** Quantification of quadrupled-positive cells in each fibroblast sub-cluster.

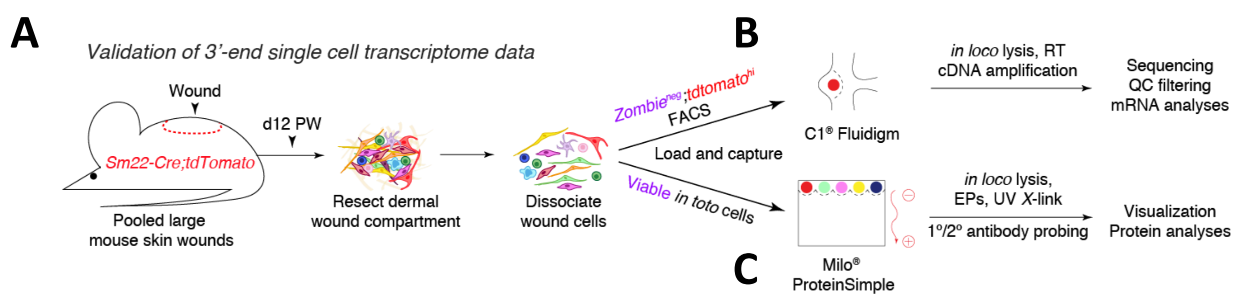


**Figure 4.9. Schematic of hematopoetic-derived myofibroblast characterization. (A)** Schematic of characterization of Lyz2-expressing myofibroblasts using (B) full length single cell RNA-sequencing and **(C)** single cell immunoblotting.

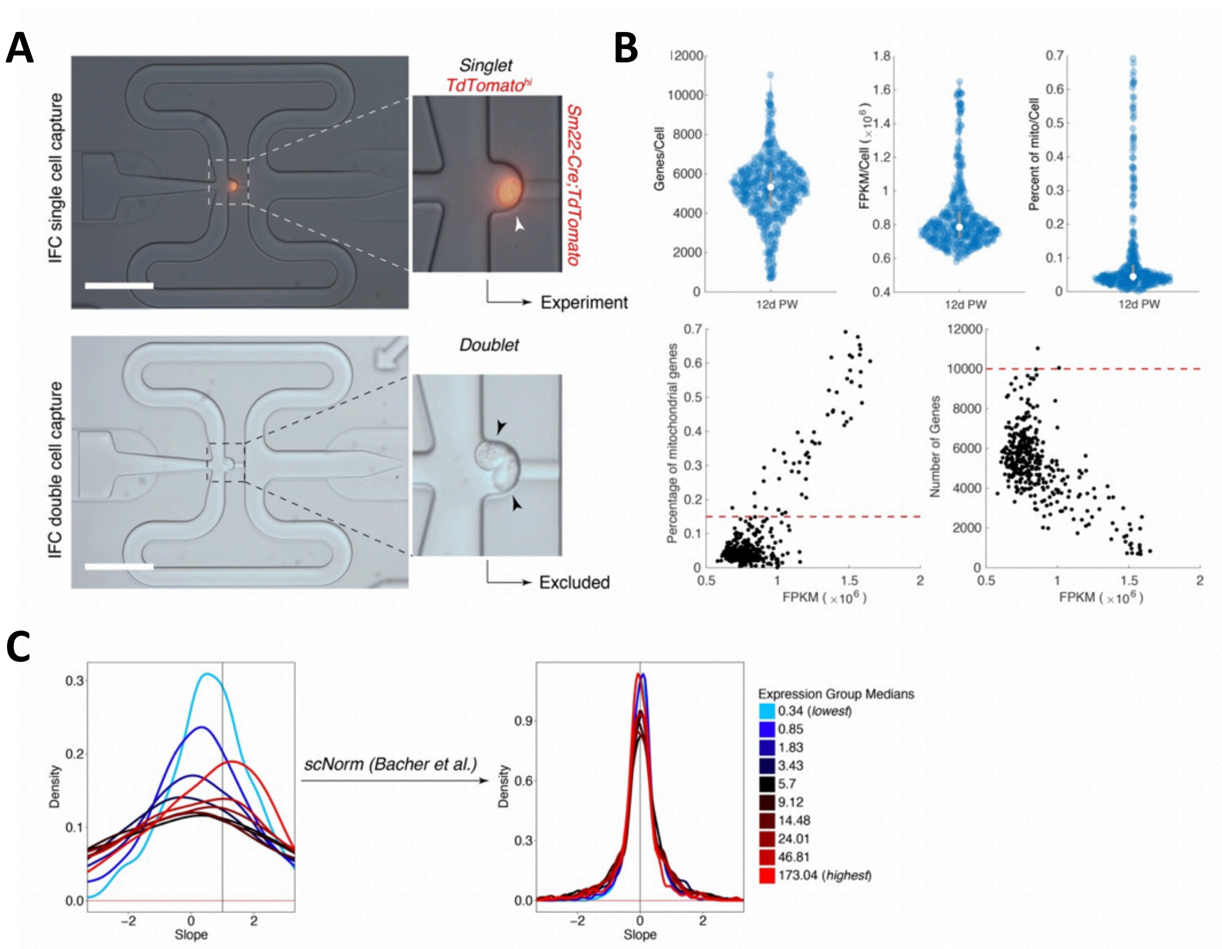


**Figure 4.10. Full length scRNA-seq quality control metrics. (A)** Visual discrimination of automated singlet and multiplet cell capture is shown. **(B)** Genes/cell, FPKM/cell, and ratio of mitochondrial (mito)/cell genes are shown. **(C)** Normalization of scRNA-seq data using scNorm. Graph on the left shows pre-normalization distribution of gene expression counts to sequencing depth for ten equally sized groups of genes. Each gene group is color-coded. Graph on the right shows post-normalization count-depth relationship. A – 125 µm.

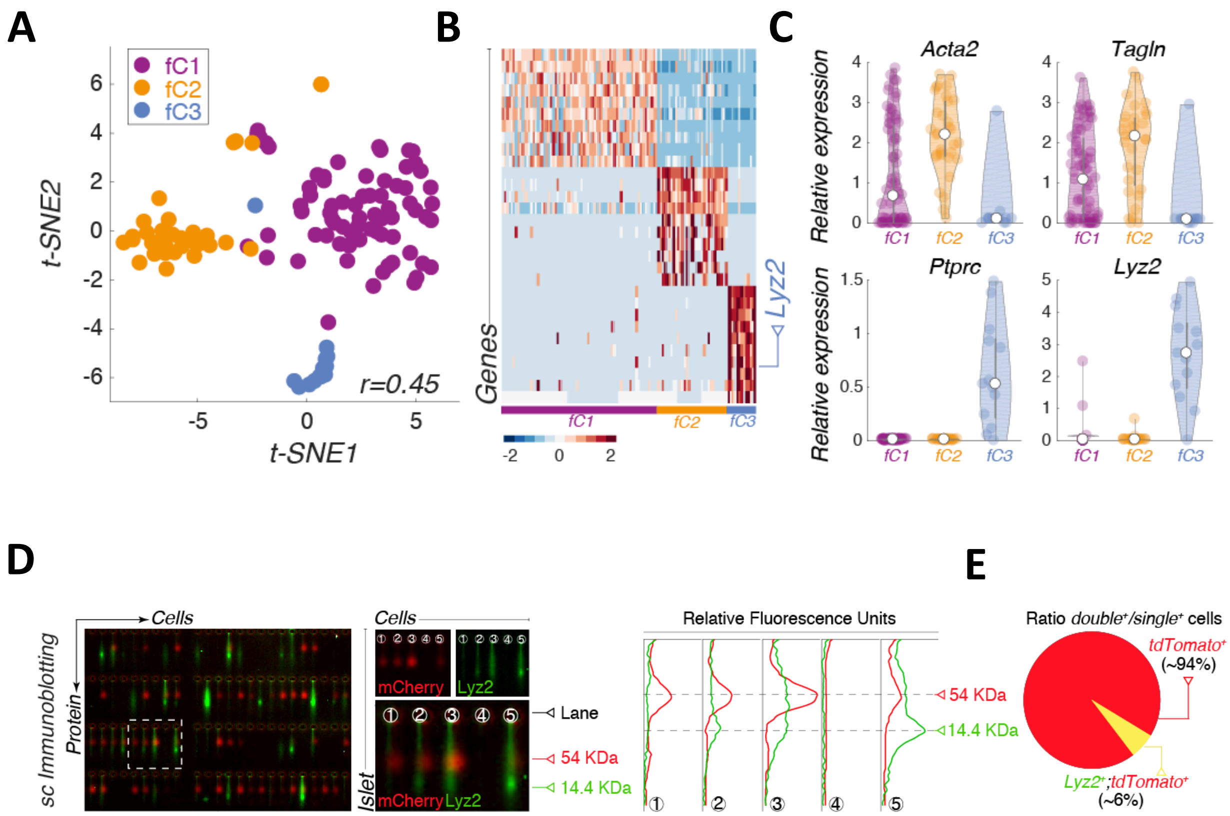


**Figure 4.11. Identification of rare hematopoietic-derived wound myofibroblasts. (A)** t-SNE plot reveals cellular heterogeneity among tdTomato$^+$ cells in day 12 skin wounds from *Sm22-Cre;tdTomato* mice. A total of 116 sequenced cells are analyzed. Three distinct cellular clusters are identified and color-coded. **(B)** Heatmap of top differentially expressed genes is shown in the center and *Lyz2* is marked. **(C)** Violin plots of contractile markers *Acta2* and *Tagln*, pan-hematopoietic marker *Ptprc* (aka *Cd45*) and myeloid marker *Lyz2* are shown on the right. **(D)** Single-cell western blot analysis on unsorted cells from day 12 post-wounding *Sm22-Cre;tdTomato* wounds reveals Lyz2-expressing myofibroblasts. Relative fluorescence units are shown. **(E)** Quantification of tdTomato$^+$/Lyz2$^+$ cells shows that approximately 6% of tdTomato-expressing wound cells were Lyz2$^+$/tdTomato$^+$ double positive (77 out of 1,293 cells).

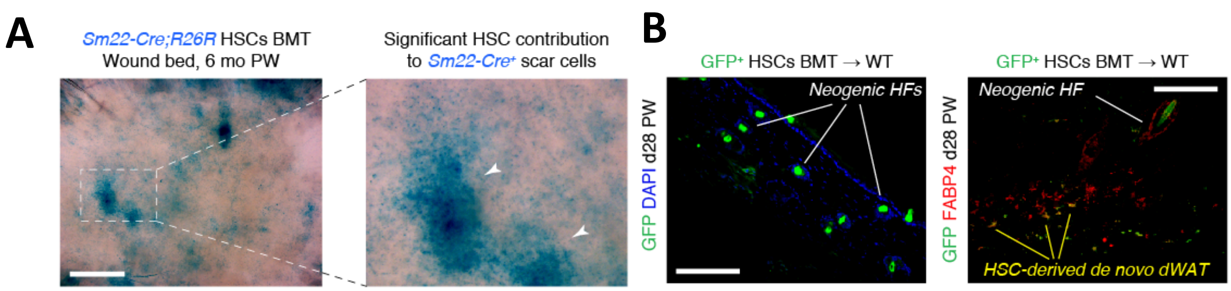


**Figure 4.12. Long term contribution of hematopoetic-derived cells to regenerating wounds. (A)** LacZ expression patterns in the wounds of *Sm22-Cre;R26R* HSCs BMT mice confirm that a portion of contractile scar cells originate from hematopoietic progenitors. **(B)** GFP expressing cells in GFP$^{+}$ HSCs BMT mice show significant contribution to the areas of hair follicles and dermal fat neogenesis 28 days post-wounding. Size bars: A – 1 mm, B – 50 µm.

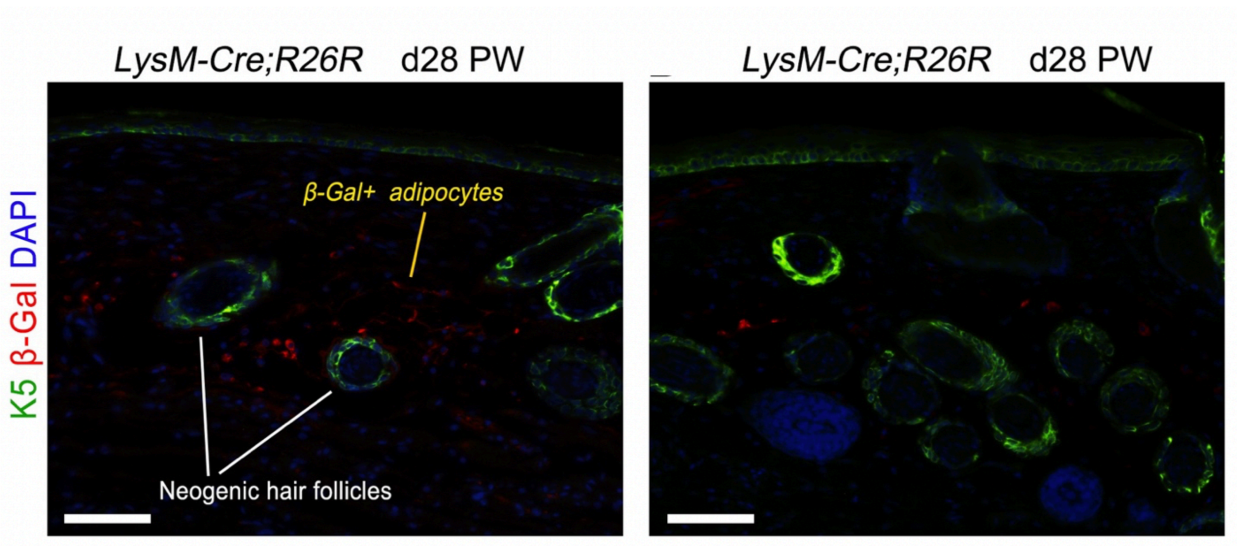


**Figure 4.13. Contribution of hematopoetic-derived cells to regenerating wounds.** β-galactosidase positive cells (red) with adipose morphology form in the wounds of myeloid-specific *LysM-Cre;R26R* mice. Size bars: 200 μm.

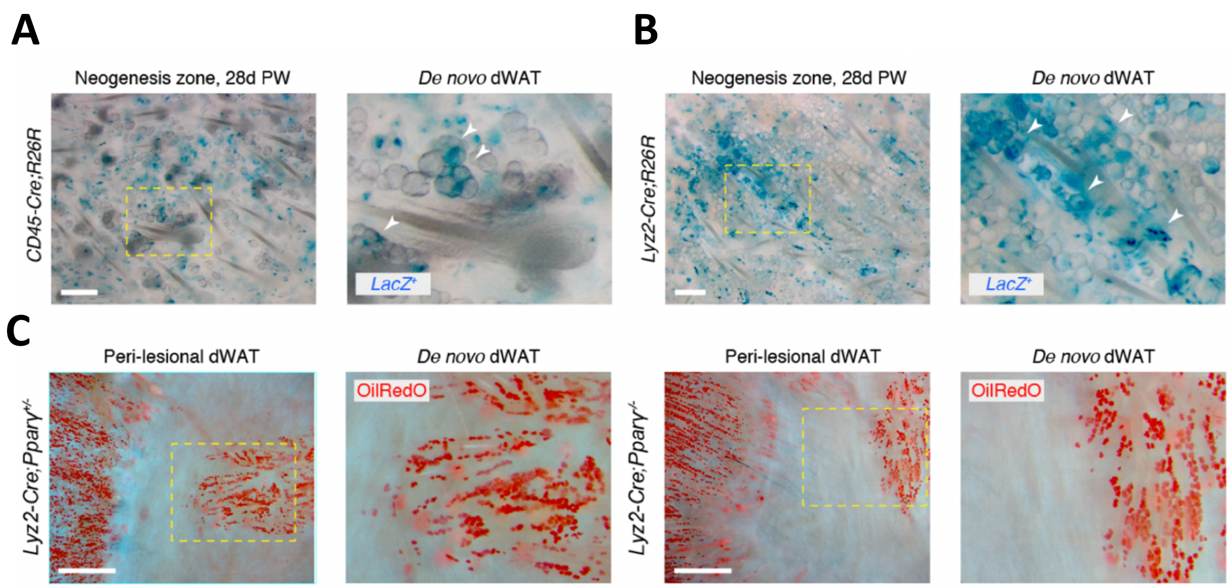


**Figure 4.14. Recruited hematopoetic progenitors contribute to regeneration of skin. (A, B)** LacZ positive clusters of adipocytes (white arrowheads) and lacZ positive dermal papillae are consistently observed in the wounds of hematopoietic specific *Cd45-Cre;R26R* and myeloid-specific *LysM-Cre;R26R* mice. **(C)** When *Pparg* is deleted in Cd45 or LysM-expressing cells, dermal adipocytes regenerate, suggesting that the contribution of hemaeopoetic-derived dermal adipocytes is limited. Size bars: A, B – 200 μm; C – 1mm.

# CHAPTER 5

## Summary, conclusions and future directions

In the works presented in this thesis, I investigated and expanded on important concepts in wound healing and regeneration previously observed in the laboratory mouse – *Mus musculus*. The paradigm in the field of wound healing suggested that mice healed wounds by scarring, and this idea prevailed for many years in the field. Skin scar tissues are different from normal, unwounded skin in that they lack appendages and may be compromised and susceptible to further injury and infection from opportunistic pathogens. In the mid 1950s, Breedis *et al*. described the ability of rabbits to regenerate hair follicles *de novo* after wounding, which partially reminisces nascent skin. Since then, several models of skin regeneration have been described. It wasn't until the 2000s when Ito and colleagues re-discovered this phenomenon in mice and fully characterized the molecular mechanisms driving it. It was termed wound induced hair neogenesis (WIHN). Because of the contradicting literature on the ability of rats to regenerate hair follicles *de novo* after wounding, I became interested in comparing their ability to regenerate with mice, the established model of skin and appendage regeneration. By performing detailed characterization of the wound healing dynamics in both systems, it was determined that both animal species can heal and carry out otherwise normal wound re-epithelialization dynamics after large excisional wound infliction. However, rats, unlike mice, consistently failed to regenerate *de novo* hair follicles. This lack of regenerative potential held true in different large injury models and strains/genetic backgrounds. I took advantage of the growing field of transcriptomics and devised a strategy to interrogate the transcript profile changes in dermis and epidermis of rats – both important for hair follicle regeneration, and compared with those in mice at a time point coincident with initiation of hair follicle neogenesis. Interspecies transcriptome analyses revealed intrinsic tissue differences between both species, whereby rat epidermis expressed an array of distinct transcriptional and epigenetic factors, markers of epidermal repair, hyperplasia, and inflammation, and lower levels of the pleiotropic WNT signaling effectors and regulators. Epigenetic regulators involved in WIHN have been seldom studied. In the interspecies analyses, several epigenetic factors were identified, suggesting that these might be important for achieving, or not, a regenerative potential. These included including *Satb1*, *Setd1b*, *Setdb1*, and *Whsc1l1*. Currently, there are many available transgenic mouse systems available that may be used to evaluate the role of the aforementioned epigenetic factors in WIHN. The number of transgenic rats, however, is rudimental. To overcome this issue, xenotransplantation rat models were used to evaluate the lack of competency of rat adult epidermis to inductive signals by dermal papillae. Indeed, it was determined that the epidermis of rats cannot be induced to regenerate hair follicles, further confirming the interspecies analyses that the epidermis of rats appears less mature. Future experiments in this area can further explore the role of transcription and epigenetic factors in WIHN in mice by taking advantage of the availability of tissue specific *Cre* and *LoxP* systems. In rats, one could exploit new technologies for *in vivo* gene KO, such as CRISPR (Wu et al., 2017), as well as *in vivo* CRISPR screens (Wu et al., 2018) to identify genes involved in regeneration *vs.* scarring in rats.

The characterization of hair follicle neogenesis in mice opened up new areas of investigation in the field of wound healing. Surprisingly, recent study identified that dermal adipocytes also regenerate in the wound area, and this process is coupled with hair follicle neogenesis. Intriguingly, the origin of dermal adipocytes was determined to be from myofibroblasts. In the past, myofibroblasts were believed to be a terminally differentiated cell type. Nonetheless, it was identified that hair follicles instruct myofibroblasts with signals to change its fate toward adipose lineage. This research opened up various research venues toward modulation of scarring and fibrogenic behavior in organs and tissues via reprogramming of myofibroblasts. This novel concept has also the potential to be applied to skin cancers. For example, modulation of myofibroblast reprogramming can have profound effects on resolution of cancer stroma formation. Future studies should aim at characterization of the roles of dermal adipocytes in wound behavior. For example, it should be determined whether dermal adipocytes can confer wounds with the ability to fight infection by *S. aureus*, the most common type of infection in soft tissues (Zhang et al., 2015) and whether they can also modulate hair cycling of neogenic hair follicles (Zhang et al., 2016). Additionally, some myofibroblasts are unable to undergo regeneration into dermal adipocytes. It should also be explored whether this is due to myofibroblast heterogeneity, or specification prior onset of hair follicle regeneration.

Although the origin of myofibroblasts is quite heterogeneous and tends to be dependent on injury type and organ, the myofibroblast tends to express contractile proteins, including alpha smooth muscle actin, when mature. By using advent single cell sequencing technologies, coupled with functional lineage tracing and bone marrow transplantation assays, the heterogeneity of early stage wounds prior the onset of regeneration was explored. First, a large repertoire of cell types were identified. These cell types ranged from endothelial, immune to several subsets of fibroblasts. Collectively, this wound ecosystem might work in concert to initiate a regenerative response in wounds. This idea should be explored in future studies. By taking advantage of tools to explore the behavior of lineage connected cells in pseudotime, the trajectory of fibroblasts toward a myofibroblast state was explored. Indeed, many putative genes were identified in this differentiation trajectory that may be important in myofibroblast differentiation. Future studies should aim at functionally testing these genes in the context of wound healing using *in vivo* CRISPR KO techniques, or tissue specific gene ablations using *Cre-Lox* technologies. Similarly, one should determine which fibroblast populations have the potential to give rise to dermal adipocytes in the wound by employing functional lineage tracing technologies and loss- or gain-of function experiments. Lastly, a hematopoetic-derived, collagen producing fibroblast was identified in the wound. This cell, indeed, exists in wounds and has the potential to maintain itself in the wound environment long term, and reprogram into a small number of dermal adipocytes during regeneration. Future studies should aim at further delineating the heterogeneity of myofibroblasts. For this, a time course of single cell analyses spanning major regenerative events in the wound bed should be performed. This type of analyses can shed light on specification of lineages important for establishment of regeneration *vs*. scarring in skin wounds.

My interest in the concept of biomimicry led to identification of novel model organisms to study wound healing and regeneration in wild environments. Studying animal behavior in their natural habitat has advantages and disadvantages. For example, it provides the researcher with the opportunity to interrogate wound healing and regeneration mechanisms under natural conditions, including under times of stress, which are largely obscured when working with already established model systems in the laboratory. One such organism is the northern elephant seal *M. angustirostris*. This large, aquatic animal provides the opportunity to study wound healing using an interval censored sampling approach. Indeed, despite the stresses *M. angustirostris* faces, which include fasting and infection, they are able to heal large predator wounds even when they become infected. Hence, this animal can enable the identification of mechanisms of innate immunity during wound healing to prevent infection, as well as the resolution of fibrogenic behavior. Thus far, I have characterized wound healing dynamics in the northern elephant seal, and they appear to undergo normal healing kinetics. Future studies should aim at resolving the microbiome of skin wounds, as well as identifying the genes important in innate immune response upon the presence of bacterial products *in vitro*. Finally, functional testing of such genes *in vivo* by means of xenotransplantation and mouse KOs will help to uncover their roles in innate immunity and wound healing.

The research presented herein expands on concepts related to cell reprogramming, tissue competency and signaling, advent single cell sequencing technologies for identification of cells with intrinsic regenerative and/or fibrogenic potential, and novel models of skin wound healing and regeneration under stressful environments to learn about efficient wound healing and regeneration of skin and shed light on the development of novel therapeutics for the treatment of conditions characterized by chronic wound healing and fibrosis (Fig. 5. 1)

.

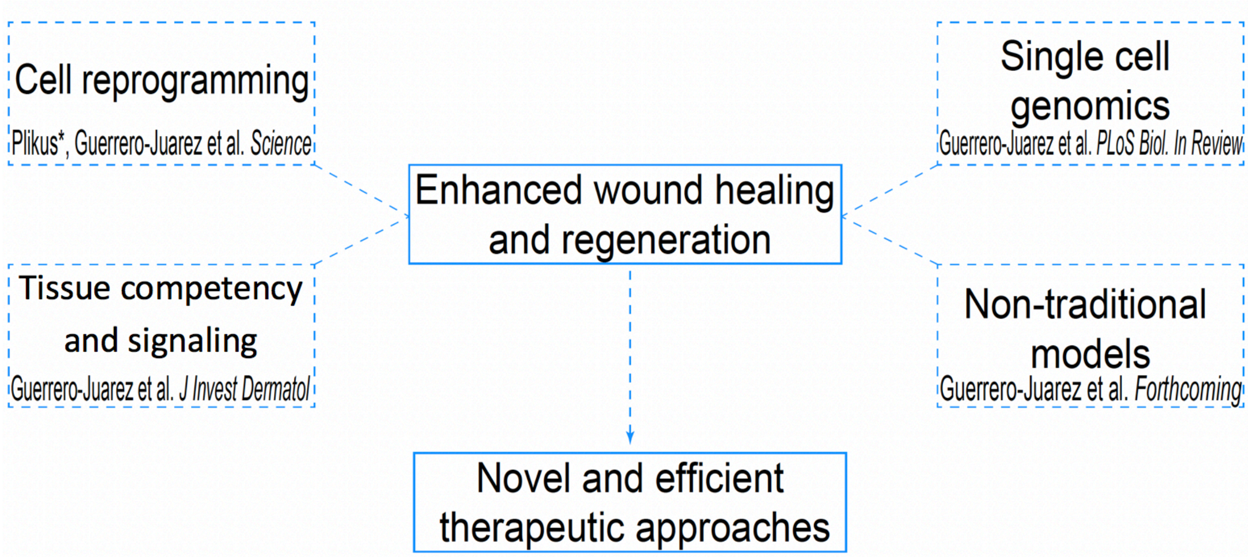


**Figure 5.1. Schematic summarizing novel concepts in study of wound healing and regeneration.** Concepts in cell reprogramming, tissue competency and signaling, single cell genomics and non-traditional models of wound healing and regeneration may shed light on enhanced wound healing and regeneration of skin for the future development of novel and efficient therapies for the treatment of chronic wounds and those prone to fibrosis.

# APPENDIX A.1

## Wound healing in Northern Elephant Seals in natural habitats

### Statement of contribution

In this study, I designed (in agreement with my thesis advisor Dr. Maksim V. Plikus) and performed experiments, analyzed data and interpreted results. My data contributes to Figs. A.1.3, A.1.4., A.1.5, A.1.6 and A.1.7. In instances, Raul Ramos (University of California, Irvine) helped to collect skin biopsies. Dr. Dorian Houser (National Marine Mammal Foundation), Dr. Daniel Crocker (Sonoma State University), and Dr. Jane Khudyakov (University of the Pacific) helped to chemically immobilize elephant seals (related to Fig. A.1.2.) and provided insightful comments, advice and criticism. Dr. Xiaoling Cao (UC Irvine/First Affiliated Hospital of Sun Yat-Sen University – People's Republic of China) aided technically with preliminary xenograft transplantation (Related to Fig. A.1.7).

**ABSTRACT**

Wound healing is an intricate process that requires coordination among the innate and adaptive immune systems, tissue stem cells, and growth factor signals to launch an effective antimicrobial defense, coupled with a robust regenerative response. The northern elephant seal (*Mirounga angustirostris*) is able to effectively repair large cutaneous wounds, as well as to regenerate prominent adnexal structures despite being influenced by factors that are known to exacerbate the healing process in humans, such as fasting and infection. Despite these stressors, *M. angustoristris* undergo normal wound healing dynamics and display normal wound closure. The closing wound displays a stratified epidermis with strong basal expression of Krt5 and actively proliferating keratinocytes. In contrast, the un-repithelialized wound center does not. Remodeling of their dermal compartment is also observed, with minimal myofibroblast presence and an intricate, yet complex composition of interweaved collagen fibers. Indeed, *M. angustoristris* is capable of undergoing hair follicle neogenesis. Preliminary xenograft transplantation studies are developed to study wound healing and modulation of infection in seal cells in an immunocompromised mouse host.

# INTRODUCTION

The northern elephant seal (NES) is a pinniped within the family *Phocidae* (Bininda-Emonds et al., 1998) of the genus *Mirounga* that follows a dichotomous lifestyle (Figure A.1.1, A.1.2) (Hindell and Perrin, 2009). Their habitat includes open oceanic waters of the Pacific coastline and range from the Gulf of Alaska to Baja California Sur, Mexico (Block et al., 2011, Robinson et al., 2012). Despite being largely aquatic, NES spend substantial time on land. In late December and early January, NES settle ashore, where females undergo parturition (Reiter et al., 1981) and estrus females breed with dominant alpha males (Leboeuf and Mesnick, 1991, Mesnick and Leboeuf, 1991). In contrast, NES undergo molting in mid-summer months – an energetically costly period (Worthy et al., 1992) characterized by synchronous shedding of club hairs (Ling, 1970). NES have a rich diet. Stomach lavage analyses in chemically-immobilized NES revealed their diet consists mainly of fish and crustaceans (Antonelis et al., 1987). NES have wound healing prominently built into their life cycle (Figure A.1.1). During the winter breeding season, alpha males engage in physical combats in efforts to establish hierarchical dominance over estrus females (Haley et al., 1994, Leboeuf, 1974). Combats are often violent and males inflict upon each other multiple abrasions. While numerous, male-male fighting-inflicted wounds are mostly deep punctures or small to medium size lacerations and are largely restricted to the male's specialized neck shield and facial proboscis – highly keratinized anatomical structures that evolved to help minimize the depth, size and prominence of such wounds. During their time in open waters, NES fall prey not only to apex-predators, which include orcas (*Orcinus orca*) (Ferguson et al., 2012), great white sharks (*Carcharodon carcharias*) (Klimey, 1994, Klimley, 1994a, 1994b, Klimley et al., 1996) and cookie cutter sharks (*Isistius brasiliensis*) (Leboeuf et al., 1987), but also to marine debris which, aside from contributing to the ghost fishing effect (Stelfox et al., 2016), inflict life-threatening wounds and often times result in malformations of the head and neck areas (Dau et al., 2009, Hanni and Pyle, 2000). Unlike combat wounds, however, wounds inflicted by apex-predators are often significant in prominence, surface area and depth.

Routine fieldwork has led to anecdotal and recorded evidence that seals are capable of rapidly and efficiently repairing skin injuries, including apex-predator-inflicted (Naessig and Lanyon, 2004, van den Hoff and Morrice, 2008), branding-inflicted (van den Hoff et al., 2004) and tagging-inflicted wounds (Paterson et al., 2011). Some of these accounts have been described also in free-roaming NES found along the Pacific coastline, as well as southern elephant seals (*Mirounga leonina*) in the coastline of Australia and Mexican islands. Stranded NES are also capable of healing in captivity upon human intervention, leading often times to their release into the wild (Higgins and Hendrickson, 2013). Because of these accounts, I became interested in characterizing wound healing dynamics and the effects natural life stressors have on wound healing outcomes in wild NES. For example, NES often heal wounds under septic conditions. Similarly, they often undergo severe stresses, which are known exacerbations of wound healing in humans and which include certain wound-specific (i.e. infection) and systemic variables (i.e. nutrition (Mrosovsky and Sherry, 1980)), and diseases and conditions (i.e. genetic skin diseases, obesity and metabolic syndrome during prolonged fast (Houser et al., 2013)) (Sun et al., 2014). The severity and extent of apex predator-inflicted wounds was analyzed using existent photographic records of free-roaming NES obtained between 1980 and 2018 from Año Nuevo State Reserve, CA, USA (37°7′59″N, 122°19′59″W). The wounds analyzed were consistent with previously reported predator-inflicted wounds and some displayed dentition marks corresponding to apex predators, including *C. carcharias*. Apart from integument rupture and loss, we found some NES sustained additional traumas, which included open bone fractures and perineal abscesses (data not shown). The nature of these secondary traumas, coupled with susceptibility to local and systemic infection posed by the septic coastline environment (Yamahara et al., 2007), may be detrimental to the health and survival of wounded NES and may negatively affect their fitness. Nevertheless, and contrary to popular expectation, large scale macrophotography and interval-censored monitoring of NES injuries corroborated previous accounts and further highlighted their superb ability to recuperate and survive from major traumatic injuries (data not shown).

## RESULTS

To interrogate the molecular mechanisms of wound healing in NES, wounds from free-roaming males (*n=3 animals total)* from a sizeable colony at Año Nuevo State Reserve obtained between August 2014 and April 2018 were sampled. Early and late healing events in non-standardized, apex predator-inflicted wounds were analyzed by taking advantage of the fact that injured seals mainly remain on shore during wound healing. This healing period coincides with the breeding season or foraging migration (1966) and seals can be approached for interval-censored sampling (Archie, 2013a). This provided the opportunity to study wounds within days of infliction, as well as late-stage wounds undergoing active re-epithelialization, remodeling and regeneration (Gurtner et al., 2008). Close examination of early-stage predator-inflicted wounds revealed a build-up of purulent exudate emanating from their surface, suggesting local infection (n=3). Furthermore, histological analyses revealed the presence of bacteria, a high degree of erosion with granular appearance – characteristic of a dense inflammatory infiltrate and increased numbers of superficially proliferating capillary plexuses, suggesting active angiogenesis (Tonnesen et al., 2000) (Figure A.1.3). In contrast, closing wounds underwent active re-epithelialization and displayed two morphologically distinct healing areas. The wound edge, displaying re-epithelialization zones, depicted a characteristic hypertrophic stratified interfollicular epidermal (IFE) structure expressing the acidic cytokeratin marker Krt5 (Moll et al., 1982, Nelson and Sun, 1983) (Fig. A.1.4). Pcna expression in the *stratum basale* (Furukawa et al., 1992) indicates actively proliferating basal keratinocytes. Of interest is the observation of regenerated Rete ridges – spatial epidermal oscillations at the interface between the regenerating epidermis and dermis. Seal wounds at this stage assume a pattern of collagen fibers similar to unwounded dermis and are also associated with low presence of α-Sma$^{+}$ myofibroblasts. Furthermore, the ECM in seals had less densely packed collagen fibers, contained more porous and weaved-like collagen bundles and elastin fibers. Future studies should follow a comparative wound healing analyses between *Mirounga* and *Mus* at the histological level (data not shown).

To establish if healed NES wounds recapitulate aspects of nascent skin (Gay et al., 2013, Guerrero-Juarez et al., 2018, Ito et al., 2007, Nelson A. M. et al., 2015, Plikus et al., 2017, Wang et al., 2015), healed wounds were sampled for evidence of *de novo* hair follicle (HF) regeneration. Evidence of mature, neogenic HFs was found on a healed dorso-lateral wound, easily identifiable by its unpigmented epidermis. Similar to mice (Gay et al., 2013, Ito et al., 2007, Nelson A. M. et al., 2015), *de novo* HFs initially localize to the center of the healed skin and at a relatively low density, and display variable follicle polarity (Figure A.1.5). This regeneration event is different from normally regenerating HFs in response to molting. At the histological level, *de novo* HFs contained an associated sebaceous gland. In contrast to normal, unwounded skin, however, dermal adipocytes were absent, suggesting *de novo* HF regeneration precedes dermal adipocyte regeneration in wild animals – similar to rodents (Plikus et al., 2017), or, in a latter case, is rudimentary (Guerrero-Juarez et al., 2018). Similar to previous observations in normal skin, the epidermis adjacent to neogenic HFs regenerated prominent Rete ridges and appears hypertrophic. Evidence of normal wound healing and subsequent tissue and appendage regeneration was surprising, however, given the septic conditions in which wound healing takes place. Evidence of WIHN suggests that an ample regenerative response over scarring might be favored during skin repair in NES, most likely to enable them to thrive and maintain their fitness in their natural habitat.

Macro-photography and histological analyses suggested that early stage NES wounds might become infected. In general, humans and rodents demonstrate poor wound healing when wounds become infected (Loesche et al., 2017, Sun et al., 2014). Indeed, a recent study that interrogated different types of chronic wounds in humans, including non-healing surgical wounds, as well as chronic diabetic foot, venous leg, and decubitus ulcers contain a uniquely distinct microbiome profile that correlates with poor healing and contain high proportions of *Staphylococcus* and *Pseudomonas* (Wolcott R. et al., 2016, Wolcott R. D. et al., 2016). Future studies will include interrogating the microbiome of seal skin wounds using 16S rRNA gene sequencing (Janda and Abbott, 2007).

The fact that NES are able to heal and regenerate skin appendages under septic beach conditions prompted me to ask whether NES possess an inherent innate ability to combat infection. Indeed, the skin is a complex heterogeneous organ system and many of the cells in the skin engage in a specific type of immune response upon infection (Nestle et al., 2009). Fibroblasts, however, tend to be highly heterogeneous and distinct subsets may be involved in eliciting an immune response. For example, primary human fibroblasts infected with DENV-2 activated TLR3 and RIG-1 signaling and up-regulated IFN-beta, TNF-alpha, HB5 and H-beta-D2, suggesting that skin fibroblasts can engage contribute to inflammation and anti-viral activities (Bustos-Arriaga et al., 2011). In addition to anti-viral properties of human fibroblasts, a recent review describes the immune responses elicited by fibroblasts in response to microorganism exposure (Bautista-Hernandez et al., 2017). For example, fibroblasts express various Toll-like receptors (TLRs) and these become activated upon presence of microbial ligands, such as PGN, LTA, and LPS. Hence, fibroblasts can recognize PAMPs via TLRs of various microorganisms, including *Staphylococcus aureus*, *Pseudomonas aeruginosa*, *Pseudomonas gingivalis*, and *Escherechia coli* and have the ability to produce antimicrobial peptides, proinflammatory cytokines, and certain chemokines (Bautista-Hernandez et al., 2017, Zhang and Gallo, 2016, Zhang et al., 2015).

Hence, I reasoned that NES dermal fibroblasts could be an important modulator of infection. To interrogate this possibility, the antimicrobial activity of NES dermal fibroblasts will be tested *in vitro*. For example, various Gram-positive and negative bacteria, including *Staphylococcus aureus*, *Pseudomonas aeruginosa*, and *Escherechia coli* will be cultured with NES and mouse dermal fibroblast conditioned media and bacterial growth will be evaluated across time. It is hypothesized that conditioned media from NES dermal fibroblasts will display heightened antimicrobial killing activity compared to that of mice. Additionally, the genes involved in this possible heightened antimicrobial killing activity will be evaluated using bulk RNA-sequencing. For example, NES dermal fibroblasts will be cultured *in vitro* and activated with the bacterial products Malp2 and LPS for 24 hours. Primary NES dermal fibroblasts have a common spindle-like morphology, possess adipogenic potential (Louis et al., 2015), and migrate into a wound area in *in vitro* wound healing assays (Louis et al., 2015) (Figure A.1.6). RNA-seq and differential gene expression analyses of Malp2-treated *vs.* control, LPS-treated *vs.* control will be conducted. Because the genome of *M. angustirostris* has not been sequenced, *de novo* transcriptome assembly of activated *M. angustirostris* dermal fibroblasts will be performed (Khudyakov et al., 2017, Khudyakov et al., 2015, Stephan et al., 2018). These analyses will help characterize the emergent properties of NES dermal fibroblasts as sentinel cells and regulators of innate immunity in wild animals. Future studies will be necessary to definitely establish the role of NES dermal fibroblasts as modulators of innate immunity. Experiments include seal-on-mouse xenotransplantations (Figure A.1.7) (Wosgrau et al., 2015) to test antimicrobial killing ability *in vivo*, as well as mouse KO experiments.

## DISCUSSION

NES is an emergent model to study wound healing under adverse healing conditions. It is evident that seals have evolved an outperforming wound healing and regeneration program that increases their fitness in wild habitats and it may partially depend on expression of certain immune modulators in skin. NES appear to be capable of healing wounds amidst facing local and systemic stressors posed by their immediate natural habitat. These stressors are known exacerbations of wound healing paradigms in humans and include wound specific- and systemic-variables, as well as certain conditions such as metabolic syndrome (Sun et al., 2014). NES demonstrate a remarkable ability to quickly repair full-thickness skin wounds inflicted by large apex-predators and might also prevent infection by tissue-specific immune modulator expression. I do not rule out, however, the possibility that abiotic factors (i.e. sea salt) (Pougatsch et al., 2017) or maggot debridement (Sherman, 2003, Tantawi et al., 2007) may confer extra protection against infection and/or modulate efficient healing.

These enhanced wound healing mechanisms are likely shared amongst other pinnipeds, including *Odobenidae* (Kryukova et al., 2012a, 2012b) and *Otariidae* (Galloreynoso and Figueroacarranza, 1992), which thrive in similar habitats, co-habit with and belong to similar food chains, and depict prominent predator-inflicted wounds and analogous healing abilities as NES. Cetaceans, in particular Indo-Pacific bottlenose dolphins *(Tursiops aduncus)*, also demonstrate similar fast-healing properties (Zasloff, 2011). Because NES can undertake prolonged fasts in connection with reproductive activities, molting and wound healing, this type of healing can have physiological implications to maintaining fitness in their respective habitats. For example, regeneration of compact pilosebaceous units can also have survival implications and help NESs cope with the demands of aquatic and terrestrial habitats, including proper insulation in water. Hence, I posit that enhanced wound regeneration in NES and other pinnipeds may have evolved convergently as an adaptation to similar predation pressures by large apex-predators and facilitate their fitness in their natural habitats (Stern, 2013). Because of its unique yearly lifecycle, *M. angustirostris* can serve as a novel model organism to study wound regeneration mechanisms under extreme environmental conditions and natural habitats.

## METHODS

**Study site and wild subjects**. Molting and non-molting juveniles, adult and sub-adult northern elephant seal males and females from a sizeable colony at Año Nuevo State Reserve, San Mateo County, CA, USA (37°7′59″N, 122°19′59″W) were sampled between 08/2014 – 05/2018. Animals were chemically immobilized as previously described (Khudyakov et al., 2017, Khudyakov et al., 2015). Animal handling was approved by National Oceanic and Atmospheric Administration Fisheries Permit No. 19108.

***In vitro* scratch assay.** Primary NES pup dermal fibroblasts were grown to confluency on Radius$^{TM}$ 24-well cell migration assay (CellBiolabs). Upon reaching confluency, the gel layer was removed as per manufacturer's directions and cell migration was evaluated at specific time points (12-96 hours). Covered area was calculated using ImageJ.

**Histology and immunohistochemistry/immunofluorescence.** Skin tissues were collected and fixed in 4% paraformaldehyde, dehydrated, paraffin embedded, and sectioned at 10 µm. Sections were stained with Hemotaxylin and Eosin (national diagnostics). When required, antigen retrieval was performed by heating histological sections in citric buffer (0.1M citric acid/0.1M sodium citrate, pH 6). Antibodies used were rabbit anti-SMA (1:200; Abcam), mouse anti-PCNA (Pcd10) (1:200, Abcam), and rabbit anti-keratin 5 (1:1000, Abcam). The AEC substrate kit was used for color development (Vector Laboratories). Secondary biotinylated antibodies (1:200, Vector) and anti-HRP (1:200, Vector) were used. Trichrome staining was performed on paraffin sections using the Trichrome stain kit (Abcam) as per manufacturer's recommendations with minor modifications. Gram and Elastin staining were performed at the UC Irvine Pathology CORE. Images were taken with a Nikon Eclipse TI inverted microscope.

**Adipocyte differentiation.** Dermal fibroblasts were isolated *in toto* from normal skin as previously described and expanded *in vitro* in DMEM (Gibco) supplemented with 10% heat-inactivated FBS (Atlanta biologics), Penn/Strep (Gibco) and Fungizone (Gibco). Upon reaching ~95% confluency, cells were switched to adipocyte differentiation medium (Cell solutions) for 48 hours and then switched to maintenance media (Cell solutions) for seven days. Cells were maintained in a water-jacketed incubator at 37°C and 5% $CO_2$ output. Lipid droplets were visualized with Bodipy® (Thermo) on day seven. Cells were harvested for RNA isolation on day seven.

**Xenograft.** Xenograft transplantation was performed as described before (Lei et al., 2017) with minor modifications using juvenile seal dermal fibroblasts and P50 mouse keratinocytes. Pelnac® was used as extracellular matrix component. Cells on Pelnac® were transplanted onto athymic mice.

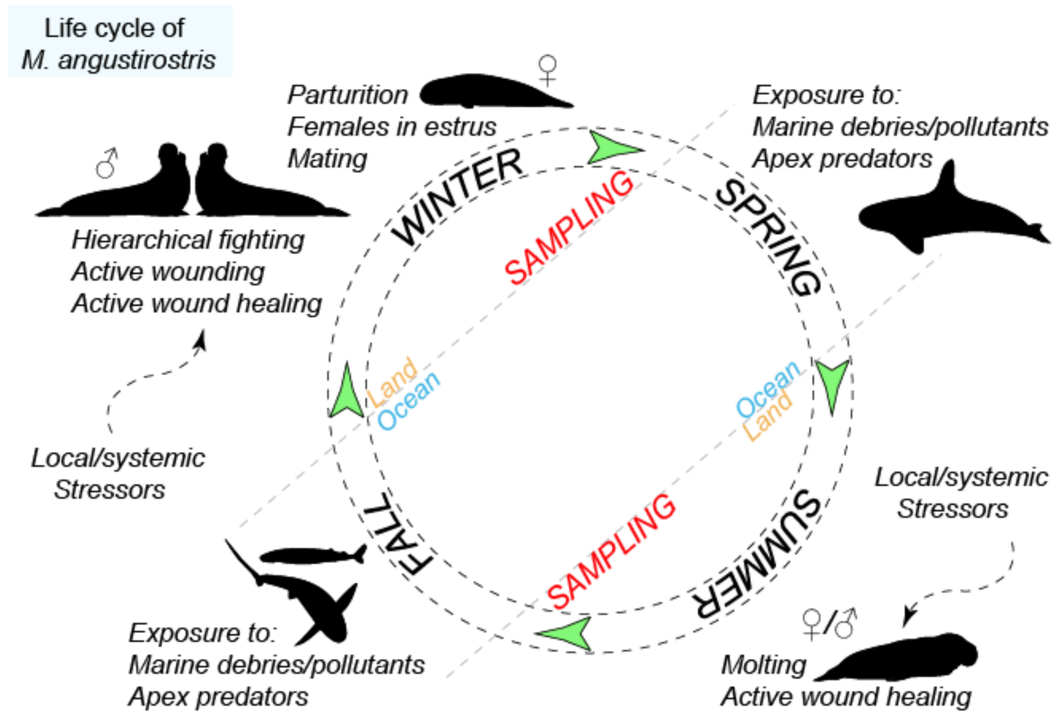


**Figure A.1.1. Schematic of life cycle of *M. angustirostris***. *M. angustirostris* is an aquatic animal that spends most of its time in water, where they are exposed to apex predators. However, during the summer and winter months, *M. angustirostris* settle ashore for mating and molting and, in the case of females, parturition. During this time, *M. angustirostris* are approached for tissue collection, interval censored sampling, and macro-photography. © Christian F. Guerrero-Juarez.

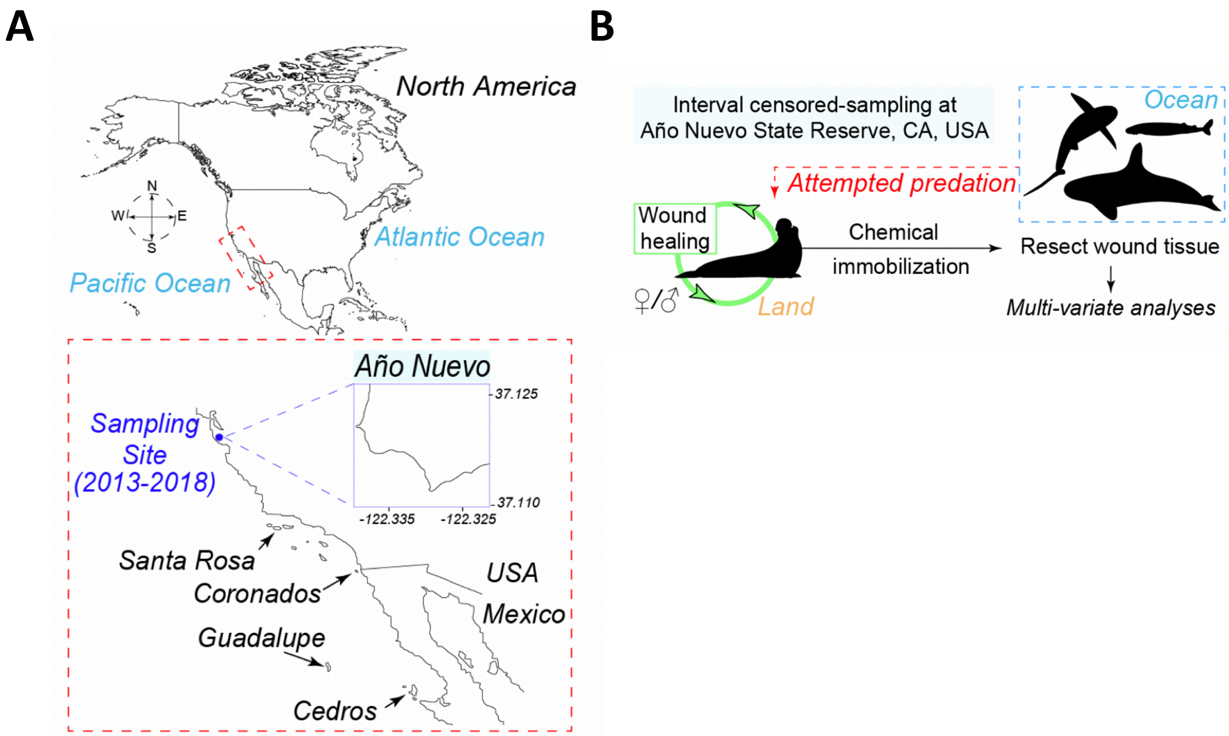


**Figure A.1.2. Schematic of habitat of *M. angustirostris* and sample collection**. **(A)** Map showing various rockeries where northern elephant seals reside during their time in land. Samples are taken from Año Nuevo State Reserve. **(B)** Samples are taken from chemically-immobilized northern elephant seals for downstream analyses. Related to A.1.2 – Map adapted from (Le Boeuf et al., 2011). © Christian F. Guerrero-Juarez.

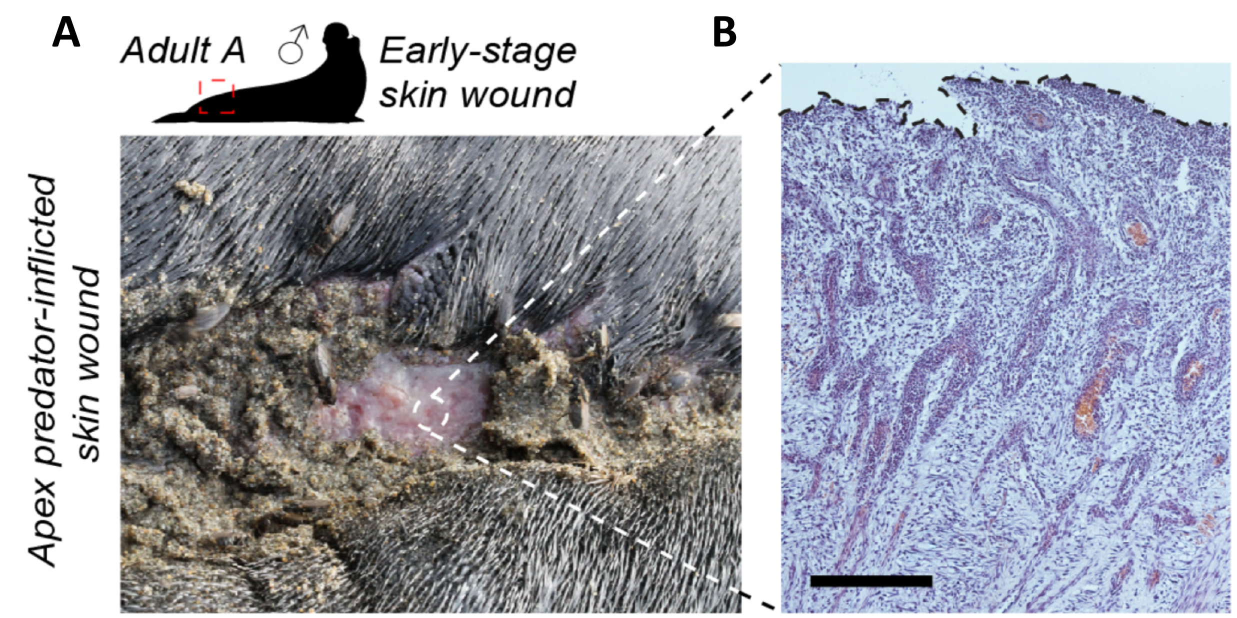


**Figure A.1.3. Histology of early stage wound in *M. angustirostris*.** Early-stage dorsal predator-inflicted wound displays high levels of infection – as shown by the presence purulent exudate. Histological analyses revealed presence of bacteria, active angiogenesis, and inflammatory infiltrate. The wound is covered in sand and flies. Size bars: B – 250 µm.

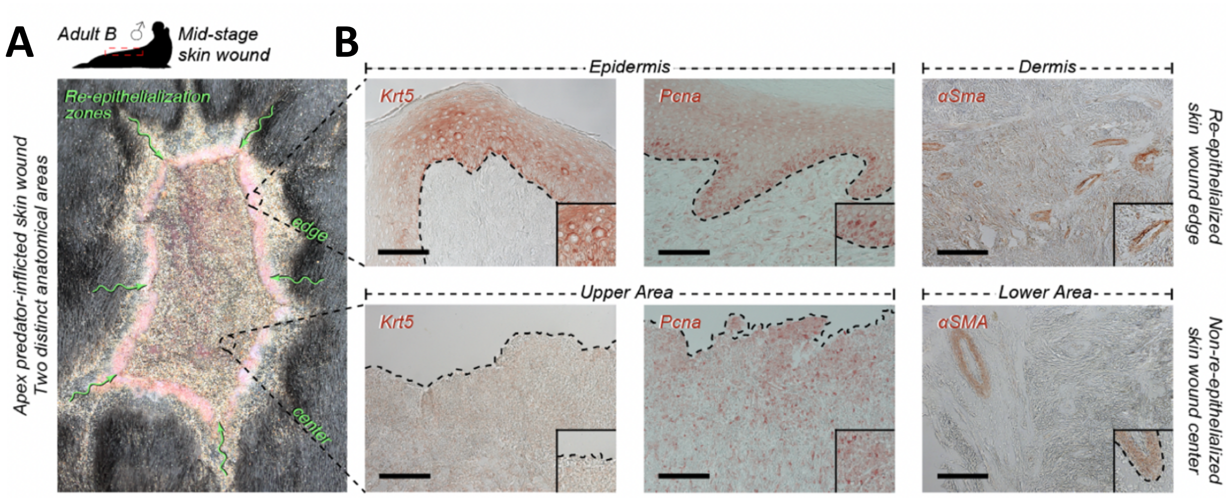


**Figure A.1.4. Histology of closing wound in *M. angustirostris*.** **(A)** Large closing wound, most likely derived from a white shark, displays active re-epithelialization zones. **(B)** The healing wound edge has undergone prominent re-epithelialization as shown by the presence of stratified epidermis – shown by Krt5$^+$ basal keratinocytes. In contrast, the wound center has not undergone re-epithelialization and lacks a stratified epidermis. Pcna$^+$ proliferating cells are observed in both wound areas albeit in distinct skin compartments. In both cases, the dermis appears reticular and is largely devoid of contractile dermal cells (myofibroblasts). Sma$^+$ cells, however, are observed in the vasculature. Size bars: B (left and middle panels) – 125 μm, (right panels) – 250 μm.

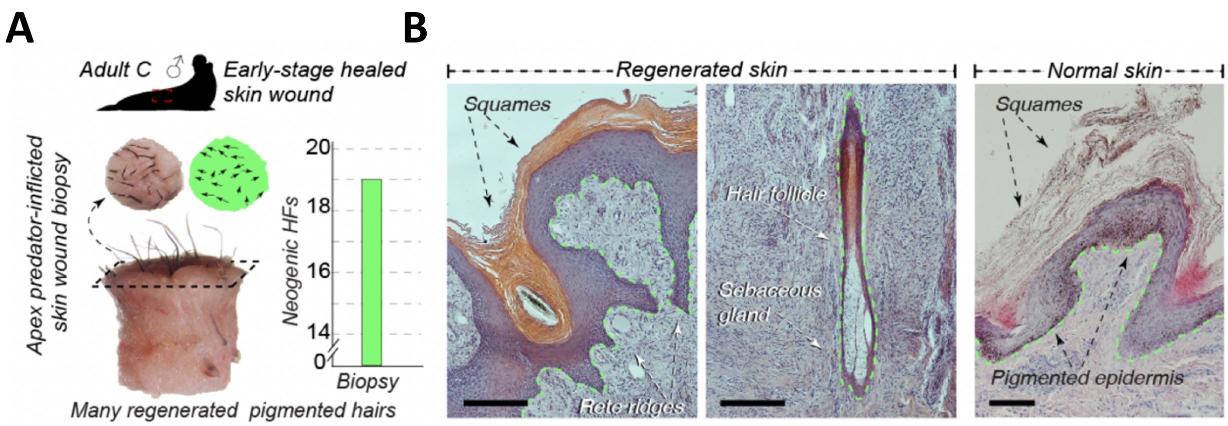


**Figure A.1.5. Histology of early stage regenerating wound in *M. angustirostris*. (A)** Healed wound from a partial lateral bite displays signs of hair follicle regeneration with many pigmented shafts emanating from the wound surface. At this stage, the epidermis remains unpigmented. In comparison, normal, unwounded skin contains both pigmented hair shafts and epidermis. **(B)** Healed *M. angustirostris* skin displays signs of enhanced regeneration, including a differentiated, stratified epidermis, composed of Rete ridges, as well as prominent regeneration of pilosebaceous units. Compared to normal, unwounded skin displays similar skin architecture and abundant adnexal structures. Size bars: B – 250 μm.

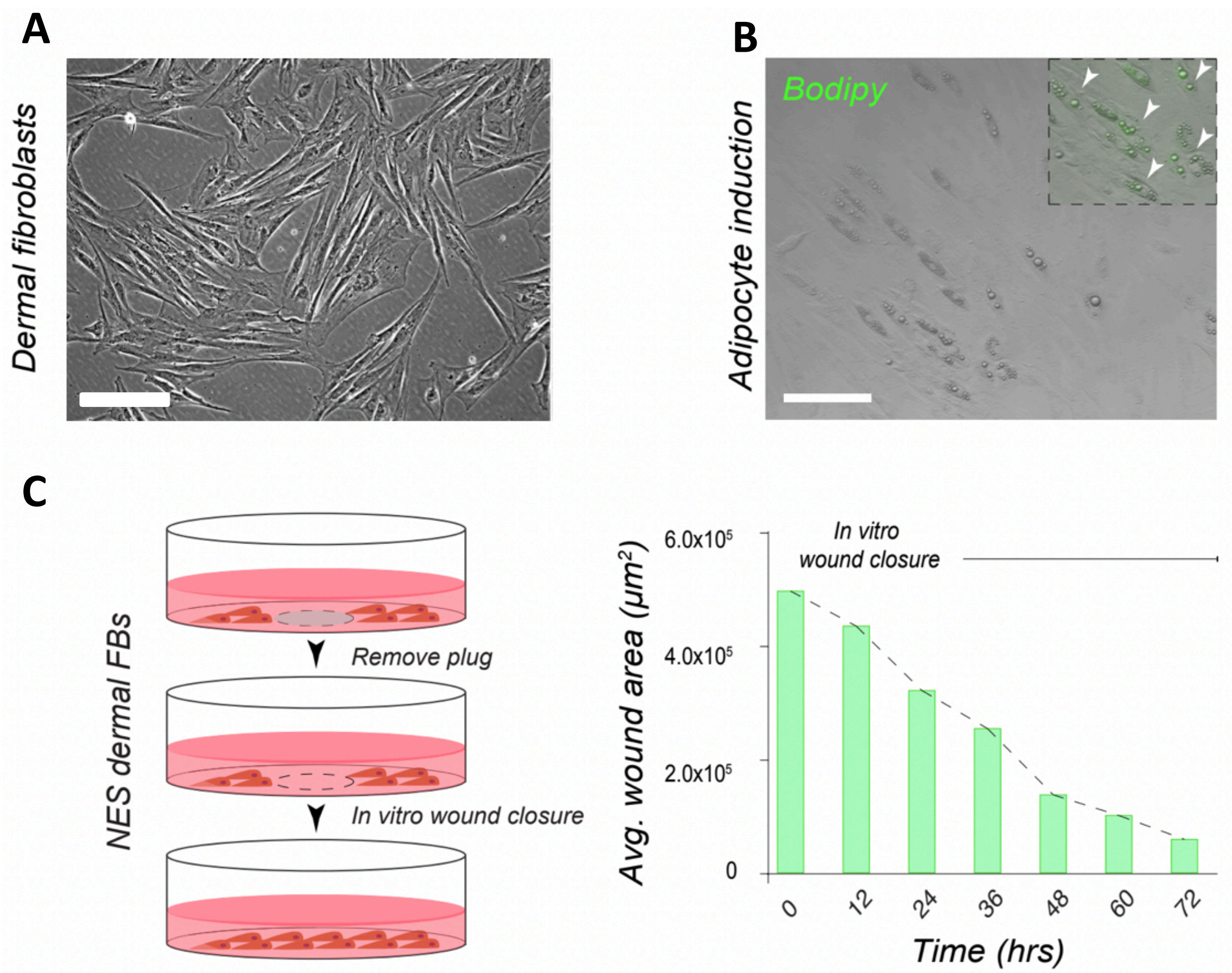


**Figure A.1.6. Characterization of *M. angustirostris* skin fbroblasts**. **(A)** Isolated fibroblasts in culture depict typical fibroblast-like morphology. **(B)** A portion of NES dermal fibroblasts display adipogenic potential, as observed by incorporation of Bodipy®. **(C)** NES dermal fibroblasts can migrate into a wound area in *in vitro* scratch assay. Size bars: B – 125 µm.

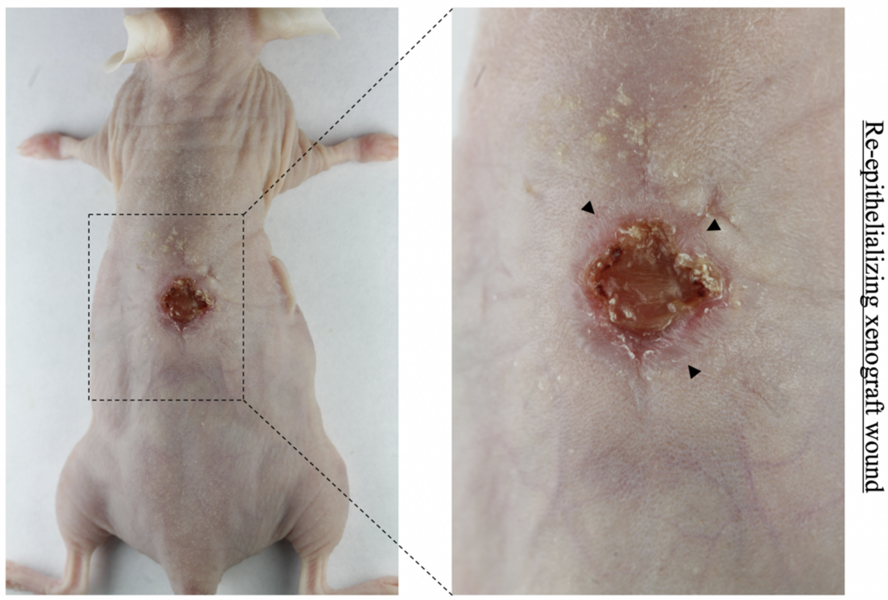


**Figure A.1.7. Example of seal-on-mouse xenograft**. Representative seal fibroblast-on-mouse xenograft model to study wound healing and infection *in vivo*. Juvenile seal dermal fibroblasts and P50 mouse keratinocytes were combined and seeded onto Pelnac®. Pelnac® was used as extracellular matrix component. Cells on Pelnac® were transplanted onto athymic mice.

# REFERENCES


Obituaries - John G Archibald - George R Barrett - Carey W Carrick - Alonzo C Cook - Benjamin F Creech - Russell L Davis - Harold Hanson Mitchell - Wd Salmon - Kendall Winfield Scott - Carl P Thompson - James Rollo Wiley. Journal of Animal Science 1966;25(4):1313-&.

Addison WN, Fu MM, Yang HX, Lin Z, Nagano K, Gori F, et al. Direct transcriptional repression of Zfp423 by Zfp521 mediates a bone morphogenic protein-dependent osteoblast versus adipocyte lineage commitment switch. Molecular and cellular biology 2014;34(16):3076-85.

Ahn RS, Taravati K, Lai K, Lee KM, Nititham J, Gupta R, et al. Transcriptional landscape of epithelial and immune cell populations revealed through FACS-seq of healthy human skin. Sci Rep 2017;7(1):1343.

Alcaraz WA, Gold DA, Raponi E, Gent PM, Concepcion D, Hamilton BA. Zfp423 controls proliferation and differentiation of neural precursors in cerebellar vermis formation. Proc Natl Acad Sci U S A 2006;103(51):19424-9.

Amamoto R, Huerta VG, Takahashi E, Dai G, Grant AK, Fu Z, et al. Adult axolotls can regenerate original neuronal diversity in response to brain injury. Elife 2016;5.

Anderson DB, Kauffman RG, Kastenschmidt LL. Lipogenic enzyme activities and cellularity of porcine adipose tissue from various anatomical locations. J Lipid Res 1972;13(5):593-9.

Antonelis GA, Lowry MS, Demaster DP, Fiscus CH. Assessing Northern Elephant Seal Feeding-Habits by Stomach Lavage. Mar Mammal Sci 1987;3(4):308-22.

Archie EA. Wound healing in the wild: stress, sociality and energetic costs affect wound healing in natural populations. Parasite Immunol 2013a;35(11):374-85.

Archie EA. Wound healing in the wild: stress, sociality and energetic costs affect wound healing in natural populations. Parasite Immunol 2013b;35(11):374-85.

Asano Y, Markiewicz M, Kubo M, Szalai G, Watson DK, Trojanowska M. Transcription factor Fli1 regulates collagen fibrillogenesis in mouse skin. Mol Cell Biol 2009;29(2):425-34.

Bacher R, Chu LF, Leng N, Gasch AP, Thomson JA, Stewart RM, et al. SCnorm: robust normalization of single-cell RNA-seq data. Nat Methods 2017;14(6):584-6.

Badiavas EV, Abedi M, Butmarc J, Falanga V, Quesenberry P. Participation of bone marrow derived cells in cutaneous wound healing. J Cell Physiol 2003;196(2):245-50.

Balemans W, Van Hul W. Extracellular regulation of BMP signaling in vertebrates: a cocktail of modulators. Dev Biol 2002;250(2):231-50.

Banerjee RR, Rangwala SM, Shapiro JS, Rich AS, Rhoades B, Qi Y, et al. Regulation of fasted blood glucose by resistin. Science 2004;303(5661):1195-8.

Barbosa FL, Chaurasia SS, Cutler A, Asosingh K, Kaur H, de Medeiros FW, et al. Corneal myofibroblast generation from bone marrow-derived cells. Exp Eye Res 2010;91(1):92-6.

Barisic-Dujmovic T, Boban I, Clark SH. Fibroblasts/myofibroblasts that participate in cutaneous wound healing are not derived from circulating progenitor cells. J Cell Physiol 2010;222(3):703-12.

Bautista-Hernandez LA, Gomez-Olivares JL, Buentello-Volante B, Bautista-de Lucio VM. Fibroblasts: The Unknown Sentinels Eliciting Immune Responses Against Microorganisms. Eur J Microbiol Immunol (Bp) 2017;7(3):151-7.

Berry R, Rodeheffer MS. Characterization of the adipocyte cellular lineage in vivo. Nat Cell Biol 2013;15(3):302-8.

Billingham RE, Russell PS. Incomplete wound contracture and the phenomenon of hair neogenesis in rabbits' skin. Nature 1956;177(4513):791-2.

Bininda-Emonds ORP, Bryant HN, Russell AP. Supraspecific taxa as terminals in cladistic analysis: implicit assumptions of monophyly and a comparison of methods. Biol J Linn Soc 1998;64(1):101-33.

Blanpain C, Fuchs E. Epidermal homeostasis: a balancing act of stem cells in the skin. Nat Rev Mol Cell Biol 2009;10(3):207-17.

Block BA, Jonsen ID, Jorgensen SJ, Winship AJ, Shaffer SA, Bograd SJ, et al. Tracking apex marine predator movements in a dynamic ocean. Nature 2011;475(7354):86-90.

Borodach GN, Montagna W. Fat in Skin of the Mouse during Cycles of Hair Growth. J Invest Dermatol 1956;26(3):229-32.

Bostrom H, Willetts K, Pekny M, Leveen P, Lindahl P, Hedstrand H, et al. PDGF-A signaling is a critical event in lung alveolar myofibroblast development and alveogenesis. Cell 1996;85(6):863-73.

Botchkarev VA, Botchkareva NV, Nakamura M, Huber O, Funa K, Lauster R, et al. Noggin is required for induction of the hair follicle growth phase in postnatal skin. Faseb J 2001;15(12):2205-14.

Botchkarev VA, Sharov AA. BMP signaling in the control of skin development and hair follicle growth. Differentiation 2004;72(9-10):512-26.

Boucher P, Gotthardt M, Li WP, Anderson RG, Herz J. LRP: role in vascular wall integrity and protection from atherosclerosis. Science 2003;300(5617):329-32.

Branton MH, Kopp JB. TGF-beta and fibrosis. Microbes Infect 1999;1(15):1349-65.

Breedis C. Regeneration of hair follicles and sebaceous glands from the epithelium of scars in the rabbit. Cancer research 1954;14(8):575-9.

Brook AH, Short BF, Lyne AG. Formation of new wool follicles in the adult sheep. Nature 1960;185:51.

Brownell I, Guevara E, Bai CB, Loomis CA, Joyner AL. Nerve-derived sonic hedgehog defines a niche for hair follicle stem cells capable of becoming epidermal stem cells. Cell Stem Cell 2011;8(5):552-65.

Bryant DM, Sousounis K, Farkas JE, Bryant S, Thao N, Guzikowski AR, et al. Repeated removal of developing limb buds permanently reduces appendage size in the highly-regenerative axolotl. Dev Biol 2017;424(1):1-9.

Bryder D, Rossi DJ, Weissman IL. Hematopoietic stem cells: the paradigmatic tissue-specific stem cell. Am J Pathol 2006;169(2):338-46.

Bustos-Arriaga J, Garcia-Machorro J, Leon-Juarez M, Garcia-Cordero J, Santos-Argumedo L, Flores-Romo L, et al. Activation of the innate immune response against DENV in normal non-transformed human fibroblasts. PLoS Negl Trop Dis 2011;5(12):e1420.

Chase HB, Montagna W, Malone JD. Changes in the Skin in Relation to the Hair Growth Cycle. Anatomical Record 1953;116(1):75-81.

Chen D, Zhao Y, Li Z, Shou K, Zheng X, Li P, et al. Circulating fibrocyte mobilization in negative pressure wound therapy. J Cell Mol Med 2017;21(8):1513-22.

Chu CC, Di Meglio P, Nestle FO. Harnessing dendritic cells in inflammatory skin diseases. Semin Immunol 2011;23(1):28-41.

Clausen BE, Burkhardt C, Reith W, Renkawitz R, Forster I. Conditional gene targeting in macrophages and granulocytes using LysMcre mice. Transgenic Res 1999;8(4):265-77.

Conesa A, Nueda MJ, Ferrer A, Talon M. maSigPro: a method to identify significantly differential expression profiles in time-course microarray experiments. Bioinformatics 2006;22(9):1096-102.
Cotsarelis G, Sun TT, Lavker RM. Label-retaining cells reside in the bulge area of pilosebaceous unit: implications for follicular stem cells, hair cycle, and skin carcinogenesis. Cell 1990;61(7):1329-37.
Coulombe PA, Kopan R, Fuchs E. Expression of keratin K14 in the epidermis and hair follicle: insights into complex programs of differentiation. J Cell Biol 1989;109(5):2295-312.
Cristancho AG, Lazar MA. Forming functional fat: a growing understanding of adipocyte differentiation. Nat Rev Mol Cell Biol 2011;12(11):722-34.
Crossno JT, Jr., Majka SM, Grazia T, Gill RG, Klemm DJ. Rosiglitazone promotes development of a novel adipocyte population from bone marrow-derived circulating progenitor cells. J Clin Invest 2006;116(12):3220-8.
Cunnington RH, Northcott JM, Ghavami S, Filomeno KL, Jahan F, Kavosh MS, et al. The Ski-Zeb2-Meox2 pathway provides a novel mechanism for regulation of the cardiac myofibroblast phenotype. J Cell Sci 2014;127(Pt 1):40-9.
Cuny GD, Yu PB, Laha JK, Xing X, Liu JF, Lai CS, et al. Structure-activity relationship study of bone morphogenetic protein (BMP) signaling inhibitors. Bioorganic & medicinal chemistry letters 2008;18(15):4388-92.
Darby I, Skalli O, Gabbiani G. Alpha-smooth muscle actin is transiently expressed by myofibroblasts during experimental wound healing. Lab Invest 1990;63(1):21-9.
Dau BK, Gilardi KVK, Gulland FM, Higgins A, Holcomb JB, Leger JS, et al. Fishing Gear-Related Injury in California Marine Wildlife. J Wildlife Dis 2009;45(2):355-62.
Depianto D, Kerns ML, Dlugosz AA, Coulombe PA. Keratin 17 promotes epithelial proliferation and tumor growth by polarizing the immune response in skin. Nat Genet 2010;42(10):910-4.
Ding J, Hori K, Zhang R, Marcoux Y, Honardoust D, Shankowsky HA, et al. Stromal cell-derived factor 1 (SDF-1) and its receptor CXCR4 in the formation of postburn hypertrophic scar (HTS). Wound repair and regeneration : official publication of the Wound Healing Society [and] the European Tissue Repair Society 2011;19(5):568-78.
Driskell RR, Clavel C, Rendl M, Watt FM. Hair follicle dermal papilla cells at a glance. J Cell Sci 2011;124(Pt 8):1179-82.
Driskell RR, Jahoda CA, Chuong CM, Watt FM, Horsley V. Defining dermal adipose tissue. Exp Dermatol 2014;23(9):629-31.
Driskell RR, Lichtenberger BM, Hoste E, Kretzschmar K, Simons BD, Charalambous M, et al. Distinct fibroblast lineages determine dermal architecture in skin development and repair. Nature 2013;504(7479):277-81.
Dulauroy S, Di Carlo SE, Langa F, Eberl G, Peduto L. Lineage tracing and genetic ablation of ADAM12(+) perivascular cells identify a major source of profibrotic cells during acute tissue injury. Nat Med 2012;18(8):1262-70.
Dunn L, Prosser HC, Tan JT, Vanags LZ, Ng MK, Bursill CA. Murine model of wound healing. J Vis Exp 2013(75):e50265.
Duran-Struuck R, Dysko RC. Principles of bone marrow transplantation (BMT): providing optimal veterinary and husbandry care to irradiated mice in BMT studies. J Am Assoc Lab Anim Sci 2009;48(1):11-22.

Ehama R, Ishimatsu-Tsuji Y, Iriyama S, Ideta R, Soma T, Yano K, et al. Hair follicle regeneration using grafted rodent and human cells. The Journal of investigative dermatology 2007;127(9):2106-15.
El Agha E, Moiseenko A, Kheirollahi V, De Langhe S, Crnkovic S, Kwapiszewska G, et al. Two-Way Conversion between Lipogenic and Myogenic Fibroblastic Phenotypes Marks the Progression and Resolution of Lung Fibrosis. Cell Stem Cell 2017;20(2):261-73 e3.
Eming SA, Martin P, Tomic-Canic M. Wound repair and regeneration: mechanisms, signaling, and translation. Sci Transl Med 2014;6(265):265sr6.
Eto H, Ishimine H, Kinoshita K, Watanabe-Susaki K, Kato H, Doi K, et al. Characterization of human adipose tissue-resident hematopoietic cell populations reveals a novel macrophage subpopulation with CD34 expression and mesenchymal multipotency. Stem Cells Dev 2013;22(6):985-97.
Fathke C, Wilson L, Hutter J, Kapoor V, Smith A, Hocking A, et al. Contribution of bone marrow-derived cells to skin: collagen deposition and wound repair. Stem Cells 2004;22(5):812-22.
Ferguson SH, Kingsley MCS, Higdon JW. Killer whale (Orcinus orca) predation in a multi-prey system. Popul Ecol 2012;54(1):31-41.
Ferraris C, Bernard BA, Dhouailly D. Adult epidermal keratinocytes are endowed with pilosebaceous forming abilities. Int J Dev Biol 1997;41(3):491-8.
Fessing MY, Mardaryev AN, Gdula MR, Sharov AA, Sharova TY, Rapisarda V, et al. p63 regulates Satb1 to control tissue-specific chromatin remodeling during development of the epidermis. J Cell Biol 2011;194(6):825-39.
Festa E, Fretz J, Berry R, Schmidt B, Rodeheffer M, Horowitz M, et al. Adipocyte lineage cells contribute to the skin stem cell niche to drive hair cycling. Cell 2011;146(5):761-71.
Filbin MG, Tirosh I, Hovestadt V, Shaw ML, Escalante LE, Mathewson ND, et al. Developmental and oncogenic programs in H3K27M gliomas dissected by single-cell RNA-seq. Science 2018;360(6386):331-5.
Foitzik K, Lindner G, Mueller-Roever S, Maurer M, Botchkareva N, Botchkarev V, et al. Control of murine hair follicle regression (catagen) by TGF-beta1 in vivo. FASEB J 2000;14(5):752-60.
Furukawa F, Imamura S, Fujita M, Kinoshita K, Yoshitake K, Brown WR, et al. Immunohistochemical localization of proliferating cell nuclear antigen/cyclin in human skin. Arch Dermatol Res 1992;284(2):86-91.
Gabbiani G. The myofibroblast in wound healing and fibrocontractive diseases. J Pathol 2003;200(4):500-3.
Gabbiani G, Ryan GB, Majne G. Presence of modified fibroblasts in granulation tissue and their possible role in wound contraction. Experientia 1971;27(5):549-50.
Gallo RL. Human Skin Is the Largest Epithelial Surface for Interaction with Microbes. J Invest Dermatol 2017;137(6):1213-4.
Galloreynoso JP, Figueroacarranza AL. A Cookiecutter Shark Wound on a Guadalupe Fur-Seal Male. Mar Mammal Sci 1992;8(4):428-30.
Gao P, Zhang Y, Liu Y, Chen J, Zong C, Yu C, et al. Signal transducer and activator of transcription 5B (STAT5B) modulates adipocyte differentiation via MOF. Cell Signal 2015;27(12):2434-43.
Gaublomme JT, Yosef N, Lee Y, Gertner RS, Yang LV, Wu C, et al. Single-Cell Genomics Unveils Critical Regulators of Th17 Cell Pathogenicity. Cell 2015;163(6):1400-12.

Gavin KM, Gutman JA, Kohrt WM, Wei Q, Shea KL, Miller HL, et al. De novo generation of adipocytes from circulating progenitor cells in mouse and human adipose tissue. FASEB journal : official publication of the Federation of American Societies for Experimental Biology 2016;30(3):1096-108.

Gavin KM, Majka SM, Kohrt WM, Miller HL, Sullivan TM, Klemm DJ. Hematopoietic-to-mesenchymal transition of adipose tissue macrophages is regulated by integrin beta1 and fabricated fibrin matrices. Adipocyte 2017;6(3):234-49.

Gawronska-Kozak B, Grabowska A, Kopcewicz M, Kur A. Animal models of skin regeneration. Reprod Biol 2014;14(1):61-7.

Gay D, Kwon O, Zhang Z, Spata M, Plikus MV, Holler PD, et al. Fgf9 from dermal gammadelta T cells induces hair follicle neogenesis after wounding. Nat Med 2013;19(7):916-23.

Gillman TP, J.; Bronks, D.; Roux, M.;. Implications of epidermal-dermal relations following injury for understanding association of carcinogenesis with hair regeneration of scars. Experientia 1955;11(12):493-4.

Gipbs HF. A study of the post-natal development of the skin and hair of the mouse. Anatomical Record 1941;80(1):61-81.

Gonzalez AC, Costa TF, Andrade ZA, Medrado AR. Wound healing - A literature review. An Bras Dermatol 2016;91(5):614-20.

Guerrero-Juarez CF, Astrowski AA, Murad R, Dang CT, Shatrova VO, Astrowskaja A, et al. Wound regeneration deficit in rats correlates with low morphogenetic potential and distinct transcriptome profile of epidermis. J Invest Dermatol 2018.

Guerrero-Juarez CF, Plikus MV. Gli-fully Halting the Progression of Fibrosis. Cell Stem Cell 2017;20(6):735-6.

Guerrero-Juarez CF, Plikus MV. Emerging nonmetabolic functions of skin fat. Nat Rev Endocrinol 2018;14(3):163-73.

Gupta RK, Arany Z, Seale P, Mepani RJ, Ye L, Conroe HM, et al. Transcriptional control of preadipocyte determination by Zfp423. Nature 2010;464(7288):619-23.

Gupta RK, Mepani RJ, Kleiner S, Lo JC, Khandekar MJ, Cohen P, et al. Zfp423 expression identifies committed preadipocytes and localizes to adipose endothelial and perivascular cells. Cell metabolism 2012;15(2):230-9.

Gurtner GC, Werner S, Barrandon Y, Longaker MT. Wound repair and regeneration. Nature 2008;453(7193):314-21.

Haley MP, Deutsch CJ, Leboeuf BJ. Size, Dominance and Copulatory Success in Male Northern Elephant Seals, Mirounga-Angustirostris. Anim Behav 1994;48(6):1249-60.

Hammarstedt A, Hedjazifar S, Jenndahl L, Gogg S, Grunberg J, Gustafson B, et al. WISP2 regulates preadipocyte commitment and PPARgamma activation by BMP4. Proceedings of the National Academy of Sciences of the United States of America 2013;110(7):2563-8.

Hanni KD, Pyle P. Entanglement of pinnipeds in synthetic materials at South-east Farallon Island, California, 1976-1998. Marine Pollution Bulletin 2000;40(12):1076-81.

Harper RA, Grove G. Human skin fibroblasts derived from papillary and reticular dermis: differences in growth potential in vitro. Science 1979;204(4392):526-7.

Hata K, Nishimura R, Ikeda F, Yamashita K, Matsubara T, Nokubi T, et al. Differential roles of Smad1 and p38 kinase in regulation of peroxisome proliferator-activating receptor gamma during bone morphogenetic protein 2-induced adipogenesis. Mol Biol Cell 2003;14(2):545-55.

Haughton CL, Gawriluk TR, Seifert AW. The Biology and Husbandry of the African Spiny Mouse (Acomys cahirinus) and the Research Uses of a Laboratory Colony. J Am Assoc Lab Anim Sci 2016;55(1):9-17.
Hausman GJ, Campion DR, Richardson RL, Martin RJ. Adipocyte development in the rat hypodermis. Am J Anat 1981;161(1):85-100.
Hausman GJ, Kauffman RG. The histology of developing porcine adipose tissue. J Anim Sci 1986;63(2):642-58.
Hausman GJ, Martin RJ. Subcutaneous adipose tissue development in Yorkshire (lean) and Ossabaw (obese) pigs. J Anim Sci 1981;52(6):1442-9.
Hausman GJ, Martin RJ. The development of adipocytes located around hair follicles in the fetal pig. J Anim Sci 1982;54(6):1286-96.
He W, Barak Y, Hevener A, Olson P, Liao D, Le J, et al. Adipose-specific peroxisome proliferator-activated receptor gamma knockout causes insulin resistance in fat and liver but not in muscle. Proc Natl Acad Sci U S A 2003;100(26):15712-7.
Henderson NC, Arnold TD, Katamura Y, Giacomini MM, Rodriguez JD, McCarty JH, et al. Targeting of alphav integrin identifies a core molecular pathway that regulates fibrosis in several organs. Nat Med 2013;19(12):1617-24.
Higashiyama R, Nakao S, Shibusawa Y, Ishikawa O, Moro T, Mikami K, et al. Differential contribution of dermal resident and bone marrow-derived cells to collagen production during wound healing and fibrogenesis in mice. J Invest Dermatol 2011;131(2):529-36.
Higgins JL, Hendrickson DA. Surgical procedures in pinniped and cetacean species. J Zoo Wildl Med 2013;44(4):817-36.
Hindell MA, Perrin WF. Elephant Seals Mirounga angustirostris and M-leonina. Encyclopedia of Marine Mammals, 2nd Edition 2009:364-8.
Hinz B, Mastrangelo D, Iselin CE, Chaponnier C, Gabbiani G. Mechanical tension controls granulation tissue contractile activity and myofibroblast differentiation. American Journal of Pathology 2001;159(3):1009-20.
Hinz B, Phan SH, Thannickal VJ, Galli A, Bochaton-Piallat ML, Gabbiani G. The myofibroblast: one function, multiple origins. Am J Pathol 2007;170(6):1807-16.
Hinz B, Phan SH, Thannickal VJ, Prunotto M, Desmouliere A, Varga J, et al. Recent developments in myofibroblast biology: paradigms for connective tissue remodeling. Am J Pathol 2012;180(4):1340-55.
Holder N, Tank PW, Bryant SV. Regeneration of symmetrical forelimbs in the axolotl, Ambystoma mexicanum. Dev Biol 1980;74(2):302-14.
Hong KM, Belperio JA, Keane MP, Burdick MD, Strieter RM. Differentiation of human circulating fibrocytes as mediated by transforming growth factor-beta and peroxisome proliferator-activated receptor gamma. J Biol Chem 2007;282(31):22910-20.
Hong KM, Burdick MD, Phillips RJ, Heber D, Strieter RM. Characterization of human fibrocytes as circulating adipocyte progenitors and the formation of human adipose tissue in SCID mice. FASEB journal : official publication of the Federation of American Societies for Experimental Biology 2005;19(14):2029-31.
Houser DS, Champagne CD, Crocker DE. A non-traditional model of the metabolic syndrome: the adaptive significance of insulin resistance in fasting-adapted seals. Front Endocrinol (Lausanne) 2013;4:164.

Hsu CK, Lin HH, H ICH, Ogawa R, Wang YK, Ho YT, et al. Caveolin-1 controls hyperresponsiveness to mechanical stimuli and fibrogenesis-associated RUNX2 activation in keloid fibroblasts. The Journal of investigative dermatology 2017.
Hsu YC, Pasolli HA, Fuchs E. Dynamics between stem cells, niche, and progeny in the hair follicle. Cell 2011;144(1):92-105.
Hu E, Liang P, Spiegelman BM. AdipoQ is a novel adipose-specific gene dysregulated in obesity. The Journal of biological chemistry 1996;271(18):10697-703.
Hughes AJ, Spelke DP, Xu Z, Kang CC, Schaffer DV, Herr AE. Single-cell western blotting. Nat Methods 2014;11(7):749-55.
Hughes MW, Jiang TX, Plikus MV, Guerrero-Juarez CF, Lin CH, Schafer C, et al. Msx2 supports epidermal competency during wound induced hair follicle neogenesis. J Invest Dermatol 2018.
Hwang J, Kita R, Kwon HS, Choi EH, Lee SH, Udey MC, et al. Epidermal ablation of Dlx3 is linked to IL-17-associated skin inflammation. Proc Natl Acad Sci U S A 2011;108(28):11566-71.
Iida M, Ihara S, Matsuzaki T. Follicular epithelia and dermal papillae of mouse vibrissal follicles qualitatively change their hair-forming ability during anagen. Differentiation; research in biological diversity 2007;75(5):371-81.
Ishida Y, Kimura A, Kondo T, Hayashi T, Ueno M, Takakura N, et al. Essential roles of the CC chemokine ligand 3-CC chemokine receptor 5 axis in bleomycin-induced pulmonary fibrosis through regulation of macrophage and fibrocyte infiltration. Am J Pathol 2007;170(3):843-54.
Ishii G, Sangai T, Sugiyama K, Ito T, Hasebe T, Endoh Y, et al. In vivo characterization of bone marrow-derived fibroblasts recruited into fibrotic lesions. Stem Cells 2005;23(5):699-706.
Ito M, Yang Z, Andl T, Cui C, Kim N, Millar SE, et al. Wnt-dependent de novo hair follicle regeneration in adult mouse skin after wounding. Nature 2007;447(7142):316-20.
Iwafuchi-Doi M, Zaret KS. Cell fate control by pioneer transcription factors. Development 2016;143(11):1833-7.
Iwaisako K, Jiang C, Zhang M, Cong M, Moore-Morris TJ, Park TJ, et al. Origin of myofibroblasts in the fibrotic liver in mice. Proc Natl Acad Sci U S A 2014;111(32):E3297-305.
Iwayama T, Steele C, Yao L, Dozmorov MG, Karamichos D, Wren JD, et al. PDGFRalpha signaling drives adipose tissue fibrosis by targeting progenitor cell plasticity. Genes Dev 2015;29(11):1106-19.
Jahoda CA. Induction of follicle formation and hair growth by vibrissa dermal papillae implanted into rat ear wounds: vibrissa-type fibres are specified. Development 1992;115(4):1103-9.
Jahoda CA, Reynolds AJ, Oliver RF. Induction of hair growth in ear wounds by cultured dermal papilla cells. The Journal of investigative dermatology 1993;101(4):584-90.
Jain R, Barkauskas CE, Takeda N, Bowie EJ, Aghajanian H, Wang Q, et al. Plasticity of Hopx(+) type I alveolar cells to regenerate type II cells in the lung. Nat Commun 2015;6:6727.
Janda JM, Abbott SL. 16S rRNA gene sequencing for bacterial identification in the diagnostic laboratory: pluses, perils, and pitfalls. J Clin Microbiol 2007;45(9):2761-4.
Jeffery E, Berry R, Church CD, Yu S, Shook BA, Horsley V, et al. Characterization of Cre recombinase models for the study of adipose tissue. Adipocyte 2014;3(3):206-11.

Jensen KB, Collins CA, Nascimento E, Tan DW, Frye M, Itami S, et al. Lrig1 expression defines a distinct multipotent stem cell population in mammalian epidermis. Cell Stem Cell 2009;4(5):427-39.
Jiang D, Correa-Gallegos D, Christ S, Stefanska A, Liu J, Ramesh P, et al. Two succeeding fibroblastic lineages drive dermal development and the transition from regeneration to scarring. Nat Cell Biol 2018;20(4):422-31.
Jin S, MacLean AL, Peng T, Nie Q. scEpath: Energy landscape-based inference of transition probabilities and cellular trajectories from single-cell transcriptomic data. Bioinformatics 2018.
Jin W, Takagi T, Kanesashi SN, Kurahashi T, Nomura T, Harada J, et al. Schnurri-2 controls BMP-dependent adipogenesis via interaction with Smad proteins. Developmental cell 2006;10(4):461-71.
Johnston AP, Yuzwa SA, Carr MJ, Mahmud N, Storer MA, Krause MP, et al. Dedifferentiated Schwann Cell Precursors Secreting Paracrine Factors Are Required for Regeneration of the Mammalian Digit Tip. Cell Stem Cell 2016;19(4):433-48.
Joost S, Zeisel A, Jacob T, Sun X, La Manno G, Lonnerberg P, et al. Single-Cell Transcriptomics Reveals that Differentiation and Spatial Signatures Shape Epidermal and Hair Follicle Heterogeneity. Cell Syst 2016;3(3):221-37 e9.
Kang S, Akerblad P, Kiviranta R, Gupta RK, Kajimura S, Griffin MJ, et al. Regulation of early adipose commitment by Zfp521. PLoS Biol 2012;10(11):e1001433.
Karbiener M, Glantschnig C, Pisani DF, Laurencikiene J, Dahlman I, Herzig S, et al. Mesoderm-specific transcript (MEST) is a negative regulator of human adipocyte differentiation. Int J Obes (Lond) 2015;39(12):1733-41.
Kaushal GS, Rognoni E, Lichtenberger BM, Driskell RR, Kretzschmar K, Hoste E, et al. Fate of Prominin-1 Expressing Dermal Papilla Cells during Homeostasis, Wound Healing and Wnt Activation. The Journal of investigative dermatology 2015;135(12):2926-34.
Kennell JA, MacDougald OA. Wnt signaling inhibits adipogenesis through beta-catenin-dependent and -independent mechanisms. J Biol Chem 2005;280(25):24004-10.
Khattak S, Tanaka EM. Transgenesis in axolotl (Ambystoma mexicanum). Methods Mol Biol 2015;1290:269-77.
Khudyakov JI, Champagne CD, Meneghetti LM, Crocker DE. Blubber transcriptome response to acute stress axis activation involves transient changes in adipogenesis and lipolysis in a fasting-adapted marine mammal. Sci Rep-Uk 2017;7.
Khudyakov JI, Preeyanon L, Champagne CD, Ortiz RM, Crocker DE. Transcriptome analysis of northern elephant seal (Mirounga angustirostris) muscle tissue provides a novel molecular resource and physiological insights. Bmc Genomics 2015;16.
Kim JK, Gavrilova O, Chen Y, Reitman ML, Shulman GI. Mechanism of insulin resistance in A-ZIP/F-1 fatless mice. J Biol Chem 2000;275(12):8456-60.
Kim W, Barron DA, San Martin R, Chan KS, Tran LL, Yang F, et al. RUNX1 is essential for mesenchymal stem cell proliferation and myofibroblast differentiation. Proceedings of the National Academy of Sciences of the United States of America 2014;111(46):16389-94.
Kimani JK. Some histological aspects of the palmar digital pads in the vervet monkey. Folia Primatol (Basel) 1983;41(1-2):147-55.

Kimura Y, Hawkins MT, McDonough MM, Jacobs LL, Flynn LJ. Corrected placement of Mus-Rattus fossil calibration forces precision in the molecular tree of rodents. Sci Rep 2015;5:14444.
Kirton JP, Crofts NJ, George SJ, Brennan K, Canfield AE. Wnt/beta-catenin signaling stimulates chondrogenic and inhibits adipogenic differentiation of pericytes: potential relevance to vascular disease? Circ Res 2007;101(6):581-9.
Kligman AM. Neogenesis of human hair follicles. Ann N Y Acad Sci 1959;83:507-11.
Kligman AM, Strauss JS. The formation of vellus hair follicles from human adult epidermis. The Journal of investigative dermatology 1956;27(1):19-23.
Kligman AM, Strauss JS. The Formation of Vellus Hair Follicles from Human Adult Epidermis1. Journal of Investigative Dermatology 1956;27(1):19-23.
Klimey AP. The Predatory Behavior of the White Shark (Vol 82, Pg 122, 1994). Am Sci 1994;82(3):205-.
Klimley AP. The Predatory Behavior of the White Shark. Am Sci 1994a;82(2):122-33.
Klimley AP. The Predatory Behavior of the White Shark (Vol 82, Pg 122, 1994). Am Sci 1994b;82(4):305-.
Klimley AP, Pyle P, Anderson SD. The behavior of white sharks and their pinniped prey during predatory attacks. Great White Sharks 1996:175-91.
Koh TJ, DiPietro LA. Inflammation and wound healing: the role of the macrophage. Expert Rev Mol Med 2011;13:e23.
Koh YJ, Kang S, Lee HJ, Choi TS, Lee HS, Cho CH, et al. Bone marrow-derived circulating progenitor cells fail to transdifferentiate into adipocytes in adult adipose tissues in mice. J Clin Invest 2007;117(12):3684-95.
Kong LL, Yang NZ, Shi LH, Zhao GH, Zhou W, Ding Q, et al. The optimum marker for the detection of lymphatic vessels. Mol Clin Oncol 2017;7(4):515-20.
Kramann R, Schneider RK, DiRocco DP, Machado F, Fleig S, Bondzie PA, et al. Perivascular Gli1+ progenitors are key contributors to injury-induced organ fibrosis. Cell Stem Cell 2015;16(1):51-66.
Kretzschmar K, Watt FM. Lineage tracing. Cell 2012;148(1-2):33-45.
Kryukova NV, Kruchenkova EP, Ivanov DI. Hunting of Killer Whales (Orcinus Orca) on Walruses (Odobenus Rosmarus Divergens) near the Retkyn Spit (Chukotka). Zool Zh 2012a;91(6):734-45.
Kryukova NV, Kruchenkova EP, Ivanov DI. Killer whales (Orcinus orca) hunting for walruses (Odobenus rosmarus divergens) near Retkyn Spit, Chukotka. Biol Bull+ 2012b;39(9):768-78.
Landsberg RL, Sero JE, Danielian PS, Yuan TL, Lee EY, Lees JA. The role of E2F4 in adipogenesis is independent of its cell cycle regulatory activity. Proc Natl Acad Sci U S A 2003;100(5):2456-61.
Lange-Asschenfeldt B, Marenbach D, Lang C, Patzelt A, Ulrich M, Maltusch A, et al. Distribution of bacteria in the epidermal layers and hair follicles of the human skin. Skin Pharmacol Physiol 2011;24(6):305-11.
Le Boeuf BJ, Condit R, Morris PA, Reiter J. The Northern Elephant Seal (Mirounga angustirostris) Rookery at Ano Nuevo: A Case Study in Colonization. Aquat Mamm 2011;37(4):486-501.
Le Goff C, Somerville RP, Kesteloot F, Powell K, Birk DE, Colige AC, et al. Regulation of procollagen amino-propeptide processing during mouse embryogenesis by specialization

of homologous ADAMTS proteases: insights on collagen biosynthesis and dermatosparaxis. Development 2006;133(8):1587-96.
LeBleu VS, Taduri G, O'Connell J, Teng Y, Cooke VG, Woda C, et al. Origin and function of myofibroblasts in kidney fibrosis. Nat Med 2013;19(8):1047-53.
Leboeuf BJ. Male-Male Competition and Reproductive Success in Elephant Seals. Am Zool 1974;14(1):163-76.
Leboeuf BJ, Mccosker JE, Hewitt J. Crater Wounds on Northern Elephant Seals - the Cookiecutter Shark Strikes Again. Fish B-Noaa 1987;85(2):387-92.
Leboeuf BJ, Mesnick S. Sexual-Behavior of Male Northern Elephant Seals .1. Lethal Injuries to Adult Females. Behaviour 1991;116:143-62.
Lee da S, Choi H, Han BS, Kim WK, Lee SC, Oh KJ, et al. c-Jun regulates adipocyte differentiation via the KLF15-mediated mode. Biochem Biophys Res Commun 2016;469(3):552-8.
Lee K, Villena JA, Moon YS, Kim KH, Lee S, Kang C, et al. Inhibition of adipogenesis and development of glucose intolerance by soluble preadipocyte factor-1 (Pref-1). J Clin Invest 2003;111(4):453-61.
Lee SH, Seo SH, Lee DH, Pi LQ, Lee WS, Choi KY. Targeting of CXXC5 by a Competing Peptide Stimulates Hair Regrowth and Wound-Induced Hair Neogenesis. The Journal of investigative dermatology 2017;137(11):2260-9.
Lehoczky JA, Robert B, Tabin CJ. Mouse digit tip regeneration is mediated by fate-restricted progenitor cells. Proc Natl Acad Sci U S A 2011;108(51):20609-14.
Lei M, Schumacher LJ, Lai YC, Juan WT, Yeh CY, Wu P, et al. Self-organization process in newborn skin organoid formation inspires strategy to restore hair regeneration of adult cells. Proc Natl Acad Sci U S A 2017;114(34):E7101-E10.
Lesko MH, Driskell RR, Kretzschmar K, Goldie SJ, Watt FM. Sox2 modulates the function of two distinct cell lineages in mouse skin. Developmental biology 2013;382(1):15-26.
Lewis CJ, Mardaryev AN, Poterlowicz K, Sharova TY, Aziz A, Sharpe DT, et al. Bone morphogenetic protein signaling suppresses wound-induced skin repair by inhibiting keratinocyte proliferation and migration. The Journal of investigative dermatology 2014;134(3):827-37.
Li B, Dewey CN. RSEM: accurate transcript quantification from RNA-Seq data with or without a reference genome. BMC Bioinformatics 2011;12:323.
Li Z, Hodgkinson T, Gothard EJ, Boroumand S, Lamb R, Cummins I, et al. Epidermal Notch1 recruits RORgamma(+) group 3 innate lymphoid cells to orchestrate normal skin repair. Nature communications 2016;7:11394.
Lindner G, Botchkarev VA, Botchkareva NV, Ling G, van der Veen C, Paus R. Analysis of apoptosis during hair follicle regression (catagen). Am J Pathol 1997;151(6):1601-17.
Ling JK. Pelage and Molting in Wild Mammals with Special Reference to Aquatic Forms. Q Rev Biol 1970;45(1):16-&.
Lobitz WC, Jr., Dobson RL. Dermatology: the eccrine sweat glands. Annu Rev Med 1961;12:289-98.
Loesche M, Gardner SE, Kalan L, Horwinski J, Zheng Q, Hodkinson BP, et al. Temporal Stability in Chronic Wound Microbiota Is Associated With Poor Healing. J Invest Dermatol 2017;137(1):237-44.

Lopez RG, Garcia-Silva S, Moore SJ, Bereshchenko O, Martinez-Cruz AB, Ermakova O, et al. C/EBPalpha and beta couple interfollicular keratinocyte proliferation arrest to commitment and terminal differentiation. Nat Cell Biol 2009;11(10):1181-90.

Louis C, Tift MS, Crocker DE, Alexander D, Smith DR, Debier C. Isolation of progenitor cells from the blubber of northern elephant seals (Mirounga angustirostris) in order to obtain an in vitro adipocyte model-preliminary results. Mar Mammal Sci 2015;31(2):764-73.

Lu CP, Polak L, Keyes BE, Fuchs E. Spatiotemporal antagonism in mesenchymal-epithelial signaling in sweat versus hair fate decision. Science 2016;354(6319).

Lu CP, Polak L, Rocha AS, Pasolli HA, Chen SC, Sharma N, et al. Identification of stem cell populations in sweat glands and ducts reveals roles in homeostasis and wound repair. Cell 2012;150(1):136-50.

Ma X, Tian Y, Song Y, Shi J, Xu J, Xiong K, et al. Msi2 Maintains Quiescent State of Hair Follicle Stem Cells by Directly Repressing the Hh Signaling Pathway. J Invest Dermatol 2017;137(5):1015-24.

Ma X, Zhang H, Yuan L, Jing H, Thacker P, Li D. CREBL2, interacting with CREB, induces adipogenesis in 3T3-L1 adipocytes. Biochem J 2011;439(1):27-38.

Maan ZN, Rennert RC, Koob TJ, Januszyk M, Li WW, Gurtner GC. Cell recruitment by amnion chorion grafts promotes neovascularization. J Surg Res 2015;193(2):953-62.

Mack M, Yanagita M. Origin of myofibroblasts and cellular events triggering fibrosis. Kidney Int 2015;87(2):297-307.

Macosko EZ, Basu A, Satija R, Nemesh J, Shekhar K, Goldman M, et al. Highly Parallel Genome-wide Expression Profiling of Individual Cells Using Nanoliter Droplets. Cell 2015;161(5):1202-14.

Madisen L, Zwingman TA, Sunkin SM, Oh SW, Zariwala HA, Gu H, et al. A robust and high-throughput Cre reporting and characterization system for the whole mouse brain. Nat Neurosci 2010;13(1):133-40.

Majka SM, Fox KE, Psilas JC, Helm KM, Childs CR, Acosta AS, et al. De novo generation of white adipocytes from the myeloid lineage via mesenchymal intermediates is age, adipose depot, and gender specific. Proc Natl Acad Sci U S A 2010;107(33):14781-6.

Mansilla E, Marin GH, Drago H, Sturla F, Salas E, Gardiner C, et al. Bloodstream cells phenotypically identical to human mesenchymal bone marrow stem cells circulate in large amounts under the influence of acute large skin damage: new evidence for their use in regenerative medicine. Transplant Proc 2006;38(3):967-9.

Mardaryev AN, Gdula MR, Yarker JL, Emelianov VU, Poterlowicz K, Sharov AA, et al. p63 and Brg1 control developmentally regulated higher-order chromatin remodelling at the epidermal differentiation complex locus in epidermal progenitor cells. Development 2014;141(1):101-11.

Mariotto A, Pavlova O, Park HS, Huber M, Hohl D. HOPX: The Unusual Homeodomain-Containing Protein. The Journal of investigative dermatology 2016;136(5):905-11.

Marshall CJ, Vousden K, Ozanne B. The involvement of activated ras genes in determining the transformed phenotype. Proc R Soc Lond B Biol Sci 1985;226(1242):99-106.

Massague J. TGF-beta signal transduction. Annu Rev Biochem 1998;67:753-91.

Matias Santos D, Rita AM, Casanellas I, Brito Ova A, Araujo IM, Power D, et al. Ear wound regeneration in the African spiny mouse Acomys cahirinus. Regeneration (Oxf) 2016;3(1):52-61.

Mayeur C, Kolodziej SA, Wang A, Xu X, Lee A, Yu PB, et al. Oral administration of a bone morphogenetic protein type I receptor inhibitor prevents the development of anemia of inflammation. Haematologica 2015;100(2):e68-71.
McElwee KJ, Kissling S, Wenzel E, Huth A, Hoffmann R. Cultured peribulbar dermal sheath cells can induce hair follicle development and contribute to the dermal sheath and dermal papilla. The Journal of investigative dermatology 2003;121(6):1267-75.
Mehlem A, Hagberg CE, Muhl L, Eriksson U, Falkevall A. Imaging of neutral lipids by oil red O for analyzing the metabolic status in health and disease. Nature protocols 2013;8(6):1149-54.
Mesa KR, Rompolas P, Zito G, Myung P, Sun TY, Brown S, et al. Niche-induced cell death and epithelial phagocytosis regulate hair follicle stem cell pool. Nature 2015;522(7554):94-7.
Mesnick SL, Leboeuf BJ. Sexual-Behavior of Male Northern Elephant Seals .2. Female Response to Potentially Injurious Encounters. Behaviour 1991;117:262-80.
Mikhail GR. Hair Neogenesis in Rat Skin. Archives of dermatology 1963;88:713-28.
Mitterberger MC, Lechner S, Mattesich M, Kaiser A, Probst D, Wenger N, et al. DLK1(PREF1) is a negative regulator of adipogenesis in CD105(+)/CD90(+)/CD34(+)/CD31(-)/FABP4(-) adipose-derived stromal cells from subcutaneous abdominal fat pats of adult women. Stem Cell Res 2012;9(1):35-48.
Mizoguchi F, Slowikowski K, Wei K, Marshall JL, Rao DA, Chang SK, et al. Functionally distinct disease-associated fibroblast subsets in rheumatoid arthritis. Nat Commun 2018;9(1):789.
Moffat GH. The growth of hair follicles and its relation to the adjacent dermal structures. J Anat 1968;102(Pt 3):527-40.
Moll R, Franke WW, Schiller DL, Geiger B, Krepler R. The catalog of human cytokeratins: patterns of expression in normal epithelia, tumors and cultured cells. Cell 1982;31(1):11-24.
Monstrey S, Middelkoop E, Vranckx JJ, Bassetto F, Ziegler UE, Meaume S, et al. Updated scar management practical guidelines: non-invasive and invasive measures. J Plast Reconstr Aesthet Surg 2014;67(8):1017-25.
Montagna W. Some particularities of human skin and the skin of nonhuman primates. G Ital Dermatol Venereol 1984;119(1):1-4.
Moon YS, Smas CM, Lee K, Villena JA, Kim KH, Yun EJ, et al. Mice lacking paternally expressed Pref-1/Dlk1 display growth retardation and accelerated adiposity. Molecular and cellular biology 2002;22(15):5585-92.
Morgan BA. The dermal papilla: an instructive niche for epithelial stem and progenitor cells in development and regeneration of the hair follicle. Cold Spring Harb Perspect Med 2014;4(7):a015180.
Mori T, Sakaue H, Iguchi H, Gomi H, Okada Y, Takashima Y, et al. Role of Kruppel-like factor 15 (KLF15) in transcriptional regulation of adipogenesis. J Biol Chem 2005;280(13):12867-75.
Morris RJ, Liu Y, Marles L, Yang Z, Trempus C, Li S, et al. Capturing and profiling adult hair follicle stem cells. Nat Biotechnol 2004;22(4):411-7.
Mortensen SB, Jensen CH, Schneider M, Thomassen M, Kruse TA, Laborda J, et al. Membrane-tethered delta-like 1 homolog (DLK1) restricts adipose tissue size by inhibiting preadipocyte proliferation. Diabetes 2012;61(11):2814-22.
Mrosovsky N, Sherry DF. Animal anorexias. Science 1980;207(4433):837-42.

Mueller AA, van Velthoven CT, Fukumoto KD, Cheung TH, Rando TA. Intronic polyadenylation of PDGFRalpha in resident stem cells attenuates muscle fibrosis. Nature 2016;540(7632):276-9.

Muller SA. Hair Neogenesis. The Journal of investigative dermatology 1971;56(1):1-9.

Muller-Rover S, Handjiski B, van der Veen C, Eichmuller S, Foitzik K, McKay IA, et al. A comprehensive guide for the accurate classification of murine hair follicles in distinct hair cycle stages. J Invest Dermatol 2001;117(1):3-15.

Murray PJ, Allen JE, Biswas SK, Fisher EA, Gilroy DW, Goerdt S, et al. Macrophage activation and polarization: nomenclature and experimental guidelines. Immunity 2014;41(1):14-20.

Muzumdar MD, Tasic B, Miyamichi K, Li L, Luo L. A global double-fluorescent Cre reporter mouse. Genesis 2007;45(9):593-605.

Mynatt RL, Stephens JM. Agouti regulates adipocyte transcription factors. Am J Physiol Cell Physiol 2001;280(4):C954-61.

Mynatt RL, Stephens JM. Regulation of PPARgamma and obesity by agouti/melanocortin signaling in adipocytes. Ann N Y Acad Sci 2003;994:141-6.

Myung PS, Takeo M, Ito M, Atit RP. Epithelial Wnt ligand secretion is required for adult hair follicle growth and regeneration. The Journal of investigative dermatology 2013;133(1):31-41.

Nacu E, Gromberg E, Oliveira CR, Drechsel D, Tanaka EM. FGF8 and SHH substitute for anterior-posterior tissue interactions to induce limb regeneration. Nature 2016;533(7603):407-10.

Naessig PJ, Lanyon JM. Levels and probable origin of predatory scarring on humpback whales (Megaptera novaeangliae) in east Australian waters. Wildlife Res 2004;31(2):163-70.

Nelson AM, Katseff AS, Ratliff TS, Garza LA. Interleukin 6 and STAT3 regulate p63 isoform expression in keratinocytes during regeneration. Exp Dermatol 2016;25(2):155-7.

Nelson AM, Loy DE, Lawson JA, Katseff AS, Fitzgerald GA, Garza LA. Prostaglandin D2 inhibits wound-induced hair follicle neogenesis through the receptor, Gpr44. The Journal of investigative dermatology 2013;133(4):881-9.

Nelson AM, Loy DE, Lawson JA, Katseff AS, FitzGerald GA, Garza LA. Prostaglandin D2 Inhibits Wound-Induced Hair Follicle Neogenesis through the Receptor, Gpr44. Journal of Investigative Dermatology 2013;133(4):881-9.

Nelson AM, Reddy SK, Ratliff TS, Hossain MZ, Katseff AS, Zhu AS, et al. dsRNA Released by Tissue Damage Activates TLR3 to Drive Skin Regeneration. Cell Stem Cell 2015;17(2):139-51.

Nelson AM, Reddy SK, Ratliff TS, Hossain MZ, Katseff AS, Zhu AS, et al. dsRNA Released by Tissue Damage Activates TLR3 to Drive Skin Regeneration. Cell Stem Cell 2015;17(2):139-51.

Nelson WG, Sun TT. The 50- and 58-kdalton keratin classes as molecular markers for stratified squamous epithelia: cell culture studies. J Cell Biol 1983;97(1):244-51.

Nestle FO, Di Meglio P, Qin JZ, Nickoloff BJ. Skin immune sentinels in health and disease. Nat Rev Immunol 2009;9(10):679-91.

Noizet M, Lagoutte E, Gratigny M, Bouschbacher M, Lazareth I, Roest Crollius H, et al. Master regulators in primary skin fibroblast fate reprogramming in a human ex vivo model of chronic wounds. Wound repair and regeneration : official publication of the Wound Healing Society [and] the European Tissue Repair Society 2016;24(2):247-62.

Nowoshilow S, Schloissnig S, Fei JF, Dahl A, Pang AWC, Pippel M, et al. The axolotl genome and the evolution of key tissue formation regulators. Nature 2018;554(7690):50-5.
Nueda MJ, Tarazona S, Conesa A. Next maSigPro: updating maSigPro bioconductor package for RNA-seq time series. Bioinformatics 2014;30(18):2598-602.
Nueda ML, Baladron V, Sanchez-Solana B, Ballesteros MA, Laborda J. The EGF-like protein dlk1 inhibits notch signaling and potentiates adipogenesis of mesenchymal cells. J Mol Biol 2007;367(5):1281-93.
Ogawa M, LaRue AC, Drake CJ. Hematopoietic origin of fibroblasts/myofibroblasts: Its pathophysiologic implications. Blood 2006;108(9):2893-6.
Oh JW, Kloepper J, Langan EA, Kim Y, Yeo J, Kim MJ, et al. A Guide to Studying Human Hair Follicle Cycling In Vivo. J Invest Dermatol 2016;136(1):34-44.
Oh MH, Oh SY, Yu J, Myers AC, Leonard WJ, Liu YJ, et al. IL-13 induces skin fibrosis in atopic dermatitis by thymic stromal lymphopoietin. J Immunol 2011;186(12):7232-42.
Ohba S, He X, Hojo H, McMahon AP. Distinct Transcriptional Programs Underlie Sox9 Regulation of the Mammalian Chondrocyte. Cell Rep 2015;12(2):229-43.
Olson LE, Soriano P. Increased PDGFRalpha activation disrupts connective tissue development and drives systemic fibrosis. Dev Cell 2009;16(2):303-13.
Opalenik SR, Davidson JM. Fibroblast differentiation of bone marrow-derived cells during wound repair. Faseb J 2005;19(11):1561-3.
Otranto M, Sarrazy V, Bonte F, Hinz B, Gabbiani G, Desmouliere A. The role of the myofibroblast in tumor stroma remodeling. Cell Adh Migr 2012;6(3):203-19.
Ou L, Shi Y, Dong W, Liu C, Schmidt TJ, Nagarkatti P, et al. Kruppel-like factor KLF4 facilitates cutaneous wound healing by promoting fibrocyte generation from myeloid-derived suppressor cells. The Journal of investigative dermatology 2015;135(5):1425-34.
Panteleyev AA, Jahoda CA, Christiano AM. Hair follicle predetermination. J Cell Sci 2001;114(Pt 19):3419-31.
Park JR, Jung JW, Lee YS, Kang KS. The roles of Wnt antagonists Dkk1 and sFRP4 during adipogenesis of human adipose tissue-derived mesenchymal stem cells. Cell Prolif 2008;41(6):859-74.
Paterson W, Pomeroy PP, Sparling CE, Moss S, Thompson D, Currie JI, et al. Assessment of flipper tag site healing in gray seal pups using thermography. Mar Mammal Sci 2011;27(2):295-305.
Pelaez-Garcia A, Barderas R, Batlle R, Vinas-Castells R, Bartolome RA, Torres S, et al. A proteomic analysis reveals that Snail regulates the expression of the nuclear orphan receptor Nuclear Receptor Subfamily 2 Group F Member 6 (Nr2f6) and interleukin 17 (IL-17) to inhibit adipocyte differentiation. Mol Cell Proteomics 2015;14(2):303-15.
Philippeos C, Telerman S, Oules B, Pisco AO, Shaw TJ, Elgueta R, et al. Spatial and single-cell transcriptional profiling identifies functionally distinct human dermal fibroblast subpopulations. The Journal of investigative dermatology 2018a.
Philippeos C, Telerman SB, Oules B, Pisco AO, Shaw TJ, Elgueta R, et al. Spatial and Single-Cell Transcriptional Profiling Identifies Functionally Distinct Human Dermal Fibroblast Subpopulations. The Journal of investigative dermatology 2018b.
Picelli S, Bjorklund AK, Faridani OR, Sagasser S, Winberg G, Sandberg R. Smart-seq2 for sensitive full-length transcriptome profiling in single cells. Nature methods 2013;10(11):1096-8.

Picelli S, Faridani OR, Bjorklund AK, Winberg G, Sagasser S, Sandberg R. Full-length RNA-seq from single cells using Smart-seq2. Nat Protoc 2014;9(1):171-81.
Pinheiro G, Prata DF, Araujo IM, Tiscornia G. The African spiny mouse ( Acomys spp.) as an emerging model for development and regeneration. Lab Anim 2018:23677218769921.
Plikus M, Wang WP, Liu J, Wang X, Jiang TX, Chuong CM. Morpho-regulation of ectodermal organs: integument pathology and phenotypic variations in K14-Noggin engineered mice through modulation of bone morphogenic protein pathway. The American journal of pathology 2004;164(3):1099-114.
Plikus MV, Baker RE, Chen CC, Fare C, de la Cruz D, Andl T, et al. Self-organizing and stochastic behaviors during the regeneration of hair stem cells. Science 2011;332(6029):586-9.
Plikus MV, Chuong CM. Complex hair cycle domain patterns and regenerative hair waves in living rodents. J Invest Dermatol 2008;128(5):1071-80.
Plikus MV, Chuong CM. Macroenvironmental regulation of hair cycling and collective regenerative behavior. Cold Spring Harb Perspect Med 2014;4(1):a015198.
Plikus MV, Gay DL, Treffeisen E, Wang A, Supapannachart RJ, Cotsarelis G. Epithelial stem cells and implications for wound repair. Semin Cell Dev Biol 2012;23(9):946-53.
Plikus MV, Guerrero-Juarez CF, Ito M, Li YR, Dedhia PH, Zheng Y, et al. Regeneration of fat cells from myofibroblasts during wound healing. Science 2017;355(6326):748-52.
Plikus MV, Mayer JA, de la Cruz D, Baker RE, Maini PK, Maxson R, et al. Cyclic dermal BMP signalling regulates stem cell activation during hair regeneration. Nature 2008;451(7176):340-4.
Plikus MV, Widelitz RB, Maxson R, Chuong CM. Analyses of regenerative wave patterns in adult hair follicle populations reveal macro-environmental regulation of stem cell activity. Int J Dev Biol 2009;53(5-6):857-68.
Pollen AA, Nowakowski TJ, Shuga J, Wang X, Leyrat AA, Lui JH, et al. Low-coverage single-cell mRNA sequencing reveals cellular heterogeneity and activated signaling pathways in developing cerebral cortex. Nat Biotechnol 2014;32(10):1053-8.
Pougatsch DA, Rader A, Rogers LC. The Use of a Sea Salt-based Spray for Diabetic Foot Ulcers: A Novel Concept. Wounds 2017;29(2):E5-E9.
Puram SV, Tirosh I, Parikh AS, Patel AP, Yizhak K, Gillespie S, et al. Single-Cell Transcriptomic Analysis of Primary and Metastatic Tumor Ecosystems in Head and Neck Cancer. Cell 2017;171(7):1611-24 e24.
Qiu X, Hill A, Packer J, Lin D, Ma YA, Trapnell C. Single-cell mRNA quantification and differential analysis with Census. Nature methods 2017a;14(3):309-15.
Qiu X, Mao Q, Tang Y, Wang L, Chawla R, Pliner HA, et al. Reversed graph embedding resolves complex single-cell trajectories. Nat Methods 2017b;14(10):979-82.
Raff MC. Surface antigenic markers for distinguishing T and B lymphocytes in mice. Transplant Rev 1971;6:52-80.
Rahman MS, Akhtar N, Jamil HM, Banik RS, Asaduzzaman SM. TGF-beta/BMP signaling and other molecular events: regulation of osteoblastogenesis and bone formation. Bone Res 2015;3:15005.
Reiter J, Panken KJ, Leboeuf BJ. Female Competition and Reproductive Success in Northern Elephant Seals. Anim Behav 1981;29(Aug):670-87.
Reynolds AJ, Jahoda CA. Cultured dermal papilla cells induce follicle formation and hair growth by transdifferentiation of an adult epidermis. Development 1992;115(2):587-93.

Rezvani M, Espanol-Suner R, Malato Y, Dumont L, Grimm AA, Kienle E, et al. In Vivo Hepatic Reprogramming of Myofibroblasts with AAV Vectors as a Therapeutic Strategy for Liver Fibrosis. Cell Stem Cell 2016;18(6):809-16.
Rinkevich Y, Lindau P, Ueno H, Longaker MT, Weissman IL. Germ-layer and lineage-restricted stem/progenitors regenerate the mouse digit tip. Nature 2011;476(7361):409-13.
Rinkevich Y, Walmsley GG, Hu MS, Maan ZN, Newman AM, Drukker M, et al. Skin fibrosis. Identification and isolation of a dermal lineage with intrinsic fibrogenic potential. Science 2015;348(6232):aaa2151.
Rivera-Gonzalez G, Shook B, Horsley V. Adipocytes in skin health and disease. Cold Spring Harb Perspect Med 2014;4(3).
Rivera-Gonzalez GC, Shook BA, Andrae J, Holtrup B, Bollag K, Betsholtz C, et al. Skin Adipocyte Stem Cell Self-Renewal Is Regulated by a PDGFA/AKT-Signaling Axis. Cell Stem Cell 2016;19(6):738-51.
Robinson PW, Costa DP, Crocker DE, Gallo-Reynoso JP, Champagne CD, Fowler MA, et al. Foraging Behavior and Success of a Mesopelagic Predator in the Northeast Pacific Ocean: Insights from a Data-Rich Species, the Northern Elephant Seal. Plos One 2012;7(5).
Rodeheffer MS, Birsoy K, Friedman JM. Identification of white adipocyte progenitor cells in vivo. Cell 2008;135(2):240-9.
Roensch K, Tazaki A, Chara O, Tanaka EM. Progressive specification rather than intercalation of segments during limb regeneration. Science 2013;342(6164):1375-9.
Rosen ED, Spiegelman BM. What we talk about when we talk about fat. Cell 2014;156(1-2):20-44.
Ross SE, Hemati N, Longo KA, Bennett CN, Lucas PC, Erickson RL, et al. Inhibition of adipogenesis by Wnt signaling. Science 2000;289(5481):950-3.
Rost F, Rodrigo Albors A, Mazurov V, Brusch L, Deutsch A, Tanaka EM, et al. Accelerated cell divisions drive the outgrowth of the regenerating spinal cord in axolotls. Elife 2016;5.
Roufosse C, Bou-Gharios G, Prodromidi E, Alexakis C, Jeffery R, Khan S, et al. Bone marrow-derived cells do not contribute significantly to collagen I synthesis in a murine model of renal fibrosis. J Am Soc Nephrol 2006;17(3):775-82.
Rowlatt U. Intrauterine wound healing in a 20 week human fetus. Virchows Arch A Pathol Anat Histol 1979;381(3):353-61.
Ryden M. On the origin of human adipocytes and the contribution of bone marrow-derived cells. Adipocyte 2016;5(3):312-7.
Ryden M, Uzunel M, Hard JL, Borgstrom E, Mold JE, Arner E, et al. Transplanted Bone Marrow-Derived Cells Contribute to Human Adipogenesis. Cell Metab 2015;22(3):408-17.
Satija R, Farrell JA, Gennert D, Schier AF, Regev A. Spatial reconstruction of single-cell gene expression data. Nat Biotechnol 2015;33(5):495-502.
Scaglione S, Kliethermes S, Cao GC, Shoham D, Durazo R, Luke A, et al. The Epidemiology of Cirrhosis in the United States A Population-based Study. J Clin Gastroenterol 2015;49(8):690-6.
Schaub JR, Huppert KA, Kurial SNT, Hsu BY, Cast AE, Donnelly B, et al. De novo formation of the biliary system by TGFbeta-mediated hepatocyte transdifferentiation. Nature 2018.
Schmidt B, Horsley V. Unravelling hair follicle-adipocyte communication. Exp Dermatol 2012;21(11):827-30.

Schmidt BA, Horsley V. Intradermal adipocytes mediate fibroblast recruitment during skin wound healing. Development 2013;140(7):1517-27.
Schmidt M, Sun G, Stacey MA, Mori L, Mattoli S. Identification of circulating fibrocytes as precursors of bronchial myofibroblasts in asthma. J Immunol 2003;171(1):380-9.
Schmidt-Ott KM. The Ebf1 knockout mouse and glomerular maturation. Kidney Int 2014;85(5):1014-6.
Schneider RK, Mullally A, Dugourd A, Peisker F, Hoogenboezem R, Van Strien PMH, et al. Gli1(+) Mesenchymal Stromal Cells Are a Key Driver of Bone Marrow Fibrosis and an Important Cellular Therapeutic Target. Cell Stem Cell 2017;20(6):785-800 e8.
Scialdone A, Natarajan KN, Saraiva LR, Proserpio V, Teichmann SA, Stegle O, et al. Computational assignment of cell-cycle stage from single-cell transcriptome data. Methods 2015;85:54-61.
Seifert AW, Kiama SG, Seifert MG, Goheen JR, Palmer TM, Maden M. Skin shedding and tissue regeneration in African spiny mice (Acomys). Nature 2012;489(7417):561-5.
Sera Y, LaRue AC, Moussa O, Mehrotra M, Duncan JD, Williams CR, et al. Hematopoietic stem cell origin of adipocytes. Exp Hematol 2009;37(9):1108-20, 20 e1-4.
Shan T, Liu W, Kuang S. Fatty acid binding protein 4 expression marks a population of adipocyte progenitors in white and brown adipose tissues. Faseb J 2013;27(1):277-87.
Shao M, Vishvanath L, Busbuso NC, Hepler C, Shan B, Sharma AX, et al. De novo adipocyte differentiation from Pdgfrbeta(+) preadipocytes protects against pathologic visceral adipose expansion in obesity. Nat Commun 2018;9(1):890.
Sherman RA. Maggot therapy for treating diabetic foot ulcers unresponsive to conventional therapy. Diabetes Care 2003;26(2):446-51.
Shi G, Sohn KC, Li Z, Choi DK, Park YM, Kim JH, et al. Expression and functional role of Sox9 in human epidermal keratinocytes. PLoS One 2013;8(1):e54355.
Sicot FX, Tsuda T, Markova D, Klement JF, Arita M, Zhang RZ, et al. Fibulin-2 is dispensable for mouse development and elastic fiber formation. Mol Cell Biol 2008;28(3):1061-7.
Siersbaek R, Nielsen R, Mandrup S. PPARgamma in adipocyte differentiation and metabolism--novel insights from genome-wide studies. FEBS Lett 2010;584(15):3242-9.
Simkin J, Gawriluk TR, Gensel JC, Seifert AW. Macrophages are necessary for epimorphic regeneration in African spiny mice. Elife 2017;6.
Sinha M, Sen CK, Singh K, Das A, Ghatak S, Rhea B, et al. Direct conversion of injury-site myeloid cells to fibroblast-like cells of granulation tissue. Nat Commun 2018;9(1):936.
Smas CM, Chen L, Sul HS. Cleavage of membrane-associated pref-1 generates a soluble inhibitor of adipocyte differentiation. Molecular and cellular biology 1997;17(2):977-88.
Smas CM, Sul HS. Pref-1, a protein containing EGF-like repeats, inhibits adipocyte differentiation. Cell 1993;73(4):725-34.
Snippert HJ, Haegebarth A, Kasper M, Jaks V, van Es JH, Barker N, et al. Lgr6 marks stem cells in the hair follicle that generate all cell lineages of the skin. Science 2010;327(5971):1385-9.
Sokolov BP, Ala-Kokko L, Dhulipala R, Arita M, Khillan JS, Prockop DJ. Tissue-specific expression of the gene for type I procollagen (COL1A1) in transgenic mice. Only 476 base pairs of the promoter are required if collagen genes are used as reporters. J Biol Chem 1995;270(16):9622-9.
Solanas G, Benitah SA. Regenerating the skin: a task for the heterogeneous stem cell pool and surrounding niche. Nat Rev Mol Cell Biol 2013;14(11):737-48.

Song GQ, Pacher M, Balakrishnan A, Yuan QG, Tsay HC, Yang DK, et al. Direct Reprogramming of Hepatic Myofibroblasts into Hepatocytes In Vivo Attenuates Liver Fibrosis. Cell Stem Cell 2016;18(6):797-808.
Soriano P. Generalized lacZ expression with the ROSA26 Cre reporter strain. Nature genetics 1999;21(1):70-1.
Sottile V, Seuwen K. Bone morphogenetic protein-2 stimulates adipogenic differentiation of mesenchymal precursor cells in synergy with BRL 49653 (rosiglitazone). FEBS Lett 2000;475(3):201-4.
Stange DE, Koo BK, Huch M, Sibbel G, Basak O, Lyubimova A, et al. Differentiated Troy+ chief cells act as reserve stem cells to generate all lineages of the stomach epithelium. Cell 2013;155(2):357-68.
Stelfox M, Hudgins J, Sweet M. A review of ghost gear entanglement amongst marine mammals, reptiles and elasmobranchs. Mar Pollut Bull 2016;111(1-2):6-17.
Stenbäck F, Niinimäki T, Dammert K. HAIR NEOGENESIS IN RAT AND RABBIT SKIN. Acta Pathologica Microbiologica Scandinavica 1967;69(3):480-.
Stephan A, Ky-Fries K, Ngo A, Busqueta LP, Abdollahi E, Sandhu G, et al. Metabolic Gene Expression in Blubber of Fasting Elephant Seals. Integr Comp Biol 2018;58:E426-E.
Stephens JM, Morrison RF, Wu Z, Farmer SR. PPARgamma ligand-dependent induction of STAT1, STAT5A, and STAT5B during adipogenesis. Biochem Biophys Res Commun 1999;262(1):216-22.
Stephenson W, Donlin LT, Butler A, Rozo C, Bracken B, Rashidfarrokhi A, et al. Single-cell RNA-seq of rheumatoid arthritis synovial tissue using low-cost microfluidic instrumentation. Nat Commun 2018;9(1):791.
Steppan CM, Bailey ST, Bhat S, Brown EJ, Banerjee RR, Wright CM, et al. The hormone resistin links obesity to diabetes. Nature 2001;409(6818):307-12.
Stern DL. The genetic causes of convergent evolution. Nat Rev Genet 2013;14(11):751-64.
Stubbington MJT, Rozenblatt-Rosen O, Regev A, Teichmann SA. Single-cell transcriptomics to explore the immune system in health and disease. Science 2017;358(6359):58-63.
Suga H, Rennert RC, Rodrigues M, Sorkin M, Glotzbach JP, Januszyk M, et al. Tracking the elusive fibrocyte: identification and characterization of collagen-producing hematopoietic lineage cells during murine wound healing. Stem Cells 2014;32(5):1347-60.
Sugiura T, Wang H, Barsacchi R, Simon A, Tanaka EM. MARCKS-like protein is an initiating molecule in axolotl appendage regeneration. Nature 2016;531(7593):237-40.
Sun BK, Siprashvili Z, Khavari PA. Advances in skin grafting and treatment of cutaneous wounds. Science 2014;346(6212):941-5.
Sun M, Wang P, Okubo T, Orringer JS, Voorhees JJ, Fisher GJ, et al. Possible Contribution of Fibrocytes to Increased Type I Collagen Synthesis during the Early Stage of Dermal Wound Repair in Human Skin. The Journal of investigative dermatology 2018;138(1):240-2.
Tabib T, Morse C, Wang T, Chen W, Lafyatis R. SFRP2/DPP4 and FMO1/LSP1 Define Major Fibroblast Populations in Human Skin. The Journal of investigative dermatology 2017.
Takeda N, Jain R, Leboeuf MR, Padmanabhan A, Wang Q, Li L, et al. Hopx expression defines a subset of multipotent hair follicle stem cells and a progenitor population primed to give rise to K6+ niche cells. Development 2013;140(8):1655-64.
Takeo M, Chou WC, Sun Q, Lee W, Rabbani P, Loomis C, et al. Wnt activation in nail epithelium couples nail growth to digit regeneration. Nature 2013;499(7457):228-32.

Tantawi TI, Gohar YM, Kotb MM, Beshara FM, El-Naggar MM. Clinical and microbiological efficacy of MDT in the treatment of diabetic foot ulcers. J Wound Care 2007;16(9):379-83.

Taylor AC. Survival of rat skin and changes in hair pigmentation following freezing. J Exp Zool 1949;110(1):77-111.

Tedder TF. B10 cells: a functionally defined regulatory B cell subset. J Immunol 2015;194(4):1395-401.

Thannickal VJ, Lee DY, White ES, Cui Z, Larios JM, Chacon R, et al. Myofibroblast differentiation by transforming growth factor-beta1 is dependent on cell adhesion and integrin signaling via focal adhesion kinase. J Biol Chem 2003;278(14):12384-9.

Thorel F, Nepote V, Avril I, Kohno K, Desgraz R, Chera S, et al. Conversion of adult pancreatic alpha-cells to beta-cells after extreme beta-cell loss. Nature 2010;464(7292):1149-54.

Tirosh I, Izar B, Prakadan SM, Wadsworth MH, 2nd, Treacy D, Trombetta JJ, et al. Dissecting the multicellular ecosystem of metastatic melanoma by single-cell RNA-seq. Science 2016a;352(6282):189-96.

Tirosh I, Venteicher AS, Hebert C, Escalante LE, Patel AP, Yizhak K, et al. Single-cell RNA-seq supports a developmental hierarchy in human oligodendroglioma. Nature 2016b;539(7628):309-13.

Tomasek JJ, Gabbiani G, Hinz B, Chaponnier C, Brown RA. Myofibroblasts and mechano-regulation of connective tissue remodelling. Nat Rev Mol Cell Biol 2002;3(5):349-63.

Tomiyama K, Murase N, Stolz DB, Toyokawa H, O'Donnell DR, Smith DM, et al. Characterization of transplanted green fluorescent protein+ bone marrow cells into adipose tissue. Stem Cells 2008;26(2):330-8.

Tonnesen MG, Feng X, Clark RA. Angiogenesis in wound healing. J Investig Dermatol Symp Proc 2000;5(1):40-6.

Trapnell C, Cacchiarelli D, Grimsby J, Pokharel P, Li S, Morse M, et al. The dynamics and regulators of cell fate decisions are revealed by pseudotemporal ordering of single cells. Nat Biotechnol 2014;32(4):381-6.

van Amerongen MJ, Bou-Gharios G, Popa E, van Ark J, Petersen AH, van Dam GM, et al. Bone marrow-derived myofibroblasts contribute functionally to scar formation after myocardial infarction. J Pathol 2008;214(3):377-86.

van den Broek LJ, Limandjaja GC, Niessen FB, Gibbs S. Human hypertrophic and keloid scar models: principles, limitations and future challenges from a tissue engineering perspective. Experimental dermatology 2014;23(6):382-6.

van den Hoff J, Morrice MG. Sleeper shark (Somniosus antarcticus) and other bite wounds observed on southern elephant seals (Mirounga leonina) at Macquarie Island. Mar Mammal Sci 2008;24(1):239-47.

van den Hoff J, Sumner MD, Field IC, Bradshaw CJA, Burton HR, McMahon CR. Temporal changes in the quality of hot-iron brands on elephant seal (Mirounga leonina) pups. Wildlife Res 2004;31(6):619-29.

van der Loop FT, Gabbiani G, Kohnen G, Ramaekers FC, van Eys GJ. Differentiation of smooth muscle cells in human blood vessels as defined by smoothelin, a novel marker for the contractile phenotype. Arteriosclerosis, thrombosis, and vascular biology 1997;17(4):665-71.

van der Maaten L, Hinton G. Visualizing Data using t-SNE. J Mach Learn Res 2008;9:2579-605.

Vaughan MB, Howard EW, Tomasek JJ. Transforming growth factor-beta1 promotes the morphological and functional differentiation of the myofibroblast. Exp Cell Res 2000;257(1):180-9.
Vecchi A, Garlanda C, Lampugnani MG, Resnati M, Matteucci C, Stoppacciaro A, et al. Monoclonal antibodies specific for endothelial cells of mouse blood vessels. Their application in the identification of adult and embryonic endothelium. Eur J Cell Biol 1994;63(2):247-54.
Versteeg HH, Heemskerk JW, Levi M, Reitsma PH. New fundamentals in hemostasis. Physiol Rev 2013;93(1):327-58.
Vidal VP, Chaboissier MC, Lutzkendorf S, Cotsarelis G, Mill P, Hui CC, et al. Sox9 is essential for outer root sheath differentiation and the formation of the hair stem cell compartment. Curr Biol 2005;15(15):1340-51.
Wakao H, Wakao R, Oda A, Fujita H. Constitutively active Stat5A and Stat5B promote adipogenesis. Environ Health Prev Med 2011;16(4):247-52.
Wang EA, Israel DI, Kelly S, Luxenberg DP. Bone morphogenetic protein-2 causes commitment and differentiation in C3H10T1/2 and 3T3 cells. Growth factors 1993;9(1):57-71.
Wang Q, Oh JW, Lee HL, Dhar A, Peng T, Ramos R, et al. A multi-scale model for hair follicles reveals heterogeneous domains driving rapid spatiotemporal hair growth patterning. Elife 2017;6.
Wang QA, Scherer PE. The AdipoChaser mouse: A model tracking adipogenesis in vivo. Adipocyte 2014;3(2):146-50.
Wang QA, Tao C, Gupta RK, Scherer PE. Tracking adipogenesis during white adipose tissue development, expansion and regeneration. Nat Med 2013;19(10):1338-44.
Wang X, Chen H, Tian R, Zhang Y, Drutskaya MS, Wang C, et al. Macrophages induce AKT/beta-catenin-dependent Lgr5+ stem cell activation and hair follicle regeneration through TNF. Nature communications 2017;8:14091.
Wang X, Hsi TC, Guerrero-Juarez CF, Pham K, Cho K, McCusker CD, et al. Principles and mechanisms of regeneration in the mouse model for wound-induced hair follicle neogenesis. Regeneration (Oxf) 2015;2(4):169-81.
Warming S, Rachel RA, Jenkins NA, Copeland NG. Zfp423 is required for normal cerebellar development. Molecular and cellular biology 2006;26(18):6913-22.
Wendling O, Bornert JM, Chambon P, Metzger D. Efficient temporally-controlled targeted mutagenesis in smooth muscle cells of the adult mouse. Genesis 2009;47(1):14-8.
Werner S, Grose R. Regulation of wound healing by growth factors and cytokines. Physiol Rev 2003;83(3):835-70.
Wilgus TA, Roy S, McDaniel JC. Neutrophils and Wound Repair: Positive Actions and Negative Reactions. Adv Wound Care (New Rochelle) 2013;2(7):379-88.
Wojciechowicz K, Gledhill K, Ambler CA, Manning CB, Jahoda CA. Development of the mouse dermal adipose layer occurs independently of subcutaneous adipose tissue and is marked by restricted early expression of FABP4. PLoS One 2013;8(3):e59811.
Wojciechowicz K, Markiewicz E, Jahoda CA. C/EBPalpha identifies differentiating preadipocytes around hair follicles in foetal and neonatal rat and mouse skin. Exp Dermatol 2008;17(8):675-80.
Wolcott R, Sanford N, Gabrilska R, Oates JL, Wilkinson JE, Rumbaugh KP. Microbiota is a primary cause of pathogenesis of chronic wounds. J Wound Care 2016;25(Sup10):S33-S43.

Wolcott RD, Hanson JD, Rees EJ, Koenig LD, Phillips CD, Wolcott RA, et al. Analysis of the chronic wound microbiota of 2,963 patients by 16S rDNA pyrosequencing. Wound Repair Regen 2016;24(1):163-74.
Woodley DT. Distinct Fibroblasts in the Papillary and Reticular Dermis: Implications for Wound Healing. Dermatol Clin 2017;35(1):95-100.
Worthy GAJ, Morris PA, Costa DP, Leboeuf BJ. Molt Energetics of the Northern Elephant Seal (Mirounga-Angustirostris). J Zool 1992;227:257-65.
Wosgrau AC, Jeremias Tda S, Leonardi DF, Pereima MJ, Di Giunta G, Trentin AG. Comparative experimental study of wound healing in mice: Pelnac versus Integra. PLoS One 2015;10(3):e0120322.
Wu Q, Tian Y, Zhang J, Tong X, Huang H, Li S, et al. In vivo CRISPR screening unveils histone demethylase UTX as an important epigenetic regulator in lung tumorigenesis. Proc Natl Acad Sci U S A 2018;115(17):E3978-E86.
Wu W, Lu Z, Li F, Wang W, Qian N, Duan J, et al. Efficient in vivo gene editing using ribonucleoproteins in skin stem cells of recessive dystrophic epidermolysis bullosa mouse model. Proc Natl Acad Sci U S A 2017;114(7):1660-5.
Wurtzel O, Cote LE, Poirier A, Satija R, Regev A, Reddien PW. A Generic and Cell-Type-Specific Wound Response Precedes Regeneration in Planarians. Dev Cell 2015;35(5):632-45.
Yamaguchi R, Takami Y, Yamaguchi Y, Shimazaki S. Bone marrow-derived myofibroblasts recruited to the upper dermis appear beneath regenerating epidermis after deep dermal burn injury. Wound Repair Regen 2007;15(1):87-93.
Yamahara KM, Layton BA, Santoro AE, Boehm AB. Beach sands along the California coast are diffuse sources of fecal bacteria to coastal waters. Environ Sci Technol 2007;41(13):4515-21.
Yang CC, Cotsarelis G. Review of hair follicle dermal cells. J Dermatol Sci 2010;57(1):2-11.
Yang H, Adam RC, Ge Y, Hua ZL, Fuchs E. Epithelial-Mesenchymal Micro-niches Govern Stem Cell Lineage Choices. Cell 2017;169(3):483-96 e13.
Yang J, Hills D, Taylor E, Pfeffer K, Ure J, Medvinsky A. Transgenic tools for analysis of the haematopoietic system: knock-in CD45 reporter and deletor mice. J Immunol Methods 2008;337(2):81-7.
Yang L, Chan T, Demare J, Iwashina T, Ghahary A, Scott PG, et al. Healing of burn wounds in transgenic mice overexpressing transforming growth factor-beta 1 in the epidermis. Am J Pathol 2001;159(6):2147-57.
Yang L, Scott PG, Dodd C, Medina A, Jiao H, Shankowsky HA, et al. Identification of fibrocytes in postburn hypertrophic scar. Wound repair and regeneration : official publication of the Wound Healing Society [and] the European Tissue Repair Society 2005;13(4):398-404.
Yilmaz OH, Kiel MJ, Morrison SJ. SLAM family markers are conserved among hematopoietic stem cells from old and reconstituted mice and markedly increase their purity. Blood 2006;107(3):924-30.
Yoshida CA, Furuichi T, Fujita T, Fukuyama R, Kanatani N, Kobayashi S, et al. Core-binding factor beta interacts with Runx2 and is required for skeletal development. Nat Genet 2002;32(4):633-8.
Yu PB, Deng DY, Lai CS, Hong CC, Cuny GD, Bouxsein ML, et al. BMP type I receptor inhibition reduces heterotopic [corrected] ossification. Nat Med 2008a;14(12):1363-9.

Yu PB, Hong CC, Sachidanandan C, Babitt JL, Deng DY, Hoyng SA, et al. Dorsomorphin inhibits BMP signals required for embryogenesis and iron metabolism. Nature chemical biology 2008b;4(1):33-41.

Yun UJ, Song NJ, Yang DK, Kwon SM, Kim K, Kim S, et al. miR-195a inhibits adipocyte differentiation by targeting the preadipogenic determinator Zfp423. J Cell Biochem 2015;116(11):2589-97.

Zasloff M. Observations on the remarkable (and mysterious) wound-healing process of the bottlenose dolphin. J Invest Dermatol 2011;131(12):2503-5.

Zhang B, Tsai PC, Gonzalez-Celeiro M, Chung O, Boumard B, Perdigoto CN, et al. Hair follicles' transit-amplifying cells govern concurrent dermal adipocyte production through Sonic Hedgehog. Genes Dev 2016;30(20):2325-38.

Zhang LJ, Gallo RL. Antimicrobial peptides. Curr Biol 2016;26(1):R14-9.

Zhang LJ, Guerrero-Juarez CF, Hata T, Bapat SP, Ramos R, Plikus MV, et al. Innate immunity. Dermal adipocytes protect against invasive Staphylococcus aureus skin infection. Science 2015;347(6217):67-71.

Zwick RK, Guerrero-Juarez CF, Horsley V, Plikus MV. Anatomical, Physiological, and Functional Diversity of Adipose Tissue. Cell Metab 2018;27(1):68-83.